International
Progress Report

IPR-04-32

Äspö Hard Rock Laboratory

Äspö Task Force

GoldSim and FrackMan/LTG Modeling Task 6A, 6B and 6B2

Performance assessment modeling using site characterisation data (PASC)

W. Dershowitz, Golder Associates Inc.
M. Uchida, JNC Tokai
D. Shuttle, Golder Associates Inc.

January 2003

Svensk Kärnbränslehantering AB
Swedish Nuclear Fuel
and Waste Management Co
Box 5864
SE-102 40 Stockholm Sweden
Tel 08-459 84 00
+46 8 459 84 00
Fax 08-661 57 19
+46 8 661 57 19

Äspö Hard Rock Laboratory

Report no.
IPR-04-32
No.
F65K
Author
W. Dershowitz
M. Uchida
D. Shuttle
Date
Jan 2003
Checked by
Masahira Uschida
Date
July 2004
Approved
Christer Svemar
Date
2004-08-30

Äspö Hard Rock Laboratory

Äspö Task Force

GoldSim and FrackMan/LTG Modeling Task 6A, 6B and 6B2

Performance assessment modeling using site characterisation data (PASC)

W. Dershowitz, Golder Associates Inc.
M. Uchida, JNC Tokai
D. Shuttle, Golder Associates Inc.

January 2003

Keywords: Fracture network modeling, solute transport, performance assessment, safety assessment, site characterisation, GoldSim, Fracman, upscaling

Forward

Site characterization is required to understand the geological environment surrounding radioactive waste repositories. Site characterization approaches and models, however, are rarely used directly in repository safety assessment. Instead, the more complex site characterization models are simplified into performance assessment (PA) type models.

This report describes a preliminary effort on the part of JNC to integrate site characterization and performance assessment modeling. The ultimate goal of this work is to quantify to effect of site characterization uncertainty on safety assessment, to help prioritize site characterization activities.

Abstract

This report describes JNC/Golder analyses in support of Task 6 of the Äspö Task Force on Groundwater Modeling. Simulations were carried out primarily on a pipe network geometry using the GoldSim performance assessment code, with supplemental simulations carried out for heterogeneous fracture planes using the MAFIC/LTG site characterization code. The simulations were designed to evaluate the influence of the difference between site characterization (Task 6A) and performance assessment (Task 6B) boundary conditions on the integration of modeling approaches. In Task 6B2, simulations were carried out using a boundary condition which replaces the downstream pumping well boundary condition used in Task 6B with a downstream fracture intersection boundary condition. The change in boundary condition can have a significant influence on the propagation of uncertainties from the SC to PA scales.

Sammanfattning

Denna rapport beskriver analyser inom Task 6 utförda av JNC/Golder för Äspö Task Force, grundvattenmodellering. Simuleringarna utfördes främst i en rörnätverksliknande geometri genom att använda förvarsfunktionskoden GoldSim. Dessutom användes platsundersökningskoden MAFIC/LTG för simulering av heterogena sprickor. Simuleringarna var konstruerade för utvärdering av skillnaden mellan experimentell platsundersökning (Task 6A) och djupförvarsrandvillkor (Task 6B) för olika modellansatser. I modelluppgift 6B2 byttes den punktformiga pumpsänkan mot en linjeformad sänka bestående av en sprickkorsning. Förändringen i randvillkor kan ha ett stort inflytande vid propagerandet av osäkerheter från platsundersökning till funktionsbedömning i förvarsskala.

Contents

List of figures

List of Tables

Executive summary

This report describes integrated site characterization (SC) and performance assessment (PA) modeling using the GoldSim PA code and the MAFIC/LTG SC code. This work focused on evaluating the extent to which the parameters which are determined from SC experiments constrain solute transport at PA time scales. This effort was carried out on a 5 to 10 m scale transport pathways from the Äspö "TRUE-1" tracer experiment "STT-1b". Simulations were carried out at both experimental and safety assessment time scales.

Site characterization scale simulations ("Task 6A") were carried out to determine the range values for transport parameters which could be consistent with measured tracer breakthrough. This uncertainty range was then compared against the physically possible range of parameters to quantify how well the experiments constrain the tracer transport parameters. Task 6A simulations determined that while the physical parameters of solute transport are not well constrained, parameter groups such as flow wetted surface and the mobile/immobile volume ratio is constrained.

The uncertainty at the SC time scale was propagated to the PA time scale by reducing the flow velocity by a factor of 1000, and increasing the simulated time scale to one million years. This effort (Task 6B) demonstrated that the residual uncertainty from site characterization does propagate to significant uncertainty at PA time scales. This is particularly true for parameters such as the available immobile zone porosity of the rock mass which are not constrained at SC time scales.

Simulations were also carried out to evaluate the influence of the difference between site characterization and performance assessment boundary conditions on the integration of modeling approaches. In "Task 6B2", simulations were carried out using a boundary condition which replaces the downstream pumping well boundary condition used in Task 6B with a downstream fracture intersection boundary condition. The change in boundary condition can have a significant influence on the propagation of uncertainties from the SC to PA scales. However, the current simulations indicate that the added uncertainty due to two-dimensional flow is less significant than other uncertainties addressed in Task 6B.

Scope

Solute transport in discrete fracture networks is a key aspect of repository safety. As a result, detailed approaches have been developed for analysis and simulation of DFN solute transport for both performance assessment (PA) and repository site characterization (SC). These approaches can be quite different, and Task 6 seeks to bridge the gap between PA and SC type models. Task 6 is focused on the 50 to 100m scale, which is the scale of many SC experiments, and also a key scale for geosphere barriers in the JNC repository program.

JNC's objectives for Task 6 are as follows:

- Identify key assumptions needed for long term prediction in PA and identify less important assumptions in PA
- Identify the most significant PA model components of a site.
- Prioritize assumptions in PA modeling and demonstrate a rationale for simplifications in PA-models by parallel application of several PA models of varying degree of simplification.
- Provide a benchmark for comparison of PA and SC models in terms of PA measures for radionuclide transport at PA temporal and spatial scales
- Establish how to transfer SC models using site characterization data to PA models, i.e., how to simplify SC models into PA models in a consistent manner

The JNC/Golder efforts for Task 6 and 6B focused on evaluating the extent to which the parameters which are determined from SC experiments constrain solute transport at PA time scales. This effort was carried out using the GoldSim code, which is a PA code capable of modeling SC experiments, and with MAFIC/LTG. MAFIC/LTG was used to study the effect of detailed in plane variations in transport properties. MAFIC/LTG is more widely used for modeling fracture networks with fully heterogeneous properties within fracture planes.

This report describes the JNC/Golder team's efforts for three tasks:

- Task 6A: Simulation of TRUE-1 Solute Transport Experiments with GoldSim PA Code
- Task 6B: Extrapolation of Experimental Results to PA Time Scales with GoldSim PA Code
- Task 6B2: Extrapolation of Single Heterogeneous Fracture Transport from SC to PA Time Scales with MAFIC/LTG SC Code

These three analyses are described in the following three report chapters. Conclusions are provided in Chapter 5.

Task 6 is phased from simple to complex, and includes sensitivity studies to maximize the amount of information obtained from the task to support both site characterization and performance assessment.

It is emphasized that up-scaling is not a primary objective of Task 6 but rather is assumed to be an implicit part of the model approaches.

1 Task 6A: Simulation of TRUE-1 Solute Transport Experiments with GoldSim PA Code

1.1 Strategy

The TRUE-1 tracer experiments provide an extensive database of solute transport behavior in a 20-meter scale fracture. The transport pathway studies for Task 6A, STT-1b, is approximately 5 meters long, and was tested with both conservative and sorbing tracers. In Task 6A, the JNC/Golder team evaluated these tracer tests using the GoldSim code (Miller, 2002), which is generally used for performance assessment (PA) rather than site characterization (SC). Previous simulations of these experiments using SC codes are described in Dershowitz et al. (2001).

The goal of the JNC/Golder team was not to determine the single "correct" set of transport pathway properties. Rather, a stochastic sensitivity study was carried out to determine the extent to which the TRUE-1 tracer breakthroughs constrain the tracer pathway properties. In effect, how much is the space of physically possible transport parameters decreased by the results for the STT-1b tracer experiments?

The conceptual model used for the transport in Task 6A is illustrated in Figure 1-1, based on the work of Winberg et al. (1999), Mazurek and Jacob (2000) (Figure 1-2). The implementation of the conceptual model in GoldSim is shown in Figure 1-3. The GoldSim model provides the following features:

- One or two transport pathways to support observed multiple peak breakthroughs observed in some TRUE-1 tracer experiments
- Pathway processes include advection, longitudinal dispersion, diffusion to immobile zones, and transfer between advective and stagnant zones within the fracture plane
- Up to three immobile zones
- Linear sorption/desorption occurs from each immobile zone (in series and parallel)

The immobile zone exchange model in GoldSim includes both diffusion to immobile zones such as breccia and wall rock, and transfer between the advective zone and the stagnant portions of the fracture. The transfer to the stagnant zone is similar to diffusion, but does not allow upstream mixing. GoldSim allows the user to explicitly represent a single stagnant dispersive zone within each one-dimensional pathway. The stagnant zone is specified in terms of the fraction of the pathway that is stagnant, and the transfer rate (1/m). The stagnant zone is assumed to have negligible advective velocity, but provides a volume available for diffusion to the immobile zones. The stagnant zone can be filled with a porous medium (to which species can sorb). Transfer between the stagnant and the mobile zone is advective, and thus varies proportionally to

the quantity of fluid flowing through the pathway. The constant of proportionality (the transfer rate) has dimensions of 1/length. It is defined as the probability of an individual solute molecule moving from the mobile zone to the stagnant zone per length of distance traveled in the mobile zone.

Because the STT-1b tracer breakthrough studied for Task 6C included only one peak, the secondary transport pathway F-G-H of Figure 1-3 was not included in the GoldSim simulation (Figure 1-4).

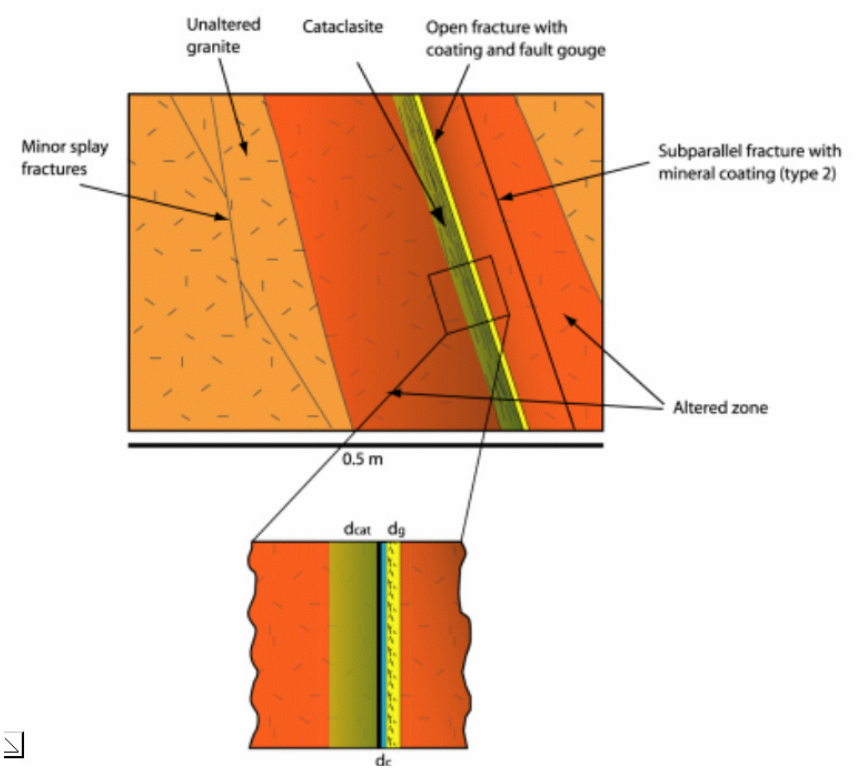

Figure 1-1 *Transport Conceptual Model after Dershowitz et al. (2002)*

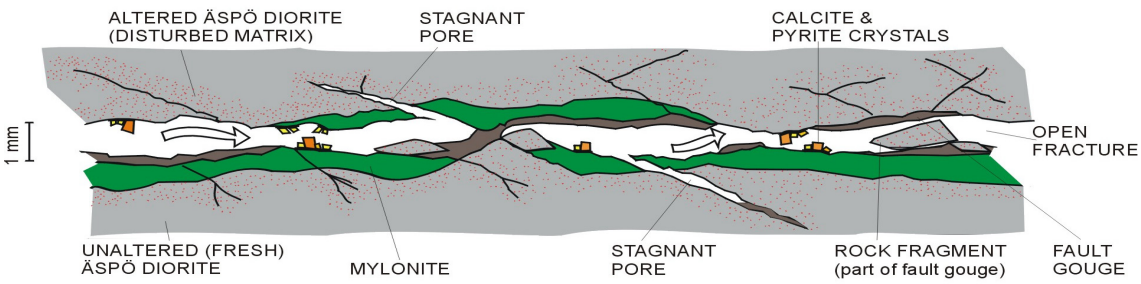

Figure 1-2 *Transport Conceptual Model Including Stagnent Zones*

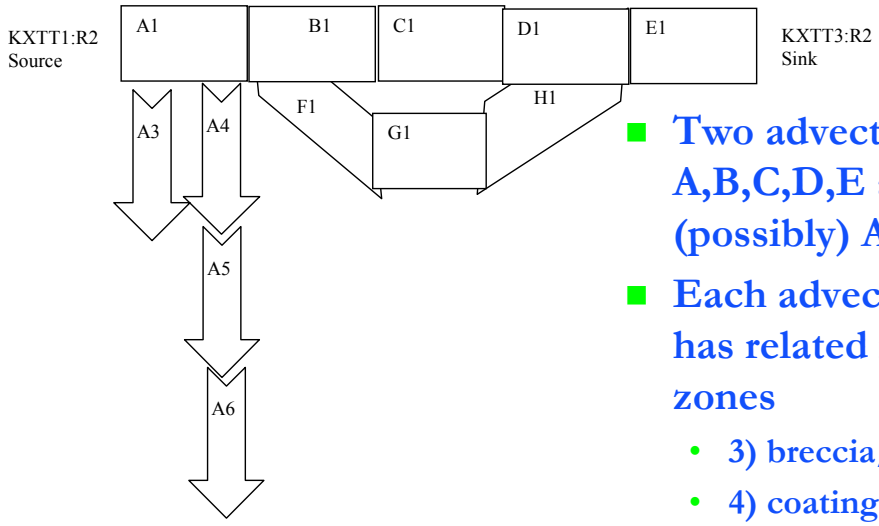

- Two advective pathways: A,B,C,D,E and (possibly) A,F,G,H,E
- Each advective pathway has related immobile zones
  - 3) breccia/infilling
  - 4) coating/mylonite
  - 5) altered wall rock
  - 6) unaltered rock mass

Note: initial simulations only use single A-E pathway

Figure 1-3 *Implementation of Conceptual Model*

.

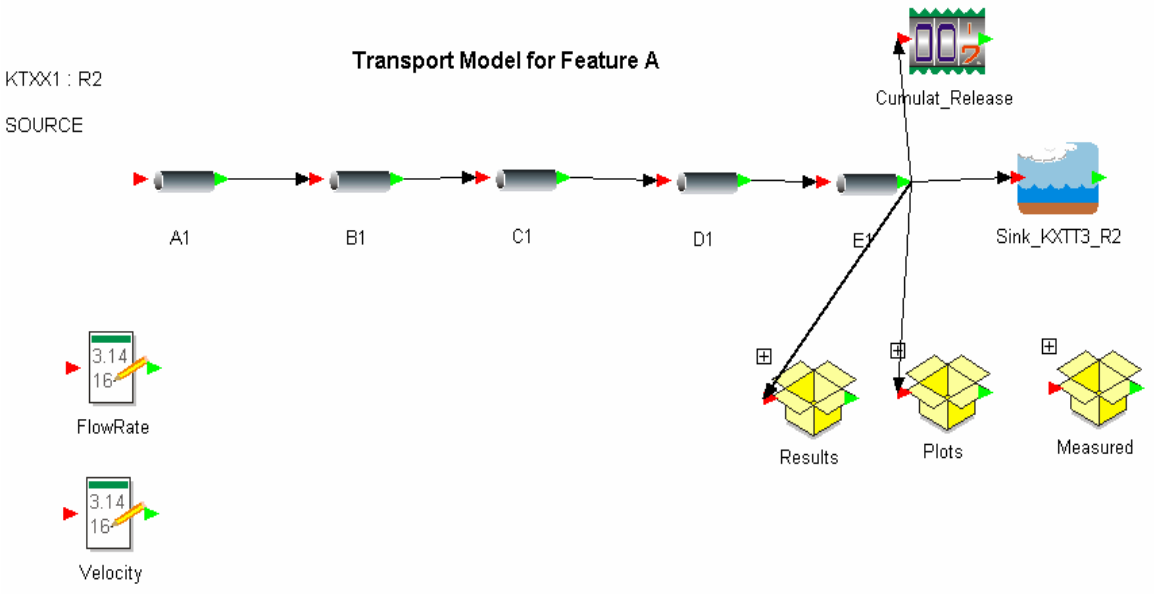

Figure 1-4 *GoldSim Implementation of Microstructure/Pathway Model*

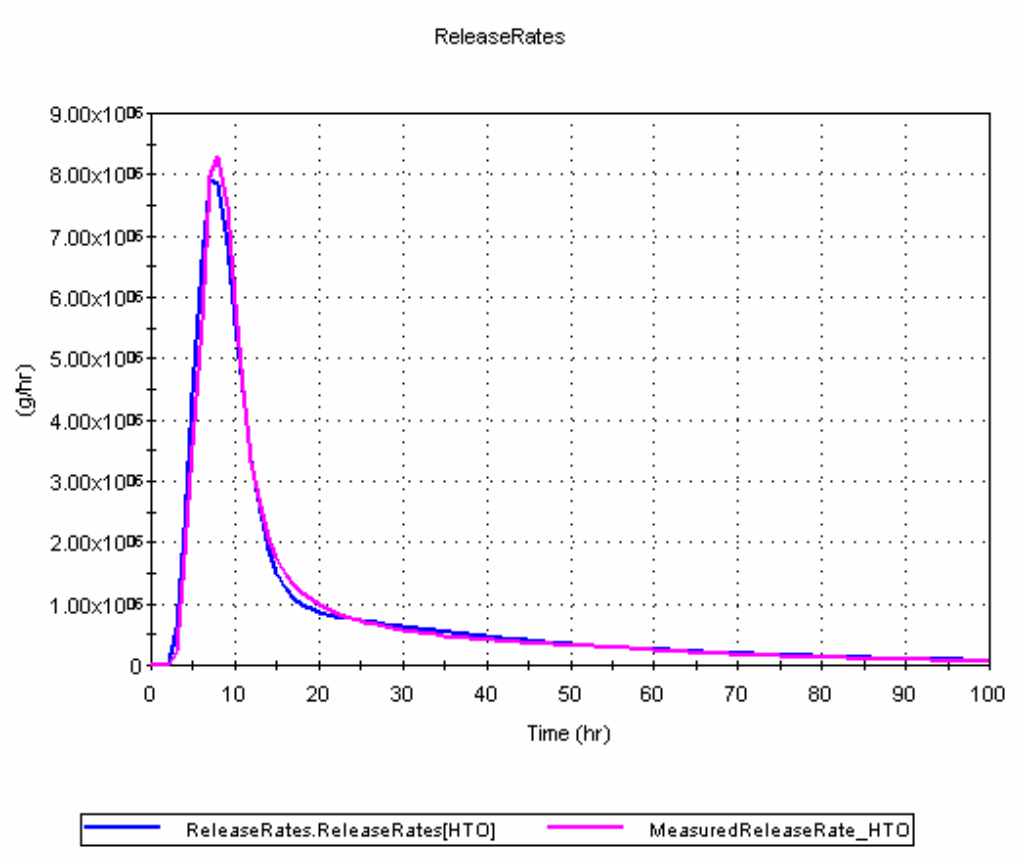

Figure 1-5 *Realization 624 – HTO Breakthrough*

Evaluation of the power of site characterization experiments to reduce uncertainty requires an understanding of the level of uncertainty before the experiment. This is given by the physically possible range of transport parameters. *Table 1-1* and *Table 1-2* lists the initial range used for each of the transport properties. These ranges were used to define the initial level of uncertainty in the transport parameters. By comparing the breakthrough curves obtained from each GoldSim realization against the measured breakthrough curves, the parameter uncertainty is then reduced by only considering those parameters and parameter combinations which provide a good match.

Table 1-1 Initial Ranges for Advective Transport Properties

Parameter	Units	Distribution	Minimum	Maximum
Width	mm	Constant	100	100
Length	m	Constant	1	1
Aperture	mm	LogUniform	0.01	0.1
Travel Time	hour	Uniform	0.5	1.5
Dispersion Length[1]	m	Discrete Values	0.05	1
Stagnant Proportion	-	-	0.8	0.8
Transfer Rate	1/m	Constant	0.1	0.1
Pathway Porosity	-	Constant	0.8	0.8
1. Dispersion length takes on 5 discrete values between min and max.				

Table 1-2 Initial Ranges for Immobile Zone Transport Properties

Rock	Parameter	Units	Distribution	Minimum	Maximum
Breccia	Dmax	mm	Uniform	0	4
	Porosity	-	Uniform	0.01	0.4
	Tortuosity	-	Discrete	0.0125	0.0125
Mylonite	Dmax	mm	Uniform	0	20
	Porosity	-	Uniform	0.005	0.2
	Tortuosity	-	Discrete	0.0125	0.0125
RockMass	Dmax	mm	Uniform	10	100
	Porosity	-	Uniform	0.001	0.005
	Tortuosity	-	Discrete	0.0125	0.0125
Transfer between mobile and immobile zones and between mobile and mobile zones occurs over the area defined by the pipe path width and length. Parameter ranges are based on Mazurek et al. (2001) and Winberg et al. (2000).					

Goodness of fit was measured by the error metric ε_T: This error metric was defined in order to consider equally the difference between simulated and measured breakthrough for all portions of the breakthrough curve.

$$\varepsilon_T = \varepsilon_{PR} + \varepsilon_{PT} + \varepsilon_5 + \varepsilon_{50} + \varepsilon_{95}$$

where ε_{PR} is the percentage error in the peak mass rate, $\varepsilon_{PT,}$ is the percentage error in the time to peak breakthrough rate, ε_5 is the percentage error in the time to 5% cumulative breakthrough, ε_{50} is the percentage error in the time to 50% cumulative breakthrough, and ε_{95} is the percentage error in the time to 95% cumulative breakthrough. Combinations of transport parameter values were considered to be more likely if they produced breakthrough curves with low error values.

1.2 Simulations

The Task 6A simulations were carried out in three stages:

- Conditioning according to conservative tracers only, directly using site characterization transport parameters (6A-1)
- Conditioning to conservative tracers using parameter groups (6A-2)
- Conditioning to conservative and sorbing tracers (6A-3).

Using each stage, the degree of uncertainty in the possible values of transport and immobile zone parameters is decreased.

1.2.1 Conditioning to Conservative Tracers (6A-1)

A total of 1500 GoldSim simulations were run using the range of parameters defining the physically possible transport parameter space of Table1-1. For each of these simulations, statistics were calculated for the magnitude of the peak breakthrough, time to peak, t5, t50, and t95. These values were then used to calculate the error metric ε_T. Table 1-3 shows the results from the 20 simulations which provided the error metric ε_T. Surprisingly, the range of values possible for all of the transport parameters within the 20 best simulations is similar to that for the full parameter space.

Table 1-3 20 "Good Fit" Pathway Realizations STT-1b HTO Breakthrough

					Breccia		Mylonite		RockMass	
Real (-)	Error Measure	Aperture (mm)	Travel Time (hr)	Dispersion (m)	Dmax (mm)	Porosity (-)	Dmax (mm)	Porosity (-)	Dmax (mm)	Porosity (-)
624	12.81%	0.0955	0.8771	0.5	2.4473	0.1186	11.3090	0.0187	52.0950	0.0030
1477	14.76%	0.0590	0.9629	0.5	0.6193	0.2739	14.6100	0.0106	29.9870	0.0027
292	16.78%	0.0671	0.5599	0.5	2.5381	0.1411	2.7768	0.0177	73.2990	0.0050
845	20.23%	0.0259	0.5909	0.5	0.6442	0.2098	16.8330	0.0071	91.2690	0.0010
602	21.28%	0.0430	0.5142	0.5	0.6608	0.3976	11.0030	0.0077	41.5360	0.0035
745	21.31%	0.0730	1.1674	0.5	2.4587	0.0678	1.6373	0.0157	78.2870	0.0024
731	22.80%	0.0632	0.5749	0.5	1.8408	0.1847	8.7847	0.0182	81.0910	0.0014
1084	22.95%	0.0679	1.0613	0.5	1.9541	0.0760	7.3231	0.0092	99.1820	0.0039
478	23.10%	0.0454	1.3132	0.5	1.5920	0.0477	8.7775	0.0100	98.1620	0.0025
1004	25.60%	0.0224	0.7993	0.5	1.0225	0.0734	19.7830	0.0089	89.4160	0.0016
893	25.83%	0.0509	1.3740	0.5	3.0949	0.0257	19.4290	0.0060	25.8680	0.0046
361	26.13%	0.0838	1.2664	0.5	0.6257	0.2397	16.9440	0.0052	58.1330	0.0013
695	27.28%	0.0112	0.5499	0.2	1.2933	0.0379	0.4726	0.0137	77.6840	0.0030
644	27.86%	0.0230	1.0208	0.5	0.4752	0.1097	8.4663	0.0087	29.4220	0.0047
1221	31.83%	0.0832	1.3865	0.5	2.0364	0.0771	8.6703	0.0192	36.0590	0.0014
625	33.70%	0.0869	1.0240	0.5	0.6912	0.2782	6.7990	0.0117	33.9660	0.0027
640	35.20%	0.0174	0.8084	0.5	0.7253	0.0772	1.0834	0.0161	90.1220	0.0017
1452	35.48%	0.0465	0.7614	0.5	0.6504	0.2279	15.1800	0.0057	90.8690	0.0045
1269	36.55%	0.0424	0.6381	0.2	3.3784	0.0497	15.4600	0.0196	93.8030	0.0014
760	37.66%	0.0361	0.7460	0.2	0.5748	0.1969	3.7313	0.0114	88.0550	0.0035
min	**n/a**	**0.0112**	**0.5142**	**0.2**	**0.4752**	**0.0257**	**0.4726**	**0.0052**	**25.8680**	**0.0010**
max	**n/a**	**0.0955**	**1.3865**	**0.5**	**3.3784**	**0.3976**	**19.7830**	**0.0196**	**99.1820**	**0.0050**

Figure 1-5 and Figure 1-6 illustrate the GoldSim modeled tracer breakthrough for the two conservative tracers HTO and I-131, for the same realization. Given the wide variation in both mobile and immobile zone parameters found in this study, the sorbing tracer breakthrough is essentially unconstrained.

1.2.2 Conditioning to Parameter Groups (6A-2)

Neretnieks (1983), Cvetkovic et al. (1999), Nagra (1994), and others have demonstrated that solute transport equations in fractured rock can be defined in terms of parameter groups. These parameters groups represent the combined affect of the fracture geometry, immobile zone properties, and site characterization parameters such as transport aperture, immobile zone depth, and reactive surface area.

Table 1-4 lists the parameter groups studied. The first three parameter groups, a_r, F, and k, are based on parameter groups commonly used. The remaining three groups are functions of these parameter groups.

Table 1-5 through Table 1-8 compares the range of parameter group values searched in 1500 simulations against the range for the ten simulations with the lowest error measure ε_T. Of the six measures, the volume ratio V_R provided the most unique constraint for which simulations were consistent with the measured breakthrough. Volume ratio V_R values for the matching simulations range over only 0.2% to 1.5% of the range for all 1500 simulations.

In the original simulations, the diffusion rate was held constant. This constrained the degree of diffusion in the model and may have reduced the ability of some models to match observed breakthrough curves. Diffusion rate was therefore added to the parameter search space for these simulations. Correspondingly, the search space for dispersion length α_L was reduced, since α_L was previously used to provide the degree of freedom for matching dispersion observed in breakthrough curves.

Table 1-4 Transport Pathway Measures

Parameter	Units	Definition
a_r	mm^2 / mm^3	2 / (aperture + 2*Dmax)
F factor (or β)	hr/m	2 * travel time / aperture
k	$(m^2/hr)^{0.5}$	porosity * $(D_{eff} * R_{matrix})^{1/2}$
k * F	$hr^{0.5}$	see above
k * F * t	$hr^{1.5}$	see above
Volume Ratio	hr	Matrix Volume / Flowing Volume * travel time * Retardation (2.Dmax+e)n/e * t * R

Table 1-5 HTO Transport Pathway Properties

		HTO					
		a_r	F factor	k	k*F	k*F *time	Volume Ratio
All 1500	min	0.24838	10.735	2.38E-06	4.515E-05	2.820E-05	0.11
	max	34.0588	292.924	8.48E-05	1.976E-02	2.856E-02	317.12
Top 10	min	0.3889	16.678	1.01E-05	4.604E-04	2.794E-04	4.46
	max	1.5413	71.454	8.44E-05	2.031E-03	1.827E-03	6.49
Proportion of Range		3.41%	19.41%	90.06%	7.97%	5.43%	**0.64%**

Table 1-6 I-131 Transport Pathway Properties

I-131							
		a_r	F factor	k	k*F	k*F *time	Volume Ratio
All 1500	min	0.248	10.73	2.380E-06	4.515E-05	2.820E-05	0.11
	max	34.059	292.92	8.480E-05	1.976E-02	2.856E-02	317.12
Top 10	min	0.282	22.33	2.949E-06	2.917E-04	2.014E-04	3.73
	max	2.786	99.68	8.031E-05	3.052E-03	1.753E-03	5.16
Proportion of Range		7.41%	27.41%	93.87%	14.00%	5.44%	**0.45%**

Table 1-7 Sr-85 Transport Pathway Properties

Sr-85							
		a_r	F factor	k	k*F	k*F *time	Volume Ratio
All 1500	min	0.248	10.73	3.527E-06	1.038E-04	8.428E-05	0.22
	max	34.059	292.92	2.265E-04	5.148E-02	7.232E-02	2045.12
Top 10	min	0.272	15.93	1.437E-05	7.223E-04	4.158E-04	10.86
	max	2.511	220.59	1.312E-04	7.101E-03	7.417E-03	14.23
Proportion of Range		6.62%	72.52%	52.42%	12.42%	9.69%	**0.16%**

Table 1-8 Co-58 Transport Pathway Properties

Co-58							
		a_r	F factor	k	k*F	k*F *time	Volume Ratio
All 1500	min	0.248	10.73	3.266E-05	8.520E-04	5.123E-04	3.70
	max	34.059	292.92	9.419E-04	2.138E-01	2.897E-01	33188.69
Top 10	min	0.587	48.11	6.119E-05	1.015E-02	1.278E-02	458.60
	max	6.026	200.27	4.191E-04	6.023E-02	6.565E-02	930.64
Proportion of Range		16.09%	53.92%	39.37%	23.52%	18.28%	**1.42%**

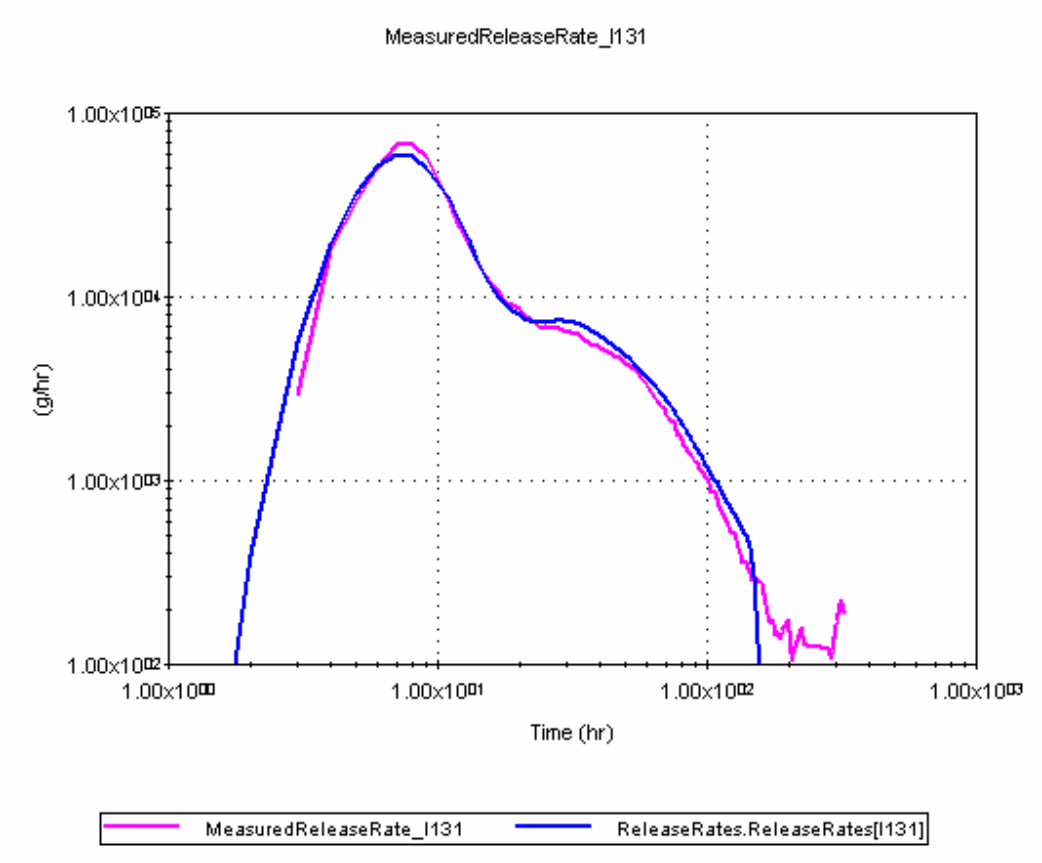

Figure 1-6 *Realization 624 – I-131 Breakthrough*

Based on the results shown in Table 1-3, the search ranges for the parameter groups was reduced as shown in Table 1-9.

The ten best simulations using the parameter ranges of Table 1-9 are shown in Table 1-10. Sensitivity studies on transport and immobile zone parameters for the best 100 realizations are shown in Figure 1-7 through Figure 1-14 for the conservative tracers. Using parameter groups constrained the simulations to provide a good match to conservative tracer breakthrough over a narrow range of parameter group values, neither diffusion distance nor immobile zone porosity are well constrained in these simulations. The range of porosity in the top 25 is biased near 0.15-0.2% for breccia porosity and 0.5 mm for breccia thickness Dmax. Figure 1-15 and Figure 1-16 illustrate the sensitivity of Sr-85 breakthrough to immobile zone parameter variability.

Table 1-9 Parameter Group Search Ranges

Parameter or Parameter Group	Original Range	Revised Range
Diffusion (Transfer Rate)	0.1 (constant)	0.01 to 1.0 (triangular)
Dispersion Length	0.05 m to 1.0 m	0.2 to 0.5 m
Area/Volume Ratio a_r	≈ 0.2 - 35	≈ 0.2 – 35
F- factor	≈ 10 – 500 hr/m	≈ 10 – 500 hr/m
k factor	≈ 2.e-6 – 1.e-4 m/hr$^{0.5}$	≈ 2.e-6 – 1.e-4 m/hr$^{0.5}$
k*F	≈ 4.5e-5 – 2e-2 hr$^{0.5}$	≈ 2.e-4 – 2.3e-2 hr$^{0.5}$
k*F*t	≈ 2.8e-5 – 3e-2 hr$^{1.5}$	≈ 4.5e-5 – 8e-2 hr$^{1.5}$
Volume Ratio V_R	0.11 to 317 hr$^{0.5}$	3.5 to 6.5 hr$^{0.5}$

Table 1-10 Results from Simulations – 10 best HTO

					Breccia / Infillings		Mylonite / Altered Wall Rock		RockMass	
Real (-)	Error Measure	Aperture (mm)	Travel Time (hr)	Dispersion (m)	Dmax (mm)	Porosity (-)	Dmax (mm)	Porosity (-)	Dmax (mm)	Porosity (-)
372	11.90%	0.017223	1.1992	0.2	2.7841	0.0120	0.3928	0.0100	25.272	0.002293
220	13.78%	0.061343	1.2072	0.2	2.9969	0.0423	3.5883	0.0146	28.353	0.004546
386	14.24%	0.077032	1.4347	0.2	2.4600	0.0509	18.0110	0.0136	61.577	0.004236
225	14.31%	0.044159	0.81627	0.5	3.8445	0.0390	19.1550	0.0055	64.103	0.003629
252	15.40%	0.027987	1.2138	0.2	1.9358	0.0281	14.9510	0.0060	71.345	0.002044
309	15.81%	0.023513	0.57681	0.5	2.2913	0.0493	16.8250	0.0077	20.117	0.003246
199	15.98%	0.086519	0.62345	0.5	2.3158	0.1739	15.5170	0.0098	71.077	0.004141
396	16.52%	0.055197	0.62606	0.5	3.6638	0.0662	16.3610	0.0136	64.104	0.002138
6	17.65%	0.068892	0.82531	0.5	3.1667	0.0712	19.2720	0.0059	40.532	0.004477
376	17.74%	0.035114	1.2359	0.2	3.5028	0.0177	3.1379	0.0132	41.868	0.004563
2	18.38%	0.082838	0.9986	0.5	1.1449	0.1864	16.4610	0.0052	82.643	0.0042
299	18.83%	0.077415	1.1643	0.2	1.9401	0.0794	3.8506	0.0118	62.918	0.0029
74	18.98%	0.03423	1.0906	0.2	0.7732	0.0997	16.0100	0.0061	72.595	0.004881
106	19.08%	0.063242	0.86335	0.5	2.1433	0.0918	12.7310	0.0107	32.894	0.001694
306	19.20%	0.035705	0.72015	0.5	0.3888	0.3788	6.6946	0.0075	35.862	0.004918
55	19.50%	0.061041	1.3734	0.2	0.2810	0.3995	7.5830	0.0142	34.615	0.003829
394	19.56%	0.058875	0.78661	0.5	3.8099	0.0530	15.8250	0.0152	25.671	0.001808
4	19.75%	0.044805	0.62563	0.5	2.6309	0.0796	9.4470	0.0165	35.09	0.001862
288	20.18%	0.055702	0.64256	0.5	2.7259	0.0967	19.1210	0.0129	86.738	0.002666
318	20.50%	0.050762	1.0349	0.2	3.1421	0.0361	18.2810	0.0106	67.131	0.002555
min	**n/a**	0.0172	0.5768	0.2	0.2810	0.0120	0.3928	0.0052	20.1170	0.0017
max	**n/a**	0.0865	1.4347	0.5	3.8445	0.3995	19.2720	0.0165	86.7380	0.0049

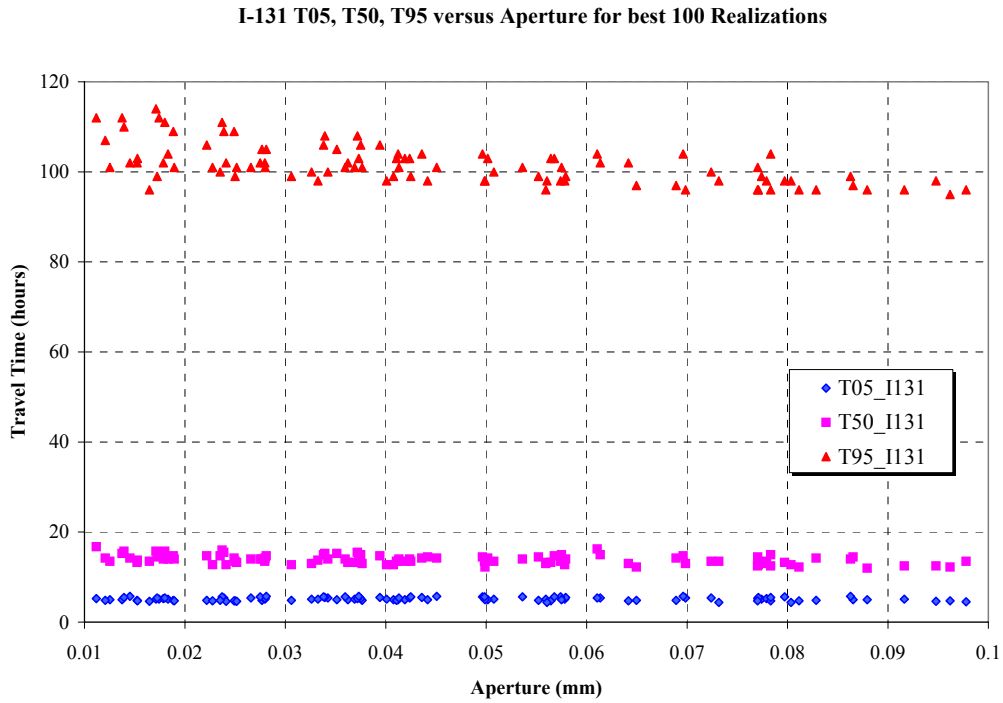

Figure 1-7 *I-131 T05, T50, T95 versus Aperture for best 100 Realizations*

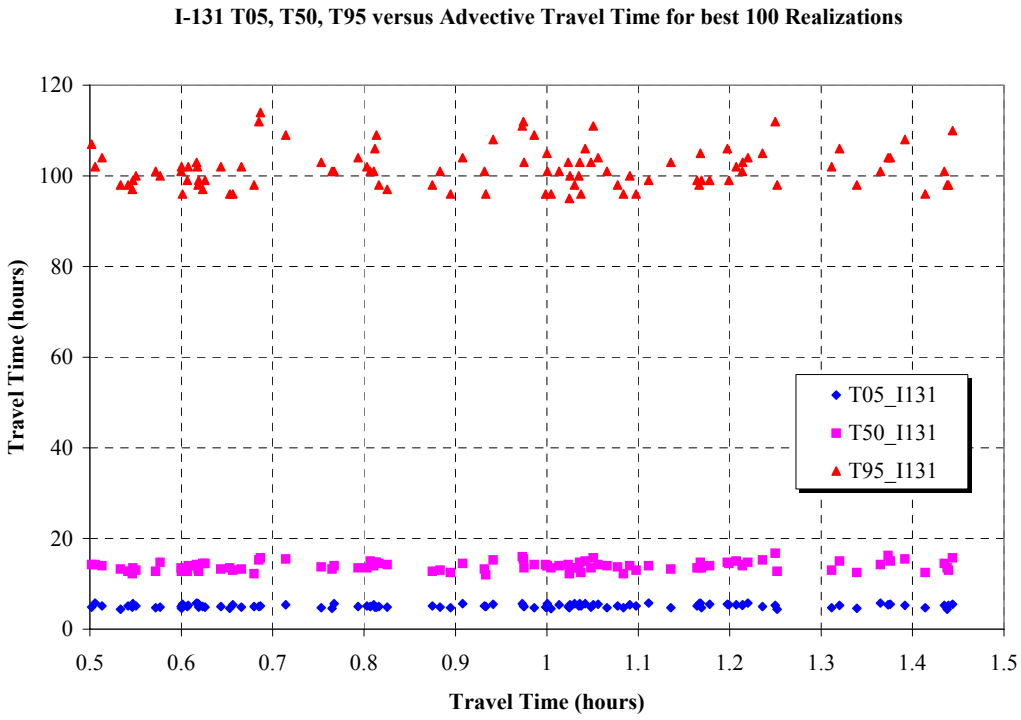

Figure 1-8 *I-131 T05, T50, T95 versus Advective Travel Time for best 100 Realization*

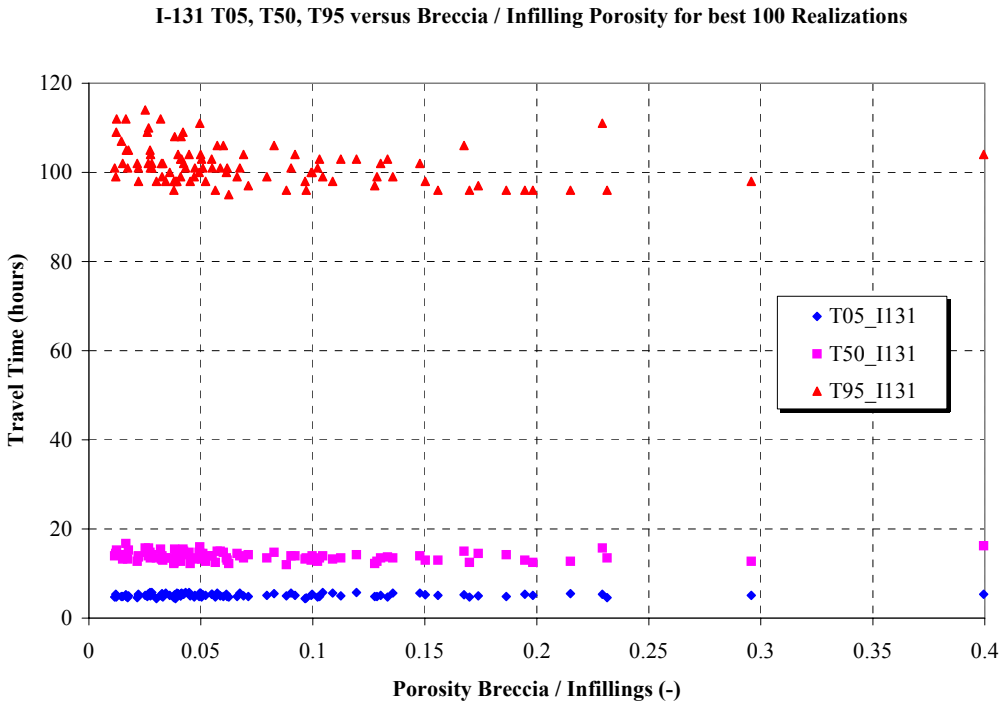

Figure 1-9 *I-131 T05, T50, T95 versus Breccia/Infilling Porosity for best 100 Realizations*

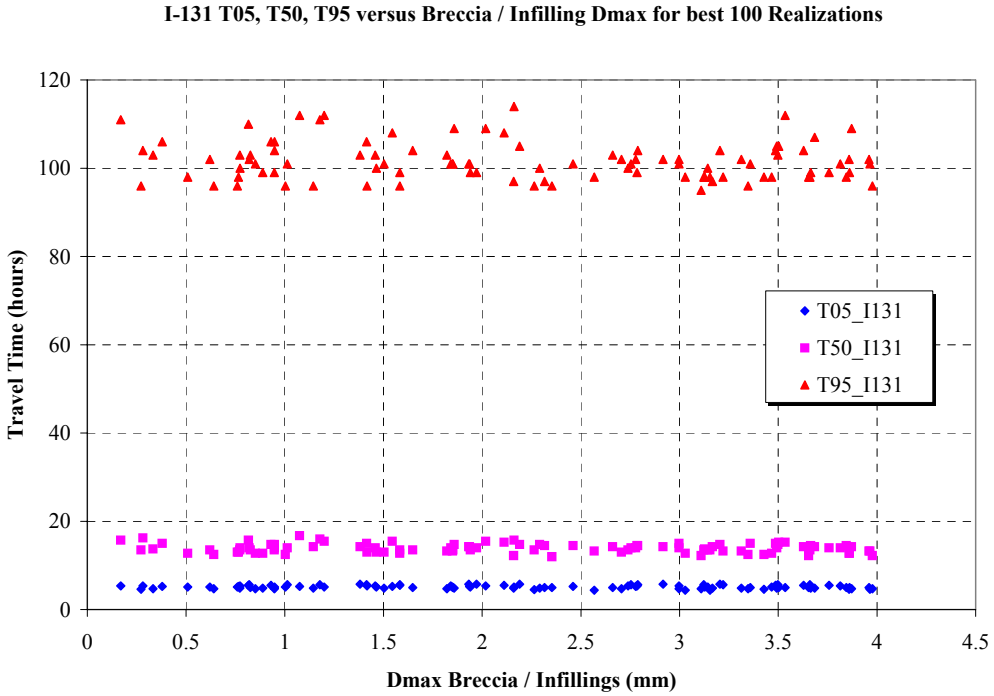

Figure 1-10 *I-131 T05, T50, T95 versus Breccia/Infilling Dmax for best 100 Realizations*

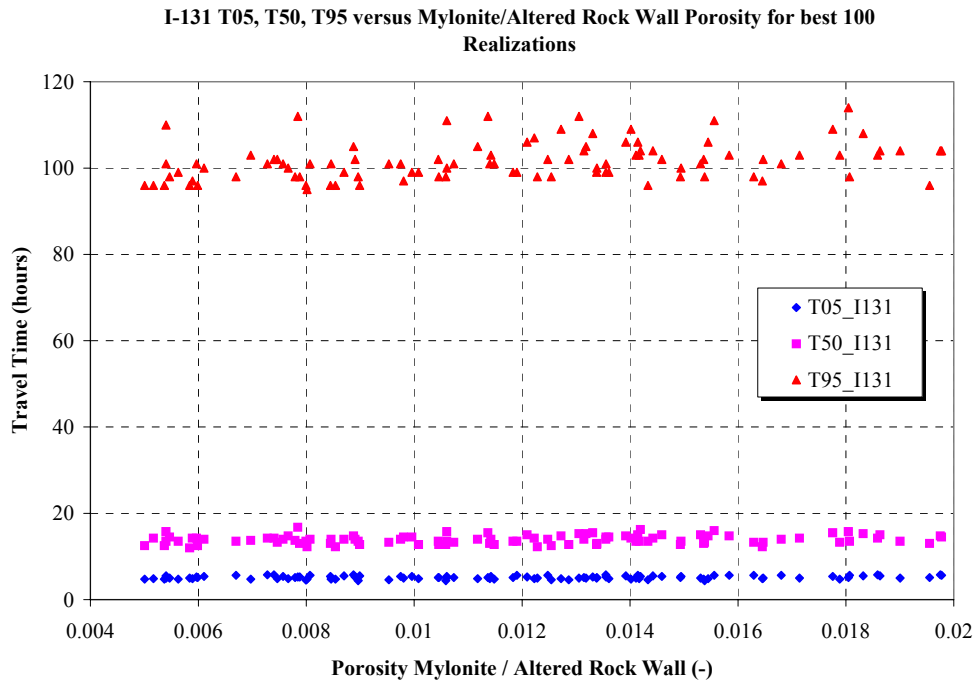

Figure 1-11 *I-131 T05, T50, T95 versus Mylonite/Altered Rock Wall Porosity for best 100 Realizations*

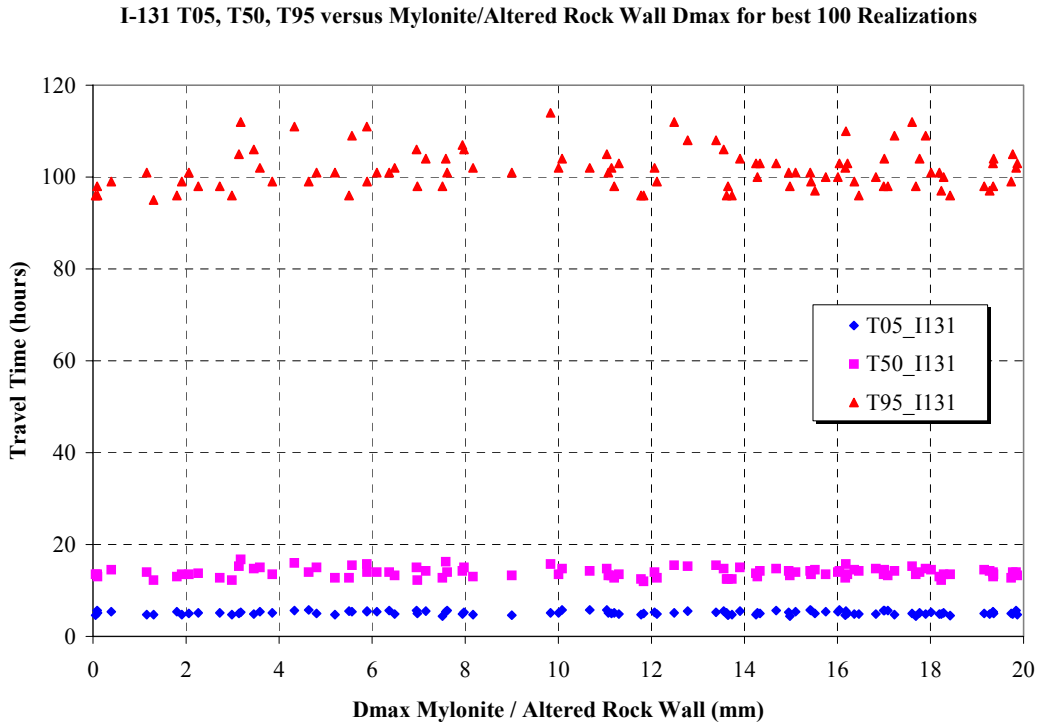

Figure 1-12 *I-131 T05, T50, T95 versus Mylonite/Altered Rock Wall Dmax for best 100 Realizations*

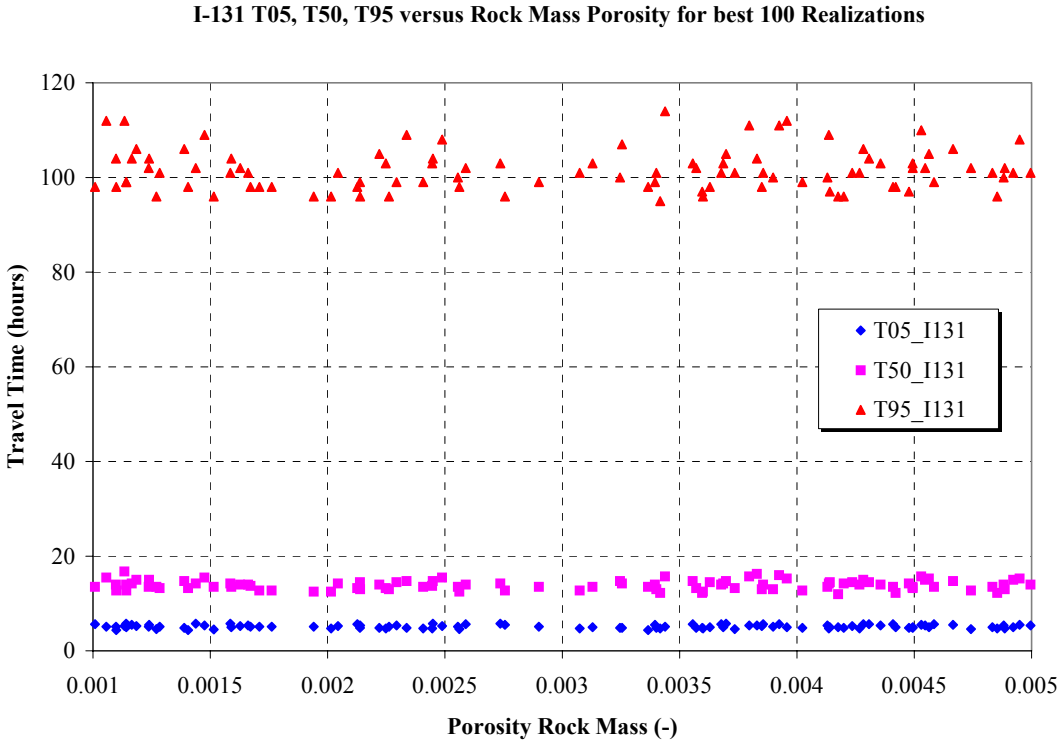

Figure 1-13 *I-131 T05, T50, T95 versus Rock Mass Porosity for best 100 Realizations*

Consequently, it can be concluded that the conservative tracer experiments of themselves cannot be used to constrain sorbing tracer response, and consequently radionuclide transport at PA time scales. Figure 1-17 through Figure 1-18 illustrate the three sets of transport parameters, which provide the best matches for the conservative tracers HTO and I-131, and how these parameters perform reasonably well for the weakly sorbing tracer Sr-85. Figure 1-19 through Figure 1-21 illustrate that these parameter sets are completely incapable of providing good constraints for the more strongly sorbing tracers Co-58, Tc-99, and Am-241.

1.2.3 Conditioning to Sorbing Tracers (6A-3)

The preceding analyses relied exclusively on conservative tracer transport results to constrain transport parameters. The next analysis constrained parameter groups and immobile zone parameters based on the error measure ε_T for the Sr-85 breakthrough curve. Future simulations will be carried out running 10,000 realizations, constrained to the total error measure ε_T for Sr-85, Co-58, and I-131. The three simulations conditioned to Sr-85 breakthrough, which provided the best match, were 385, 299, and 241. These breakthrough curves are illustrated in Figure 1-22 through Figure 1-27. Of these three realizations, only 385 really provided a good match to Sr-85 breakthrough. Realizations 299 and 241 illustrate how the variation in immobile zone parameters possible within the match to Sr-85 breakthrough still produce a good match for the conservative tracers, but leave a high degree of variability in the breakthrough for the more strongly sorbing tracers.

1.3 Discussion

The simulations carried out for Task 6A clearly demonstrated the degree of residual uncertainty in immobile zone parameters following conditioning to conservative and sorbing tracer experiments. Conservative tracer experiments provide a poor constraint on the micro-scale immobile zone parameters, which determine sorbing tracer breakthrough. Conditioning to sorbing tracer experiments provides a much better constraint. However, uncertainty in immobile zone parameters, which are unimportant for weakly sorbing tracers, can propagate to larger uncertainties in more strongly sorbing tracer breakthrough.

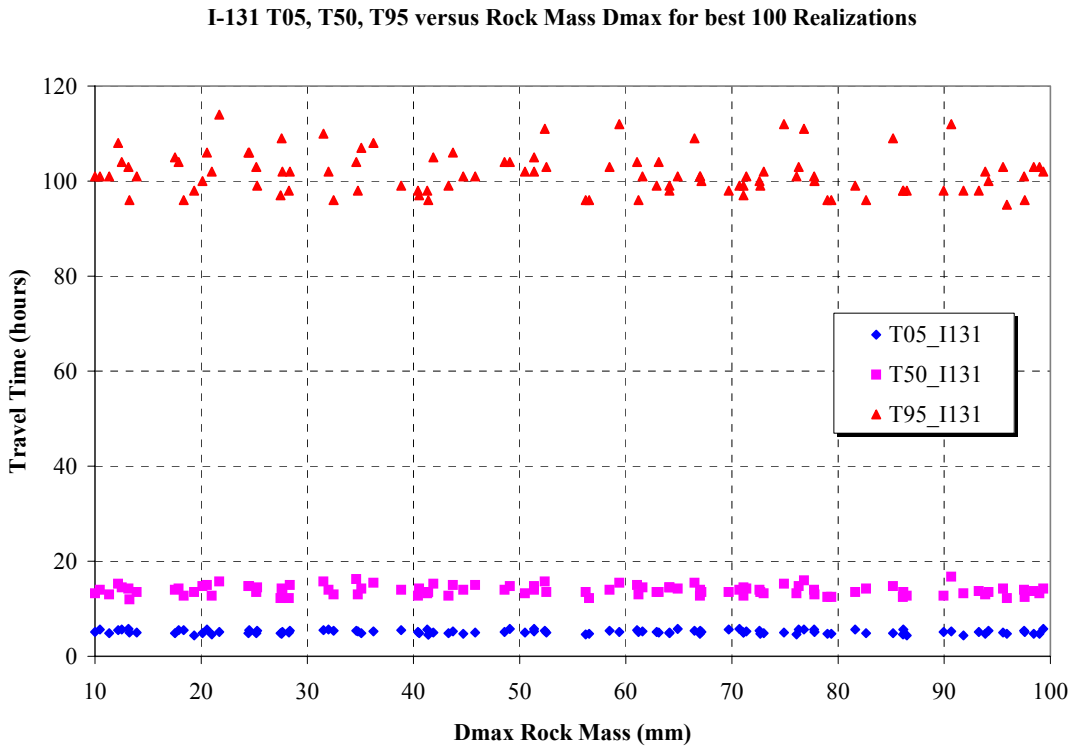

Figure 1-14 *I-131 T05, T50, T95 versus Rock Mass Dmax for best 100 Realizations*

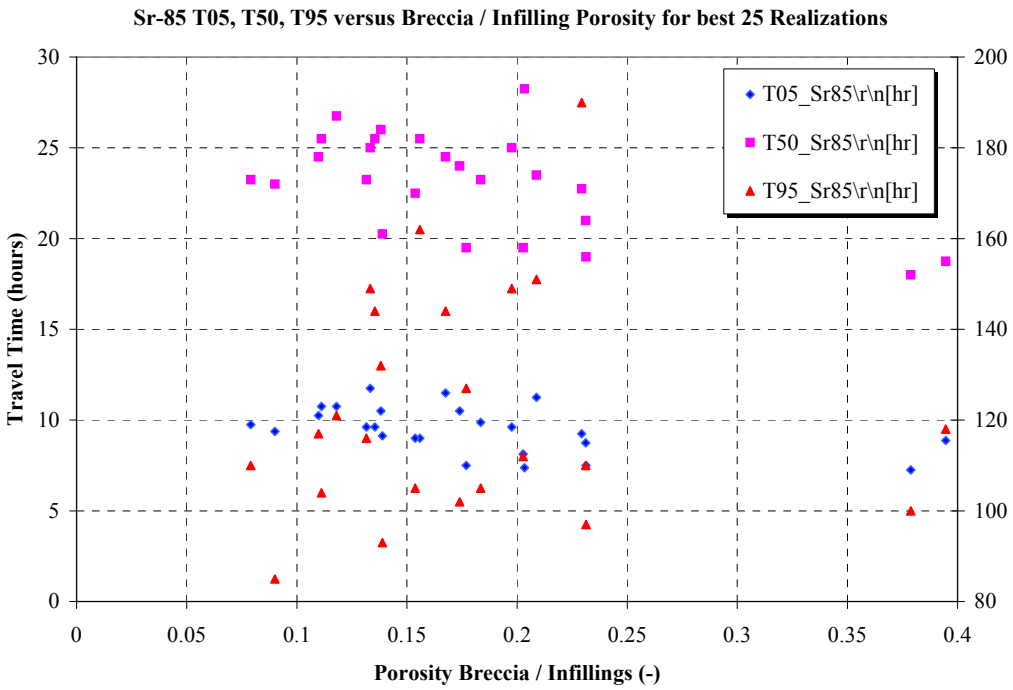

Figure 1-15 *Sr-85 T05, T50, T95 versus Breccia/Infilling Porosity for best 25 Realizations*

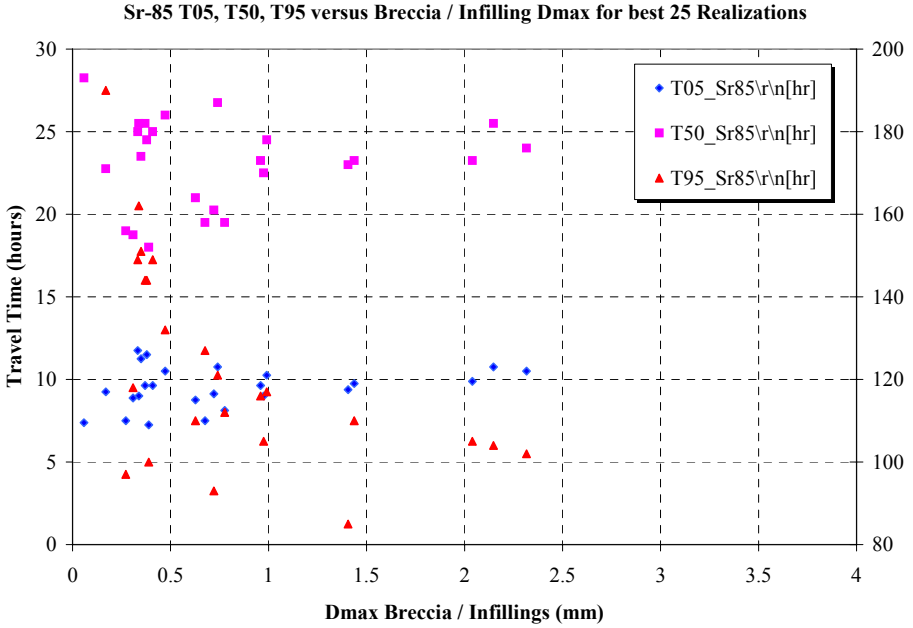

Figure 1-16 *Sr-85 T05, T50, T95 versus Breccia/Infilling Dmax for best 25 Realizations*

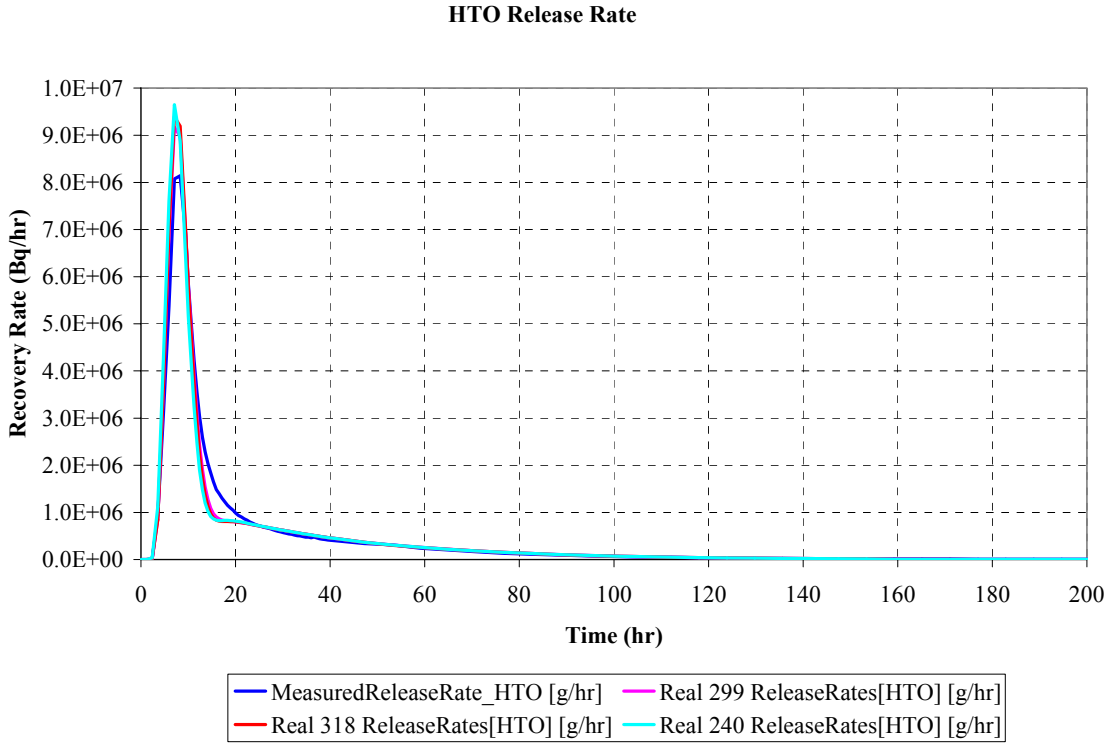

Figure 1-17 *HTO Breakthrough Realizations 299, 318 & 240*

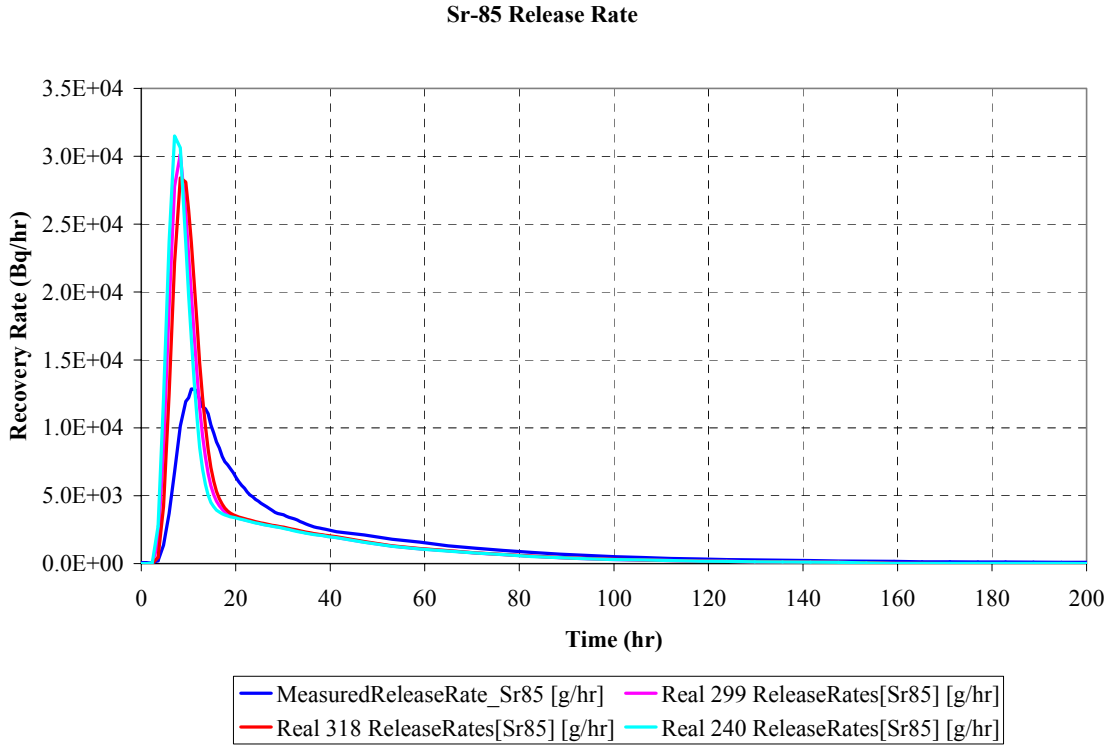

Figure 1-18 *Sr-85 Breakthrough Realizations 299, 318, & 240*

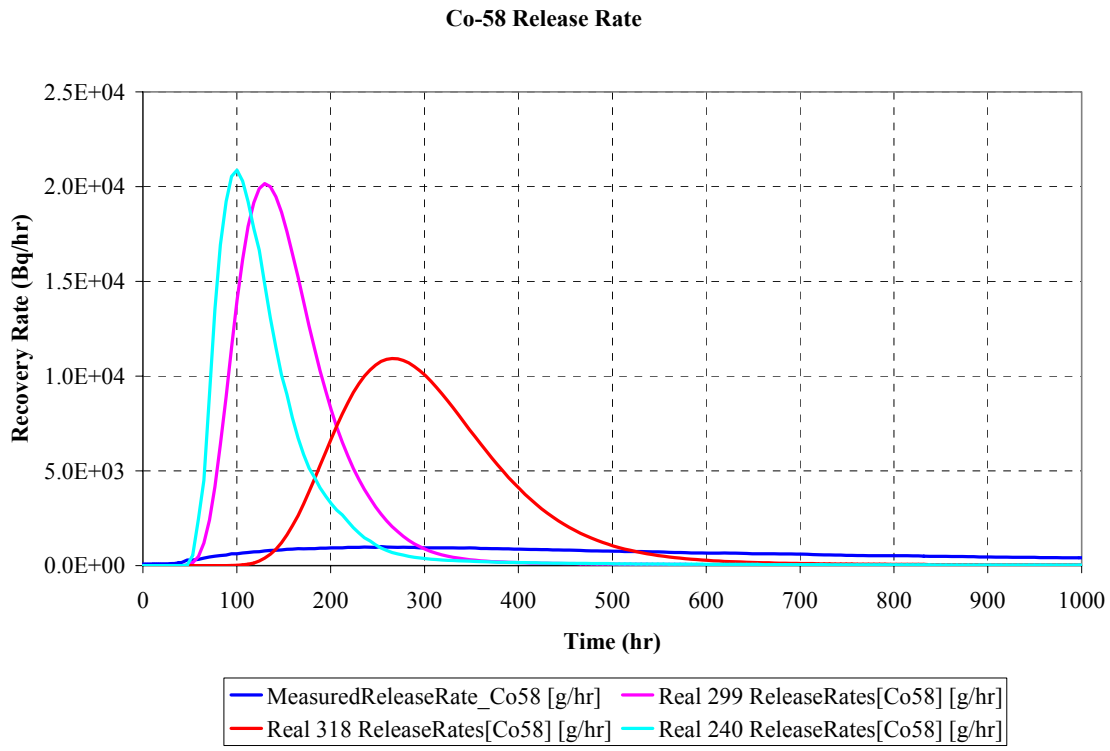

Figure 1-19 *Co-58 Breakthrough Realizations 299, 318, & 240*

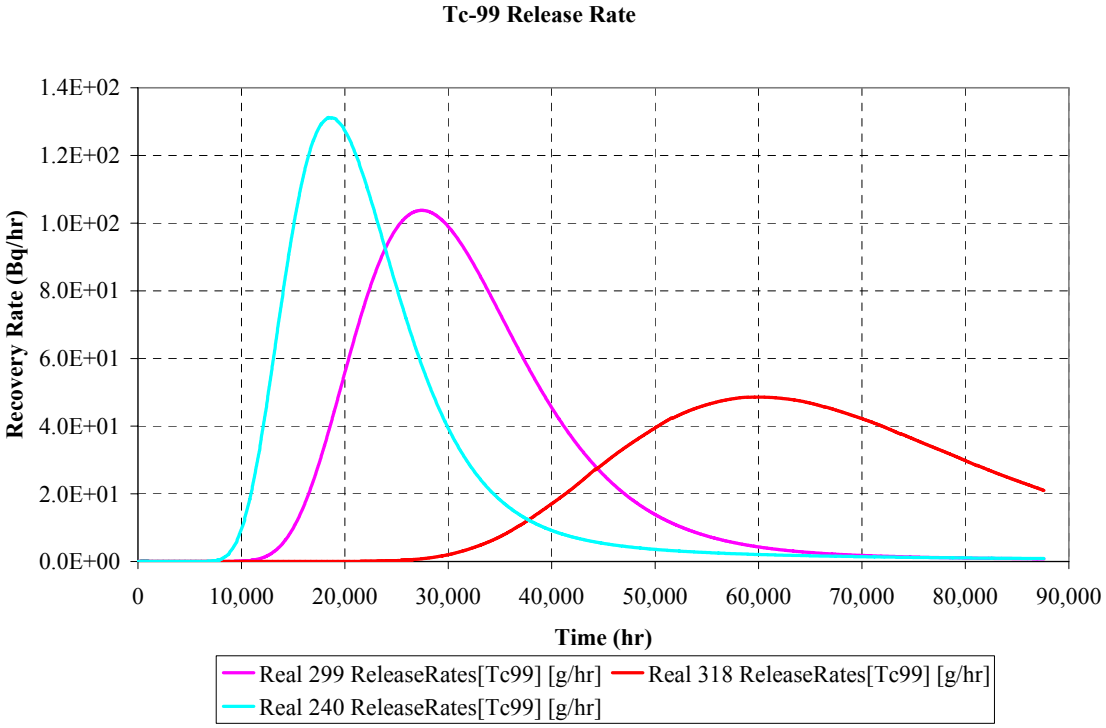

Figure 1-20 *Tc-99 Breakthrough Realizations 299, 318, & 240*

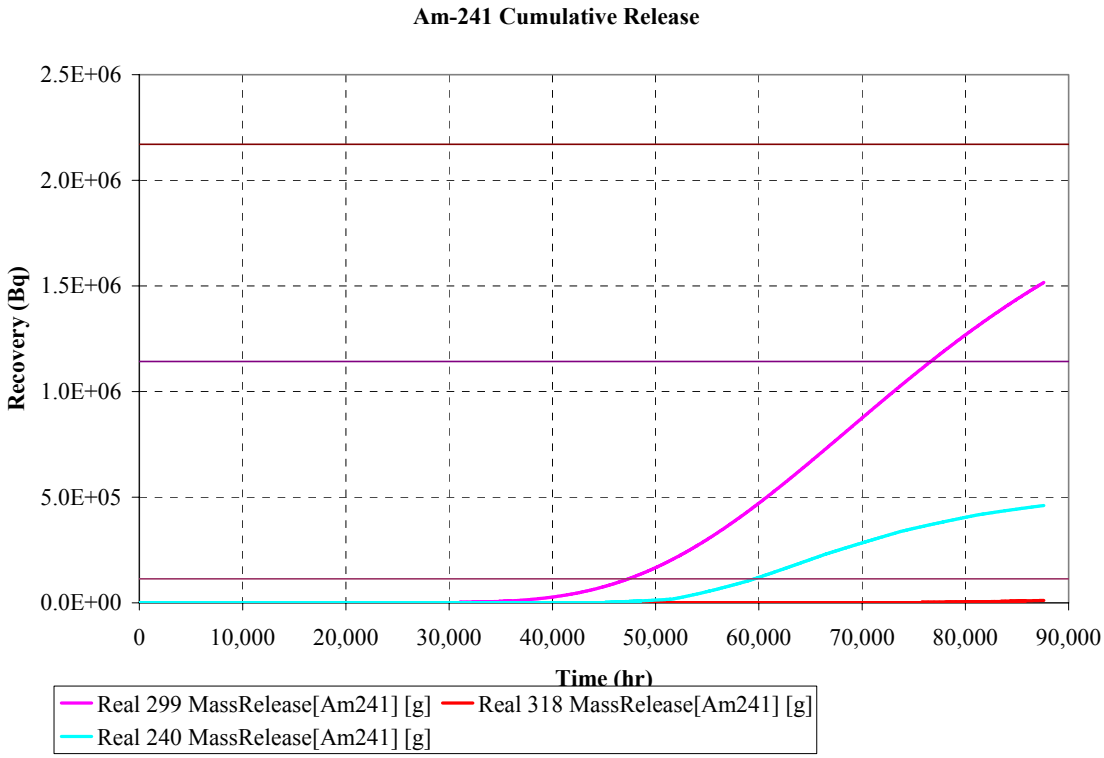

Figure 1-21 *Am-241 Breakthrough realizations 299, 318, & 240*

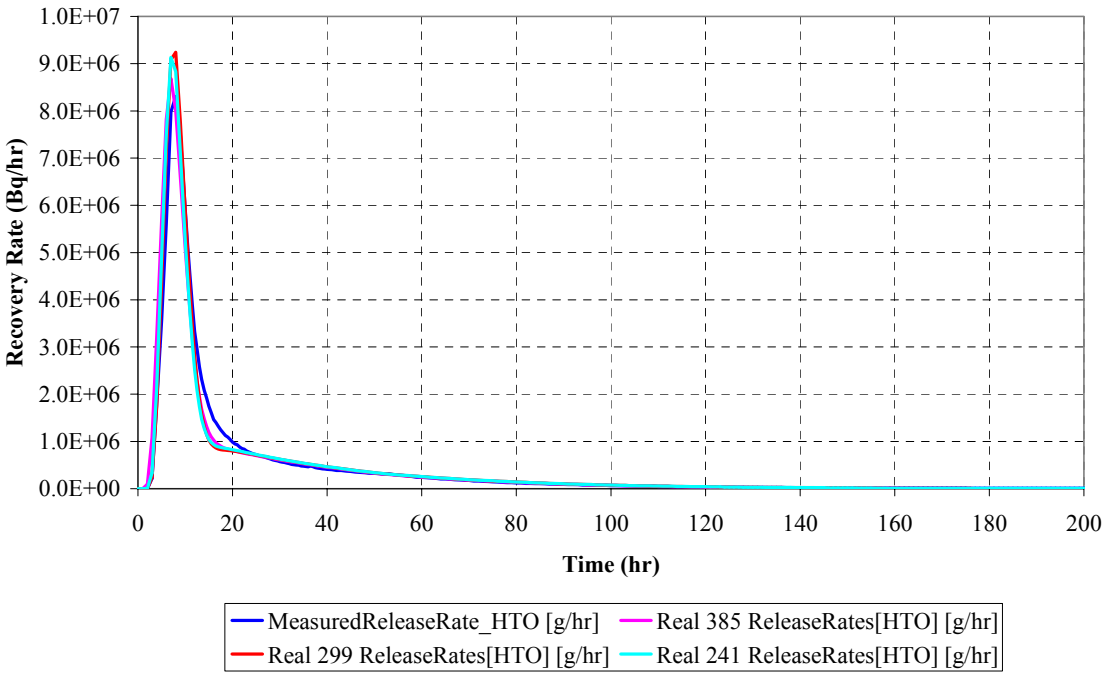

Figure 1-22 *HTO Breakthrough Realizations 385, 299, & 241*

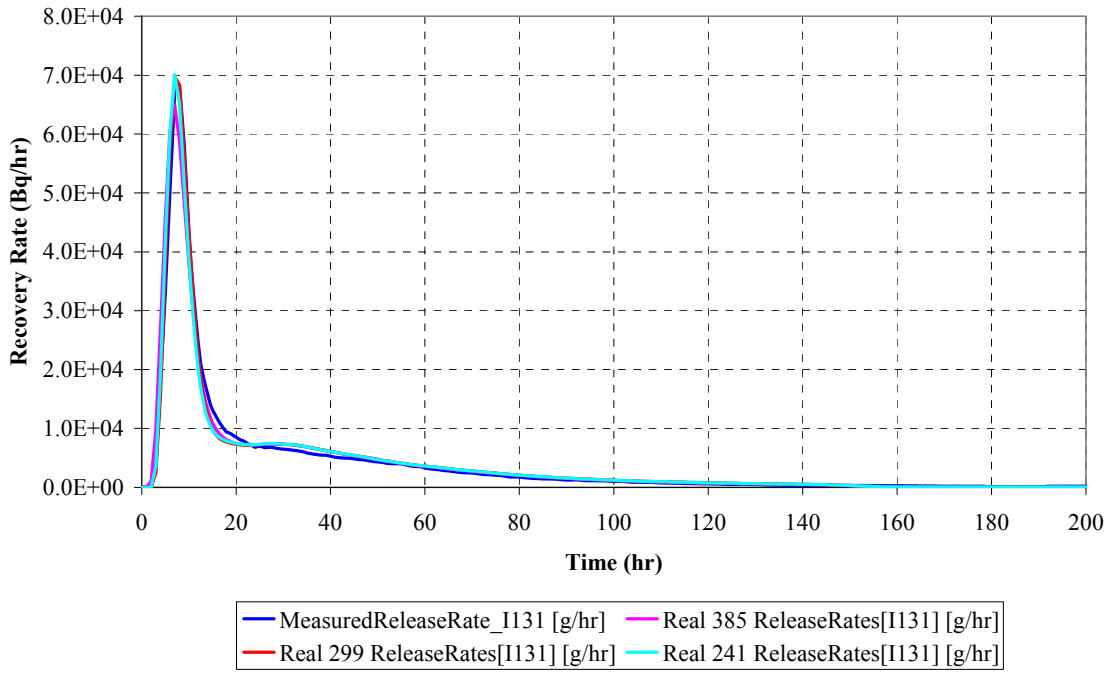

Figure 1-23 *I-131 Breakthrough Realizations 385, 299, & 241*

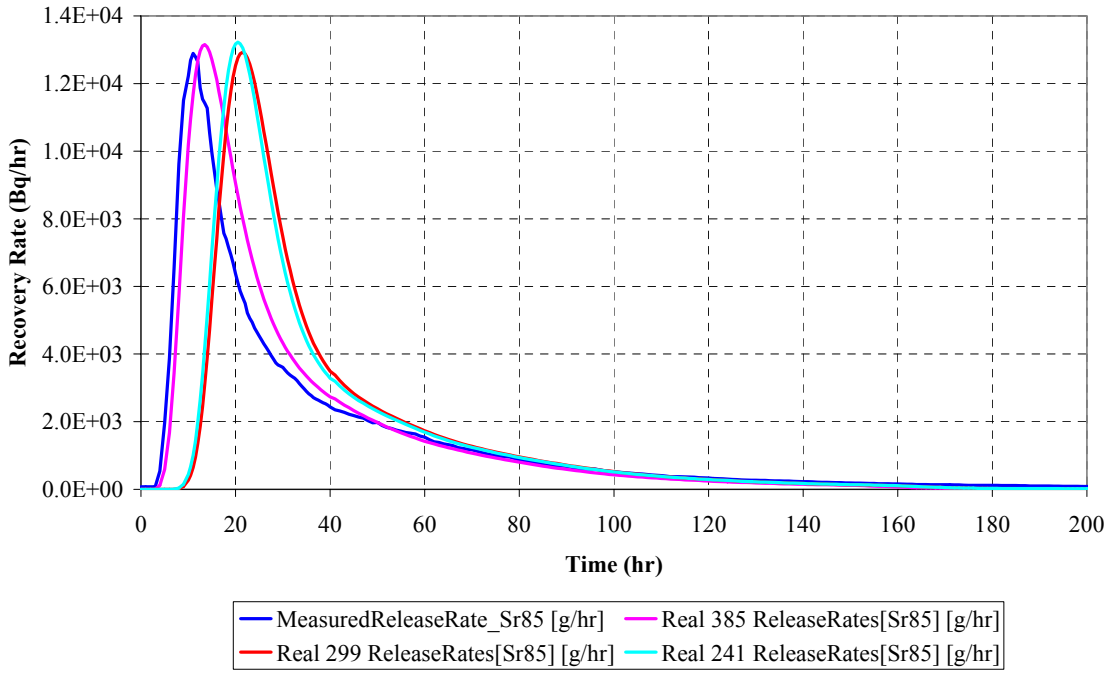

Figure 1-24 *Sr-85 Breakthrough Realizations 385, 299, & 241*

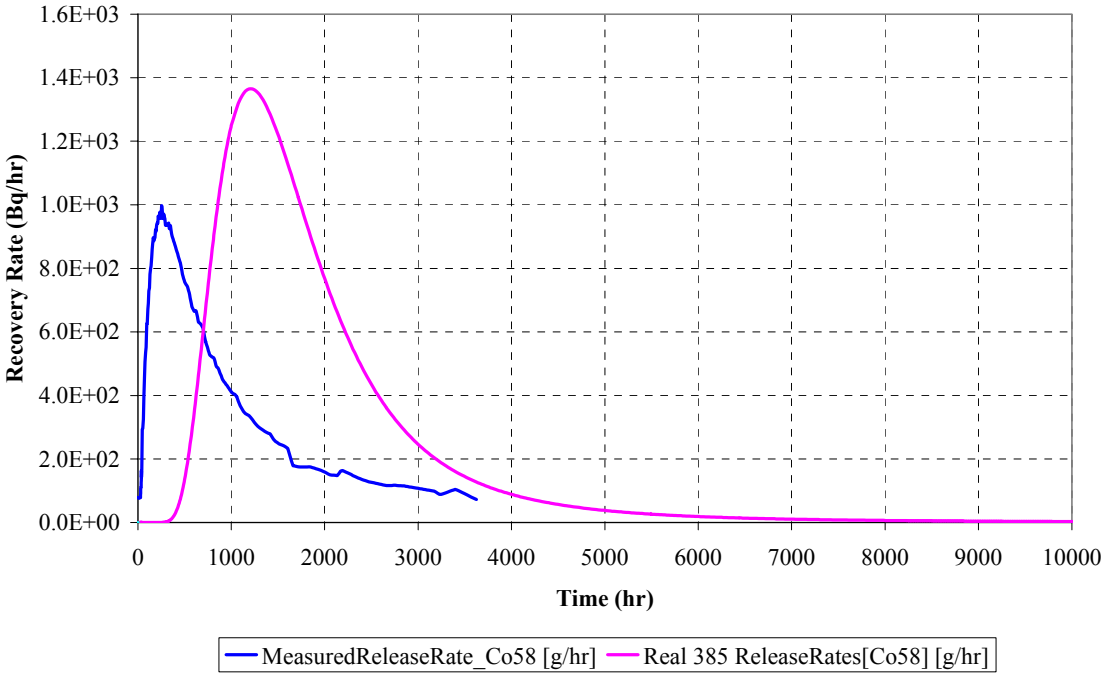

Figure 1-25 *Co-58 Breakthrough Realization 385*

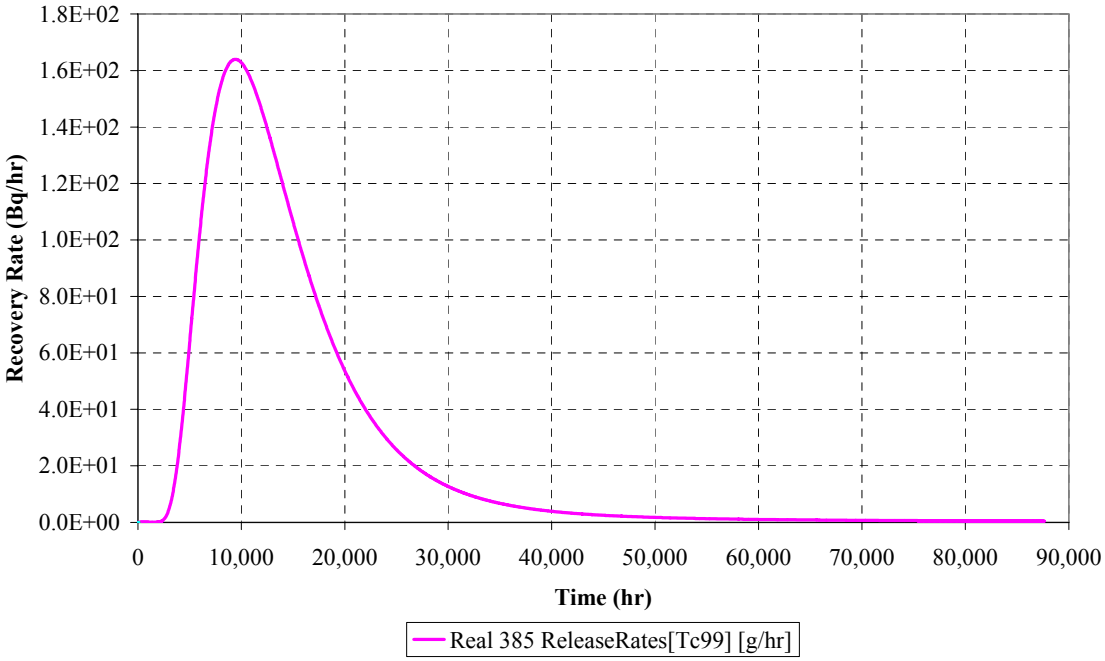

Figure 1-26 *Tc-99 Breakthrough Realization 385*

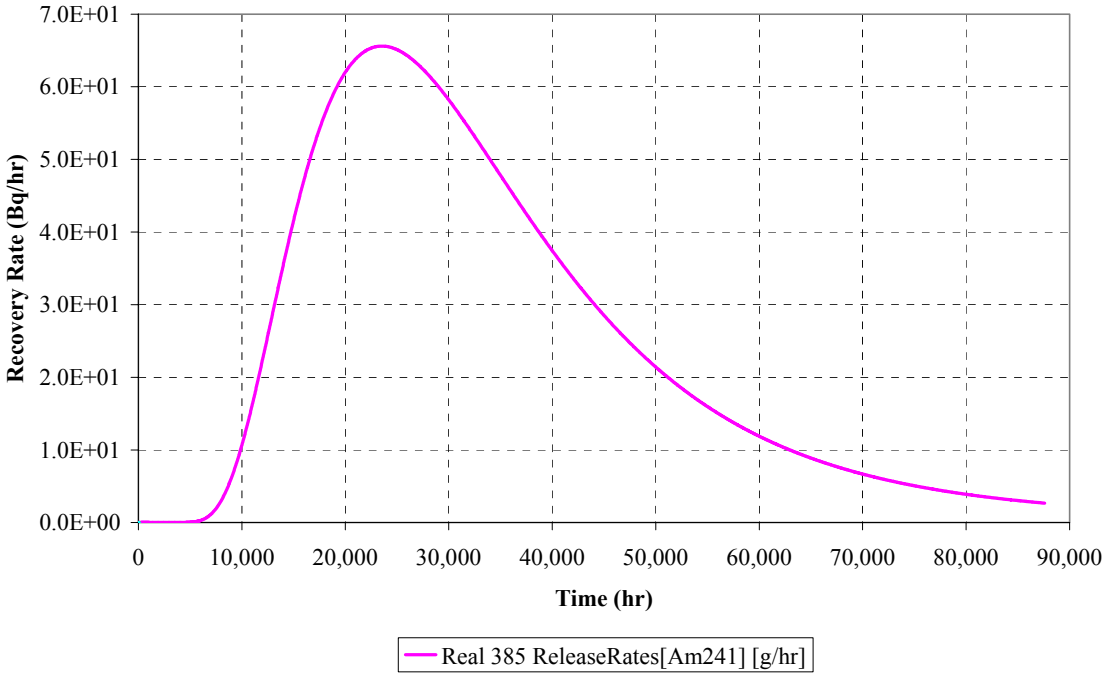

Figure 1-27 *Am-241 Breakthrough Realization 385*

2 Task 6B: Extrapolation of SC Experimental Results to PA Time Scales with GoldSim PA Code

2.1 Strategy

Task 6B was run using the realizations 385, 299, and 241 which were conditioned to Sr-85 tracer breakthrough at the experimental time scales. In Task 6B, the experimental determination of transport and immobile zone parameters was propagated to PA time scale model. However, at the PA time scale, the immobile zone parameters for the rock mass dominate. The rock mass immobile zone parameters are completely unimportant at experimental time scales.

2.2 Simulations

Figure 2-1 through Figure 2-6 illustrate the PA time scale breakthrough using the transport parameters of realizations 385, 299, and 241, but reducing the advective velocity by a factor of 1000. The breakthrough times for conservative tracers HTO and I-131, and weakly sorbing tracer Sr-85 and Co-85 are well constrained, indicating that the variability in immobile zone parameters remaining following experimental tracer tests is not important at PA time scales for conservative and weakly sorbing tracers. For the strongly sorbing tracers Tc-99 and Am-241 the time for 50% breakthrough varies on the order of 50,000 years. However, these strongly sorbing tracers are generally considered much less important for PA calculations, and the residual uncertainty, once quantified, may be within tolerable limits.

3.3 Discussion

The Task 6B simulations illustrate the power of the use of stochastic simulation and sensitivity studies to quantify the residual uncertainty at PA time scales based on models conditioned to in situ experiments. Further refinement of the conditioning to sorbing tracers at the experimental time scales would not improve the conditioning for the rock mass immobile zone which dominates at the PA time scale.

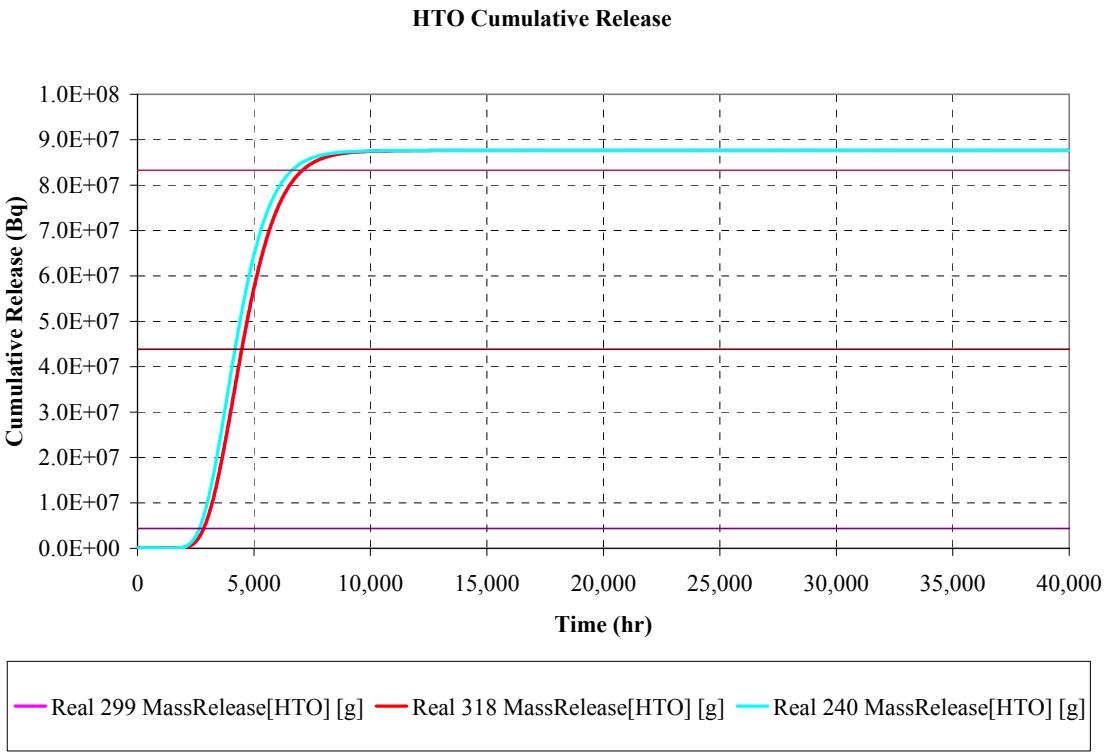

Figure 2-1 *HTO Breakthrough at PA time Scales Real 299, 318, & 240*

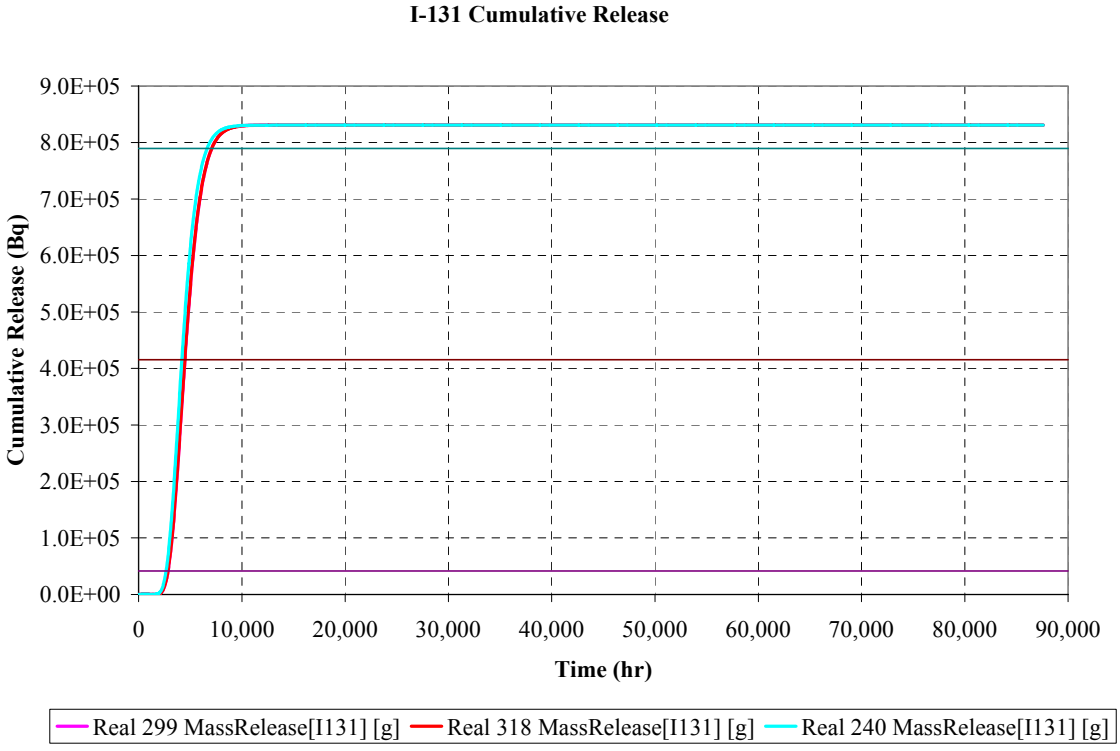

Figure 2-2 *I-131 Breakthrough at PA Time Scales Real 299, 318, &240*

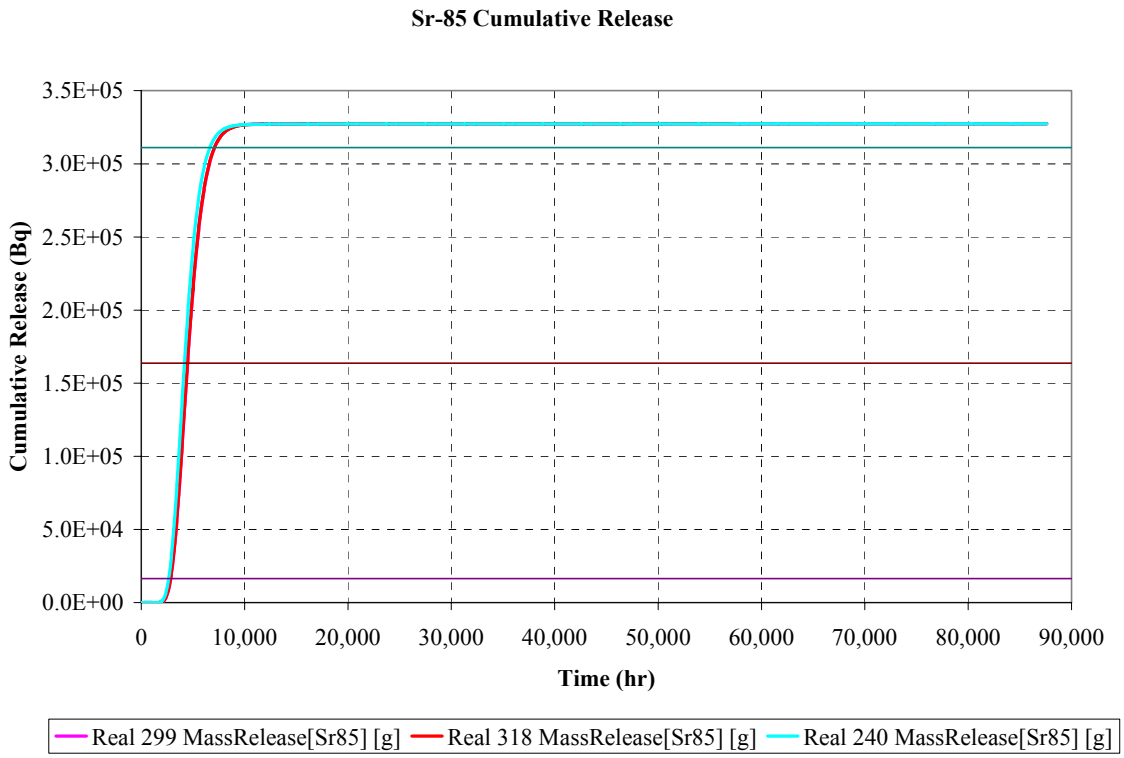

Figure 2-3 *Sr-85 Breakthrough at PA Time Scales Real 299, 318, & 240*

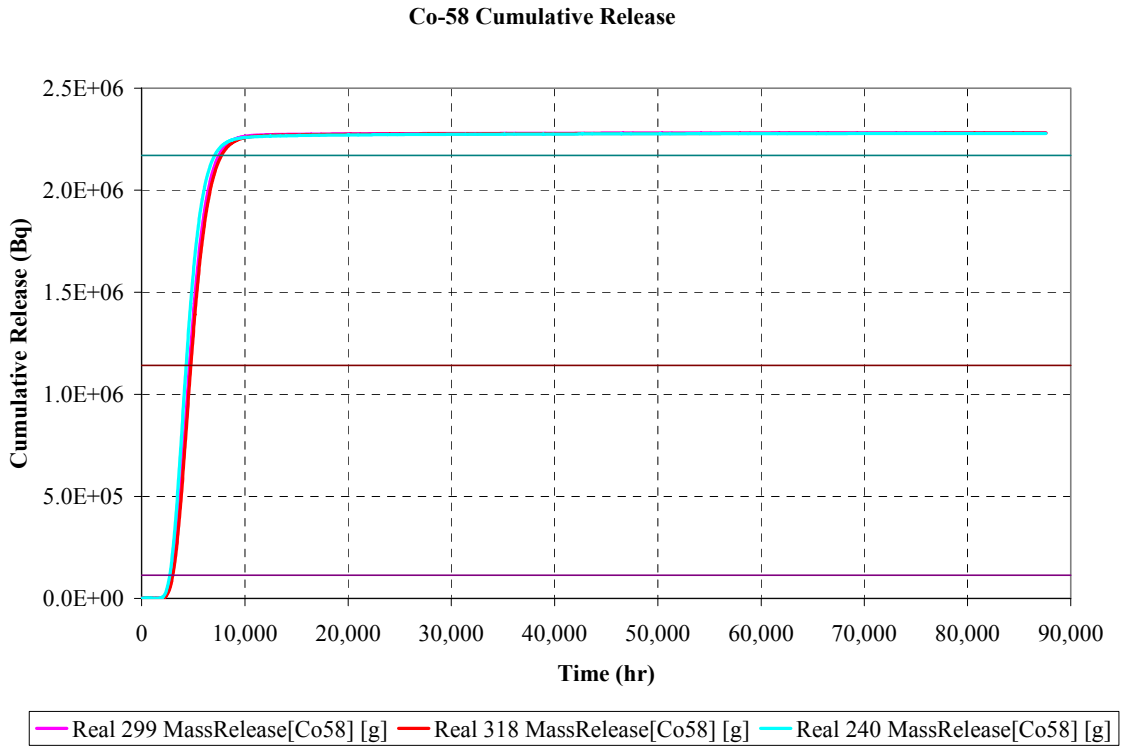

Figure 2-4 *Co-58 Breakthrough at PA Time Scales Real 299, 318, & 240*

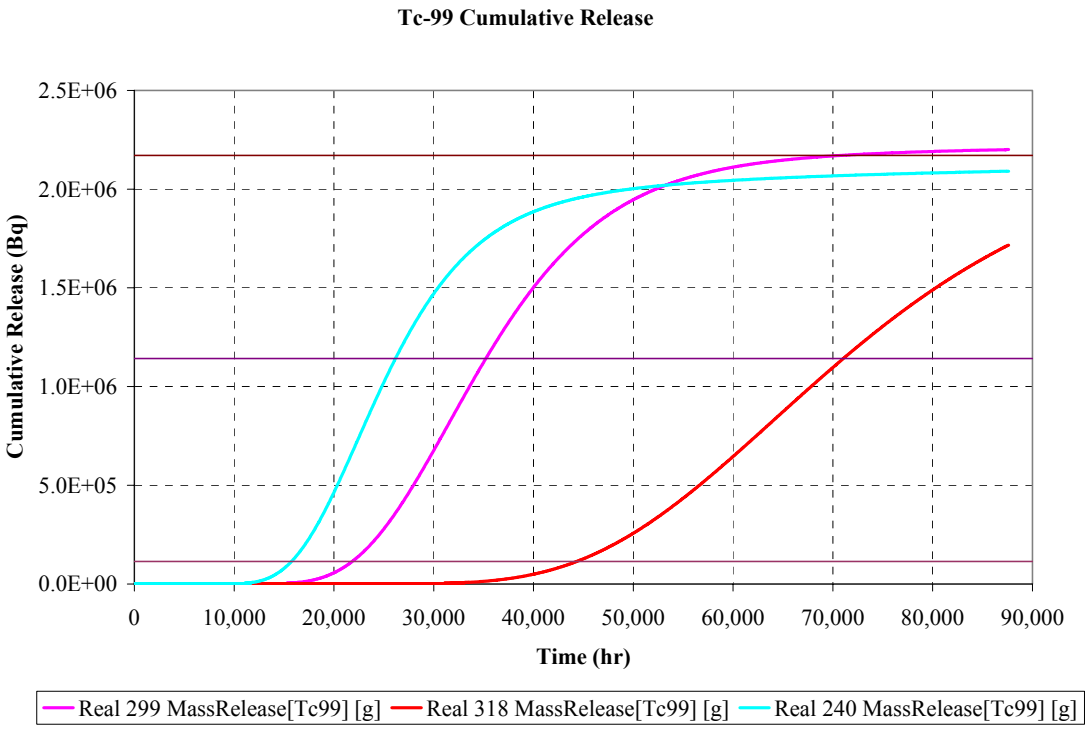

Figure 2-5 *Tc-99 Breakthrough at PA Time Scales Real 299, 318, & 240*

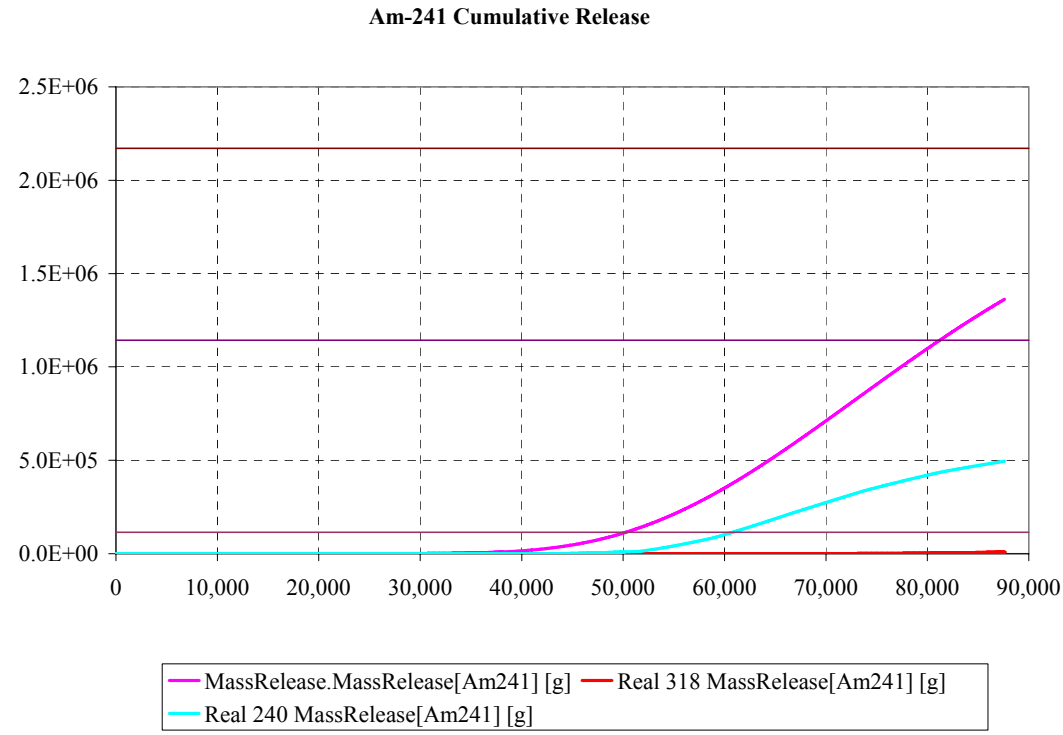

Figure 2-6 *Am-241 Breakthrough at PA Time Scales Real 299, 318, & 240*

3 Task 6B2: Extrapolation of Single Heterogeneous Fracture Transport from SC to PA Time Scales with MAFIC/LTG SC Code

3.1 Strategy

Tasks 6A and 6B were run using a radially converging flow boundary condition between two boreholes. This type of boundary condition is realistic for site characterization, but is somewhat questionable for PA, where transport is generally driven by natural rather than forced gradients. Radially converging flow is essentially 1-D, and is therefore ideally suited for the pipe transport representation, at least over small distance scales. At PA time and distance scales, however, more complex flow regimes may need to be considered.

Two sets of simulations were carried out for Task 6B2. The initial simulations, described in Section 4.2 below used the same 1/1000 advective velocity used in Task 6B to approximate PA conditions, but set the downstream boundary condition as a line sink, representing the effect of an intersecting fracture in a fracture network. In the TRUE-1 rock block, this fracture might be NE-2, for example.

In the second set of simulations, described in Section 4.3 below, the boundary conditions are modified to correspond to the task specification established at the 15th Task Force meeting in Goslar, Germany. These boundary conditions are designed to produce flow and transport over a larger area of Feature A. The input boundary is no longer a point source and the tracers are assumed to be collected in a fracture intersecting Feature A (Figure 3-1).

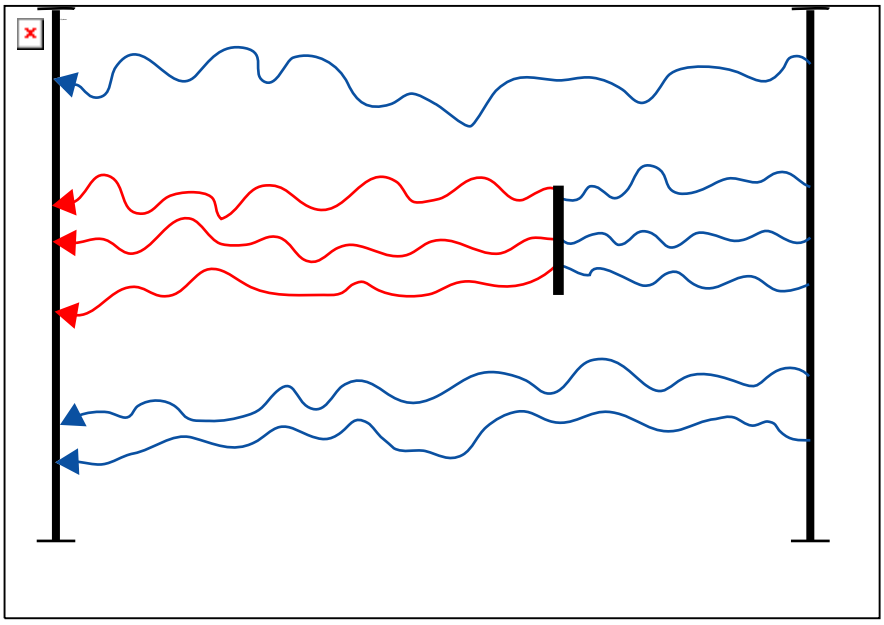

Figure 3-1 *Principle geometry for Task 6B2 seen in the plane of Feature A (Elert and Selroos, 2001)*

The JNC/Golder strategy for Task 6B2 focuses on how transport is influenced by different hypotheses regarding the in plane heterogeneity of "Feature A". Task 6B2 simulations are carried out using a discrete fracture stochastic continuum model, FracMan/EdMesh to generate 2D heterogeneous realizations of feature A, and MAFIC/LTG to solve solute transport in 2D with multiple immobile zones.

The microstructural conceptual model used for transport in this study (Figure 2-1) is the same as that used for Tasks 6A and 6B (Sections 2 and 3 above) with the following exceptions

- MAFIC/LTG solves diffusion directly rather than "advective exchange" as in the GoldSim model.
- MAFIC/LTG solves flow and transfer over the entire fracture surface, subject to assumed boundary conditions, rather than restricting flow to a pipe channel of prescribed width
- MAFIC/LTG provides for variation in the advective flow properties (aperture and transmissivity) and immobile zone properties (thickness, porosity, tortuosity) over the fracture surface.

Advection within the fracture plane is controlled by fracture transmissivity, which determines the advective flux (m^2/s).

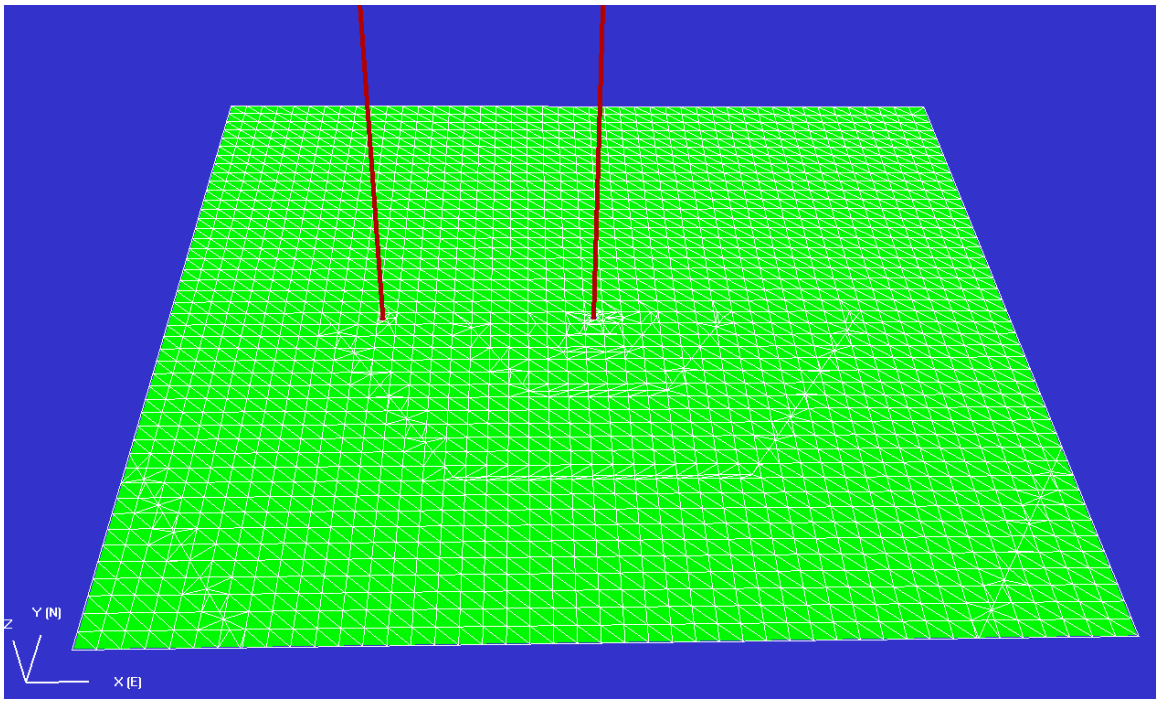

Figure 3-2 *Single Fracture Representation of Feature A*

The MAFIC/LTG transport conceptual model provides for five immobile zones:

- breccia/gouge inside the fracture plane
- surface sorption to fracture plane coatings
- mylonite/cataclasite altered wall rock
- intact rock mass accessible through the altered wall rock (in series)

Rather than the pipe network with a single branch, as shown in Figure 1-3, the Task 6B2 model represents Feature A as a planar feature (Figure 3-2).

3.2 Dipole flow fields

3.2.1 Assumptions

The initial Task 6B2 simulations were carried out using boundary conditions based on those used in Task 6A and 6B. Two boundary conditions implemented were run: RC (radially converging) and BG (background flow). The RC boundary conditions used the same injection and pumping well boundary conditions as in Task 6B, and applied a constant head of 0 at each of the four edges of the fractures to provide a 2D flow field. The BG boundary condition assumed injection from a borehole as in Task 6B, with collection at the down-gradient edge. A gradient of 8e-4 (0.016m over 20m was applied from the up-gradient to down-gradient edges of the fracture to provide travel times comparable to the Task 6B boundary conditions. No-flow was assumed for the fracture edges parallel to the flow direction. These two boundary conditions were used to provide a basis for selecting to boundary conditions to be used in the Task 6B2 specification (Section 4.3).

Three tracer injection boundary conditions were evaluated in these simulations. The first is the Task 6B injection time history. The second and third are simple Dirac delta and continuous injections. These two were provided to study the extremes of possible injection time histories for future simulations.

Three alternative transmissivity fields were implemented on Feature A to make it possible to evaluate the effect of this micro-scale variability at PA time scales: homogeneous transmissivity, geostatistical variability (Figure 3-3) and non-stationary variability (Figure 3-4). Parameters for the stochastic fields are as follows:

- Homogeneous Field: Constant Transmissivity 4.17e-7 m^2/s
- Geostatistical Field: Mean 4.e-7 m^2/s, Std Dev 1.e-6 m^2/s. Correlation Length = 0 m. (Exponential variogram)
- Non-stationary field: Peak/Trough density 5 m^{-3} (3-D), Std. Dev. 2.e-4 m^2/s, Peaks Mean 8.e-4, Std. Dev. 5.e-6 m^2/s, Troughs Mean 5.e-9, Std. Dev. 1.e-8 m^2/s (See Dershowitz et al., 2000)

For each of these fields, transport aperture e_t is correlated to transmissivity as $e_t = 0.025 * T^{0.5}$

The BG flow field for Task 6B2 is defined by injecting tracer at the same rate and boundary condition as in Task 6B, but applying a background gradient of 0.25% instead of the pumping rate of 6.67 x 10^{-8} m^3/s applied for Task 6B. This background gradient is generally consistent with the background gradients assumed in PA for deep repositories. The head field resulting from this boundary condition (Figure 3-5) can be compared directly to the head field resulting from the radially converging flow boundary condition which was used in the STT-1b (Winberg, 2000) experiment (Figure 3-6). Tracer transport parameters for the Task 6B2 simulations are shown in Table 3-1. The tracer source for Task 6B2 uses a step pulse function with the same injection rate (1.6 x 10^{-10} m^3/s) used in Task 6B.

3.2.2 Simulations

Figure 3-7 and Figure 3-8 present a direct comparison of simulation results for the radially converging (RC) Task 6B using the STT-1b borehole sink boundary condition and the background gradient (BG) Task 6B2 boundary conditions and the non-stationary heterogeneity fracture transmissivity field. Both transport pathways produced breakthrough with a similar peak, but the BG simulation shows more diffusion as indicated by the larger diffusive tail.

Figure 3-9 illustrates the pattern of breakthrough to the down-gradient side of "Feature A" in the Task 6B2 simulations. The highest concentrations correspond to the location of the injection well. At 1000 years, the location directly down gradient from the injection location has a much higher concentration, and the concentration falls off rapidly with lateral distance. However, as time progresses, the plume spreads, and the differences across the plume decrease significantly.

Figure 3-10 through Figure 3-21 present the breakthrough, cumulative breakthrough, and plume pattern for the conservative tracer I-131, and the sorbing tracers Sr-85, Co-58, Tc-99, and Am-241. These simulations were carried out using the Task 6B2 BG flow boundary conditions. For comparison, results are also provided for a radially converging (RC) boundary condition. As expected, more strongly sorbing tracers have a greater difference between the RC and BG flow patterns with greater reactive area available for exchange with immobile zones and sorption in immobile zones.

Table 3-1 Transport Properties for 6B and 6B2

Initial Example uses the properties from GoldSim Rev5, Realization 385

Property	Units	Parameter Value
Aperture	mm	$0.025\ T^{0.5}$
Dispersion Length	m	0.5
Breccia Porosity	-	0.2314
Breccia Dmax	mm	0.272
Mylonite Porosity	-	0.014
Mylonite Dmax	mm	0.054
Rock Mass Porosity	-	0.00127
Rock Mass Dmax	mm	56.2
Tortuosity	-	0.0125

Tracer	Property	Units	Value
HTO	Kd	m^3/kg	0.0
	D_0	m^3/s	2.4×10^{-9}
I-131	Kd	m^3/kg	0.0
	D_0	m^3/s	1.66×10^{-9}
Sr-85	Kd	m^3/kg	1.3×10^{-4}
	D_0	m^3/s	7.9×10^{-10}

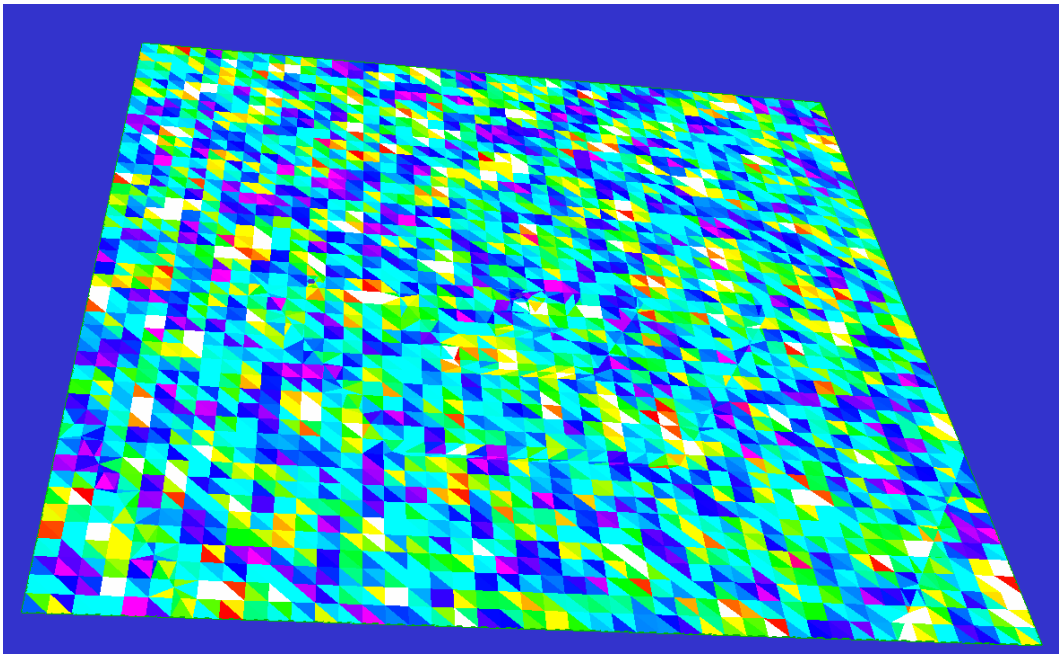

Figure 3-3 *Geostatistical Transmissivity Distribution*

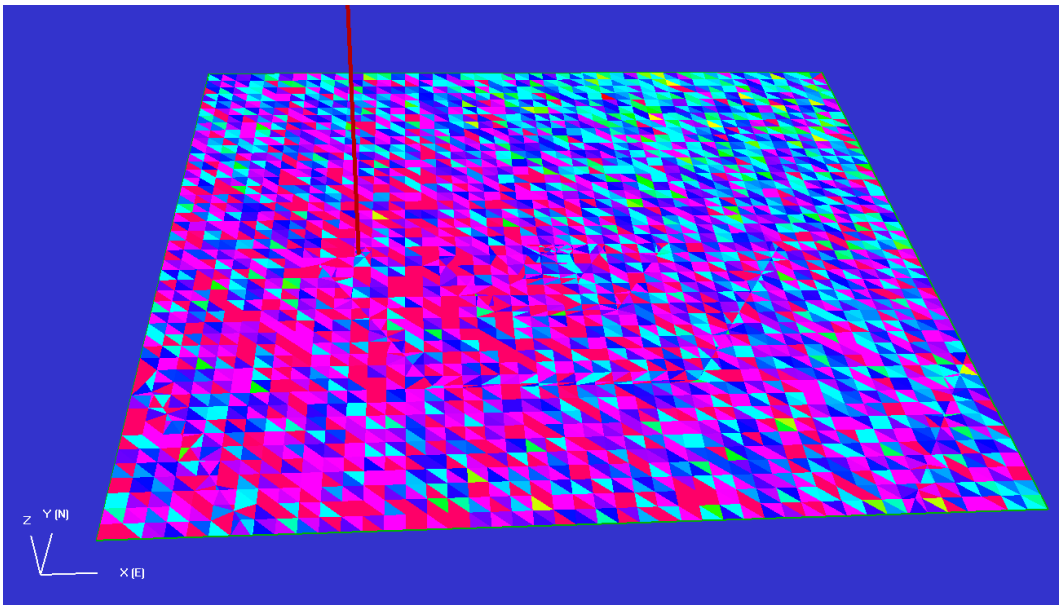

Figure 3-4 *Non-Stationary Spatial Process Transmissivity Distribution*

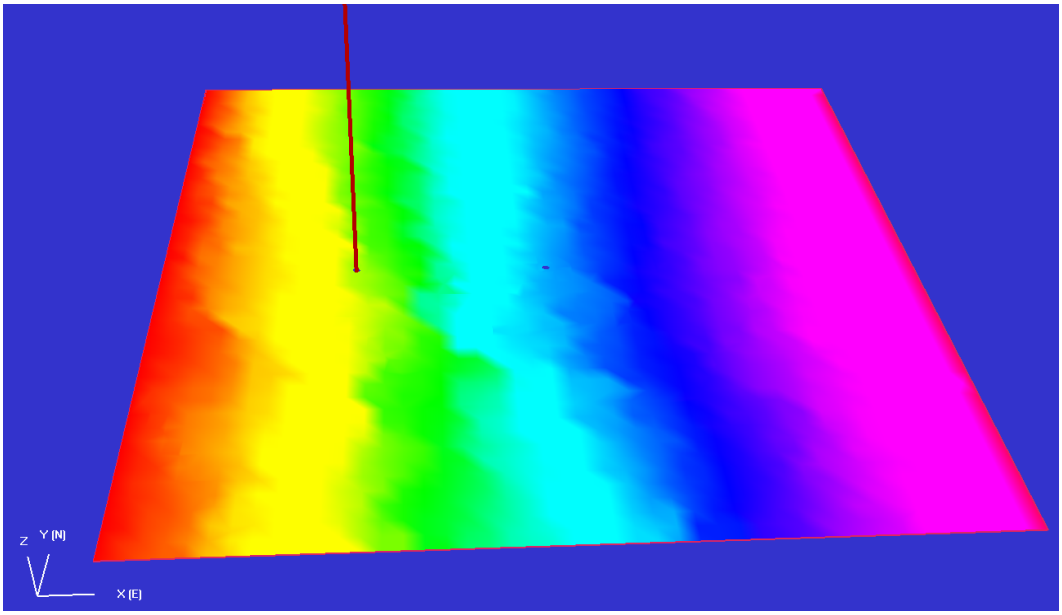

Figure 3-5 *Head Solution for Task 6B2 2D Flow Field (BG)*

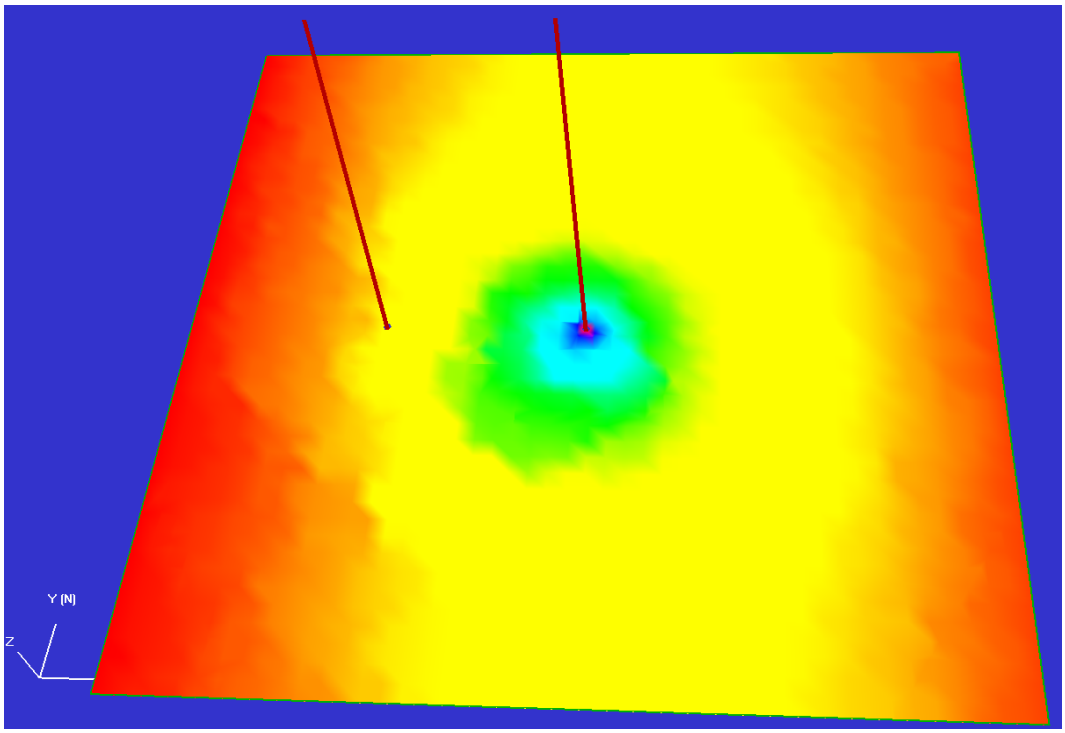

Figure 3-6 *Head Solution for Task 6A (STT-1b) Flow Boundary Conditions (RC)*

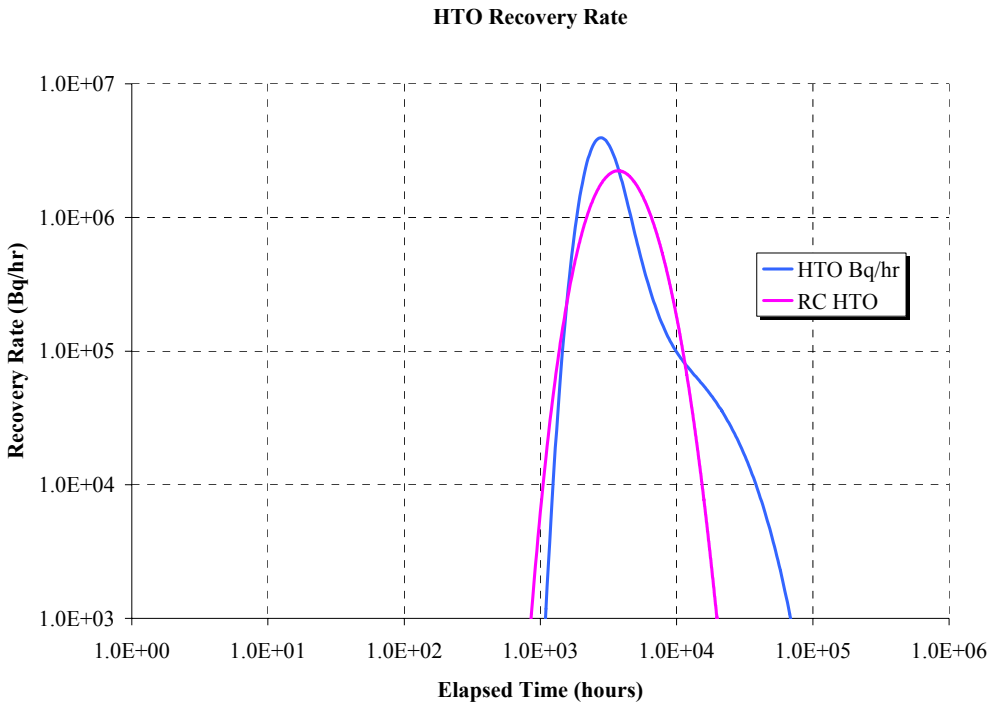

Figure 3-7 *Task 6B Conservative Tracer Breakthrough (RC and BG Boundary Conditions)*

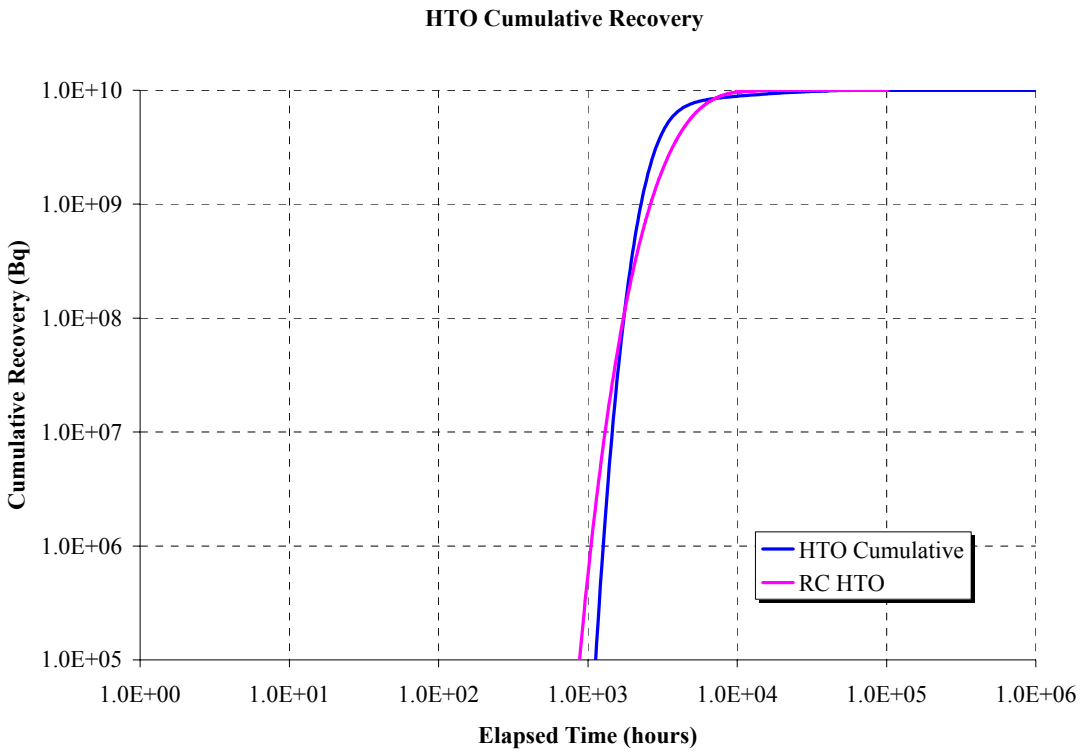

Figure 3-8 *Task 6B Conservative Tracer Breakthrough (RC and BG Boundary Conditions)*

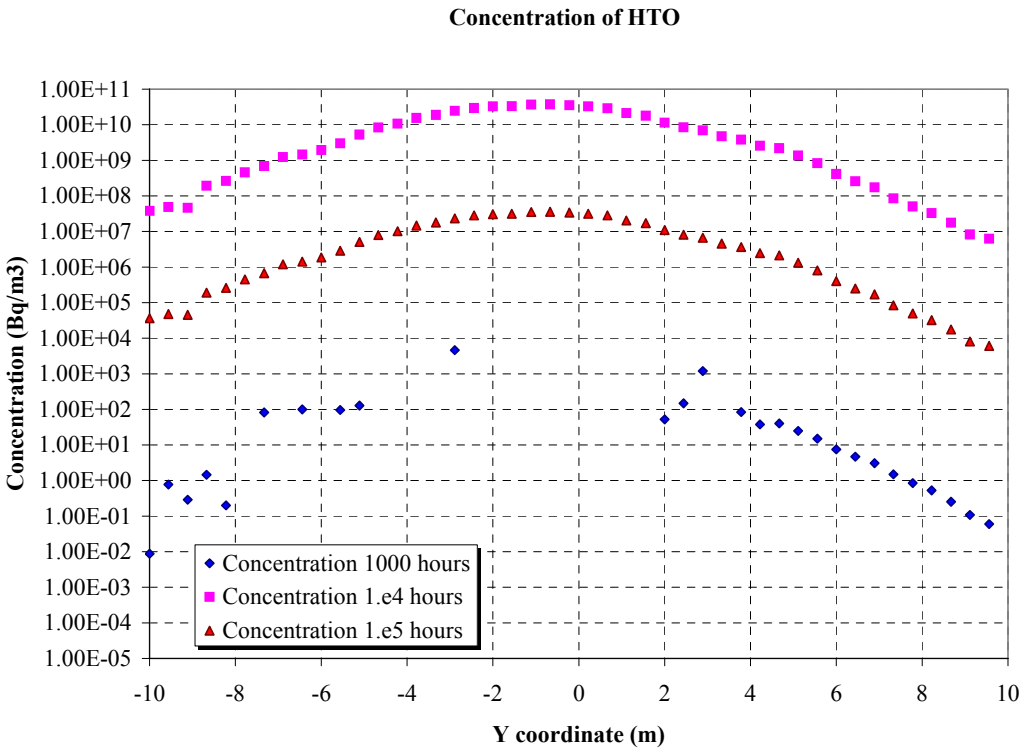

Figure 3-9 *Task 6B2 Conservative Tracer Breakthrough (BG Boundary Condition)*

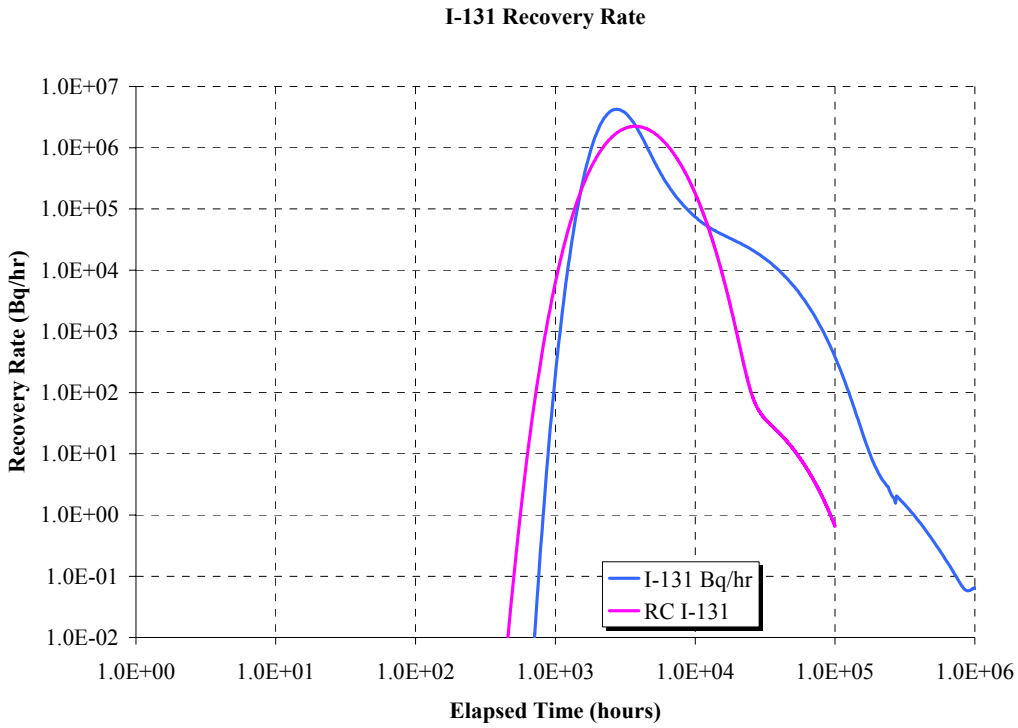

Figure 3-10 *I-131 Tracer Breakthrough (RC and BG Boundary Conditions)*

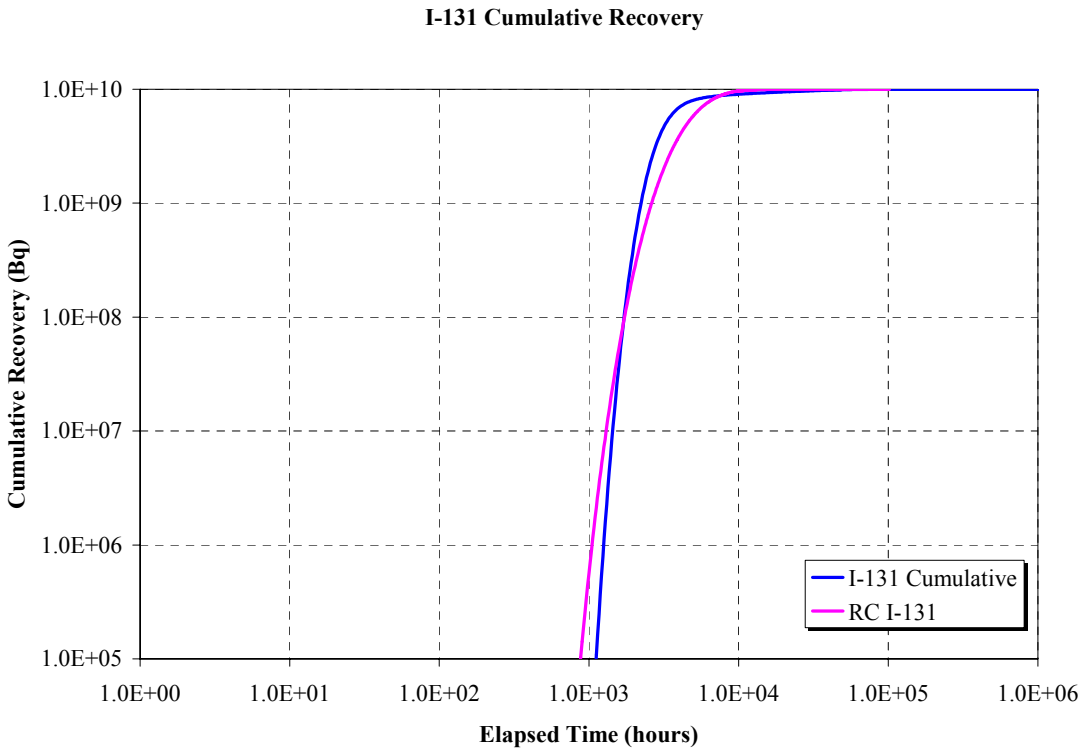

Figure 3-11 *I-131 Tracer Breakthrough (RC and BG Boundary Conditions)*

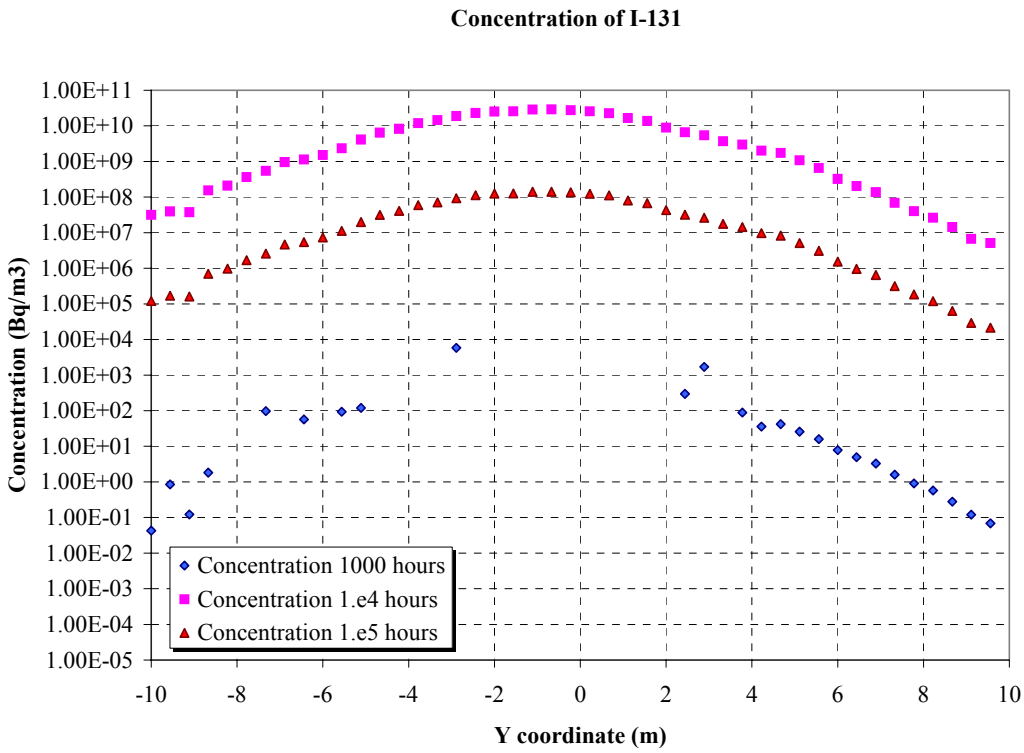

Figure 3-12 *I-131 Tracer Breakthrough (BG Boundary Condition)*

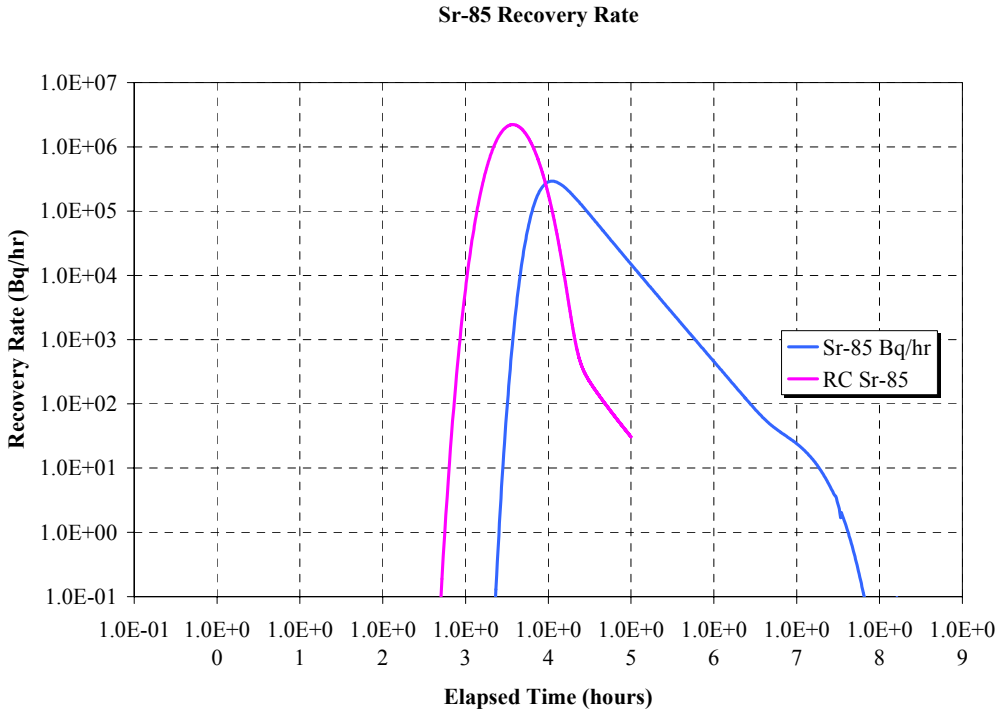

Figure 3-13 *Sr-85 Tracer Breakthrough (RC and BG Boundary Conditions)*

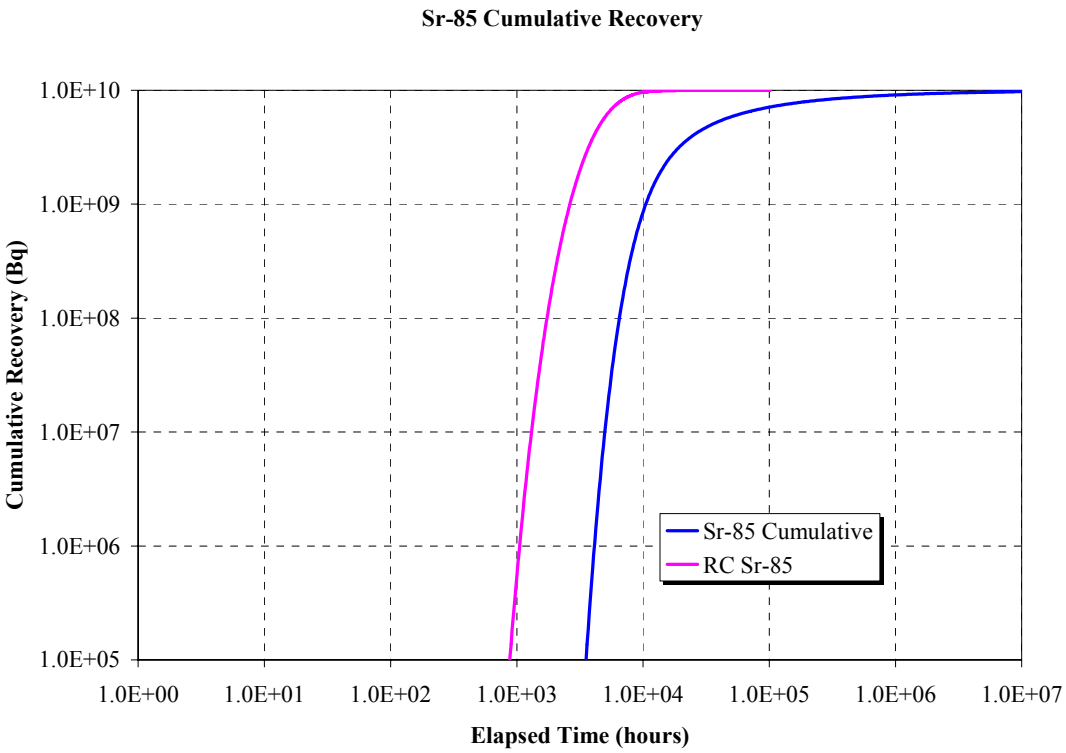

Figure 3-14 *Sr-85 Tracer Breakthrough (RC and BG Boundary Conditions)*

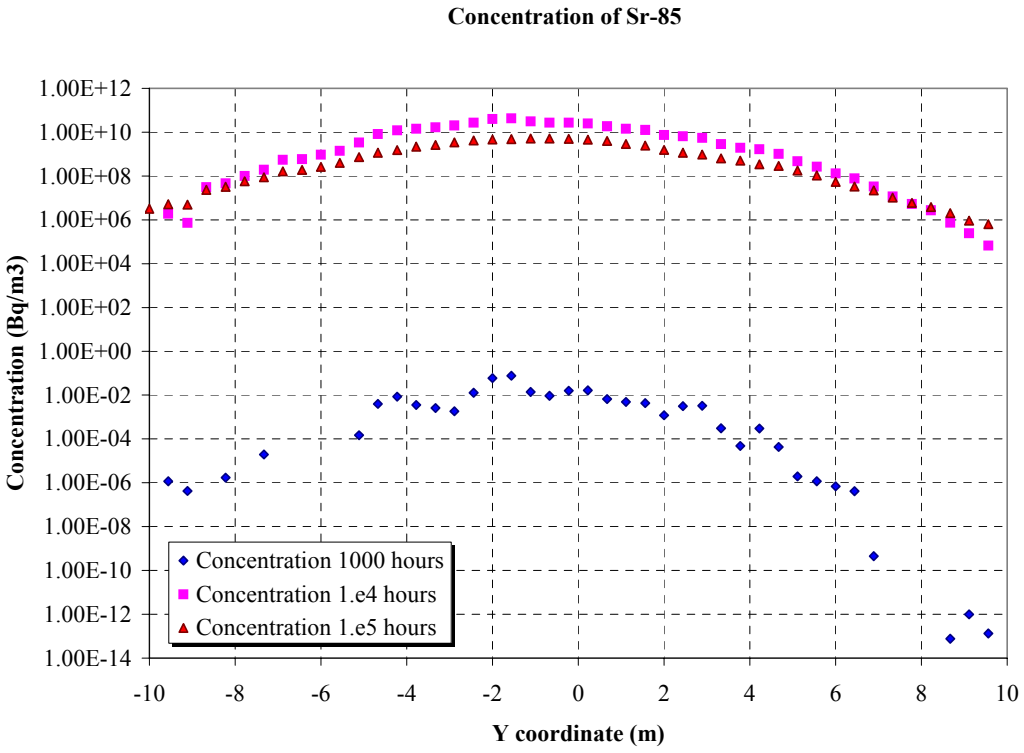

Figure 3-15 *Sr-85 Tracer Breakthrough (BG Boundary Condition)*

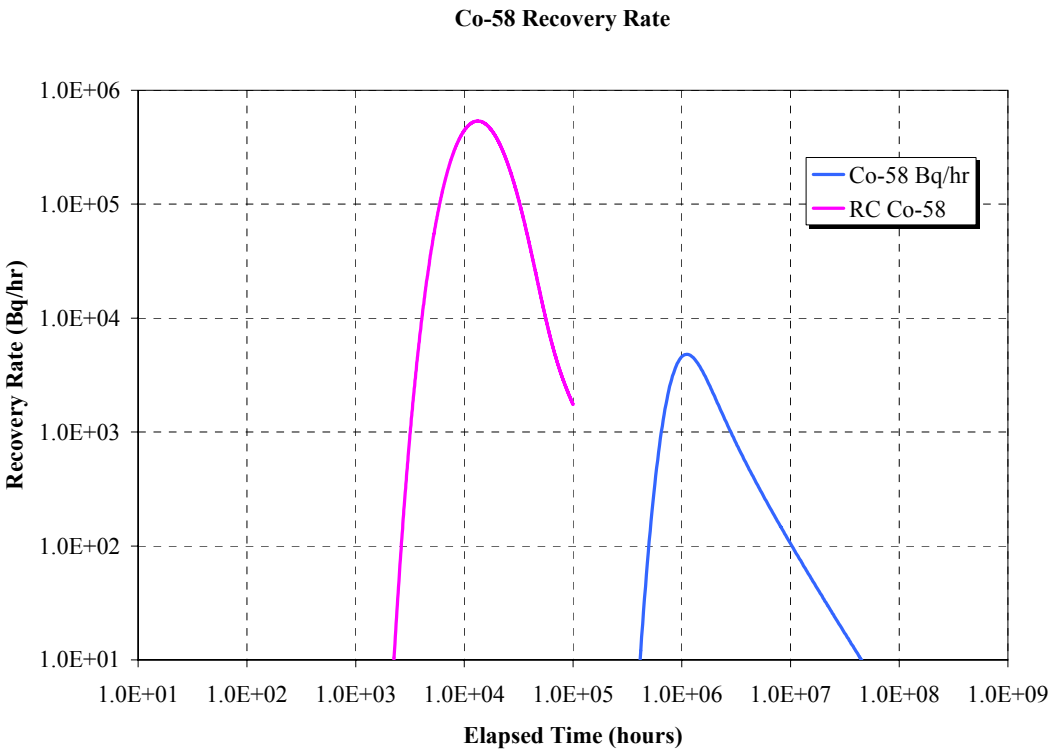

Figure 3-16 *Co-58 Tracer Breakthrough (RC and BG Boundary Conditions)*

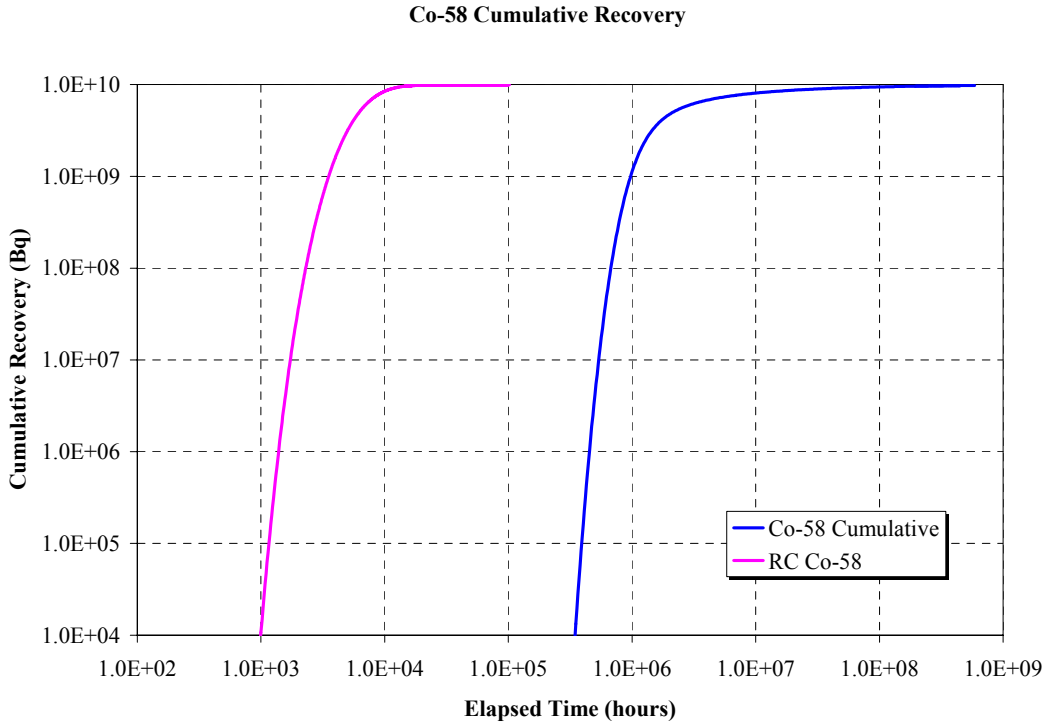

Figure 3-17 *Co-58 Tracer Breakthrough (RC and BG Boundary Conditions)*

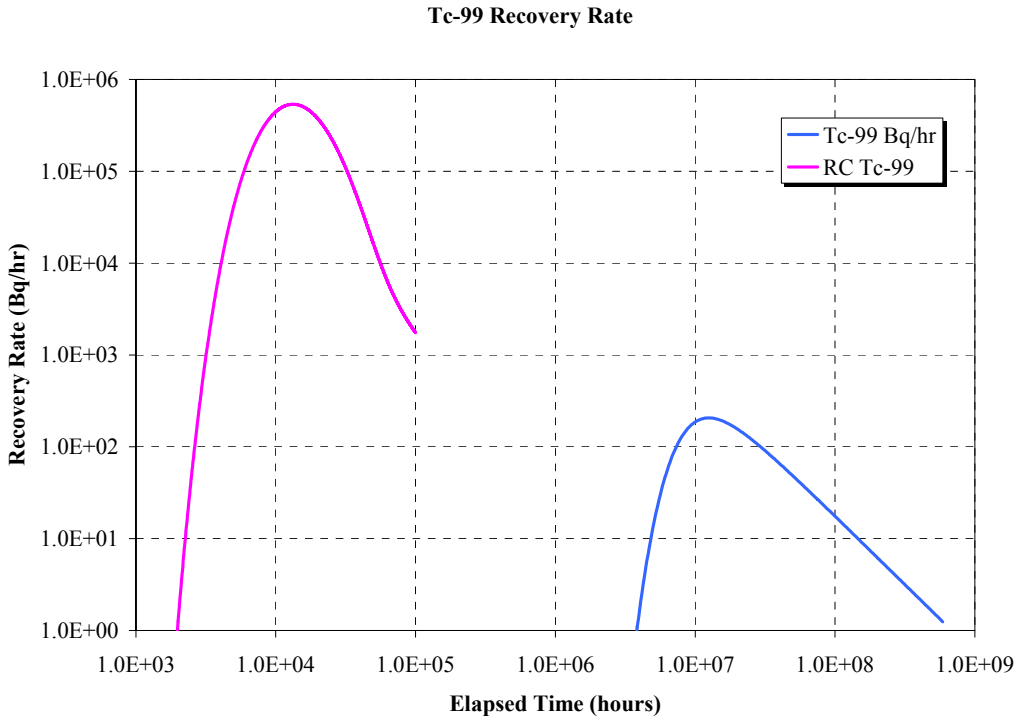

Figure 3-18 *Tc-99 Tracer Breakthrough (RC and BG Boundary Conditions)*

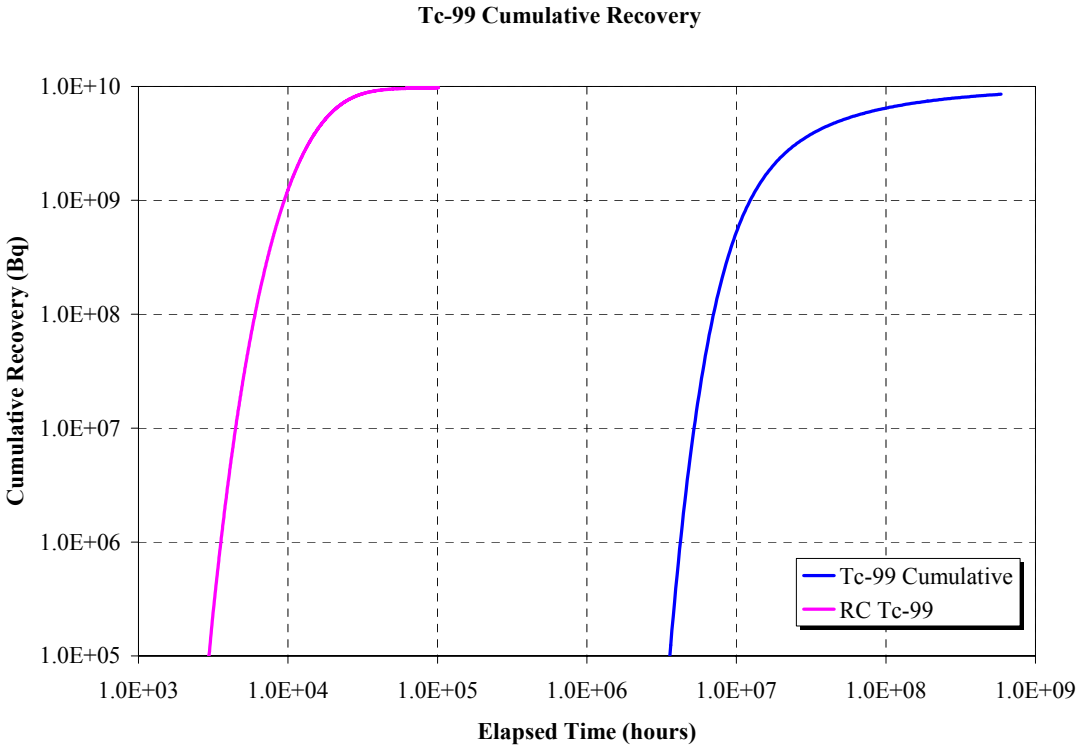

Figure 3-19 *Tc-99 Tracer Breakthrough (BG Boundary Condition)*

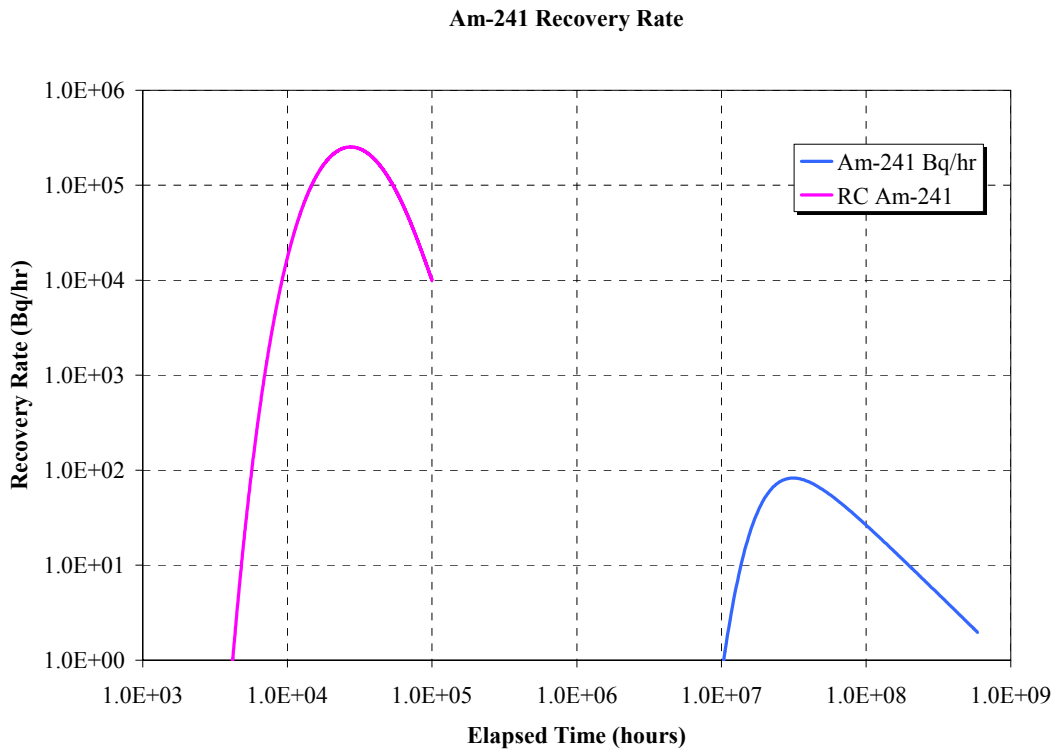

Figure 3-20 *Am-241 Tracer Breakthrough (RC and BG Boundary Conditions)*

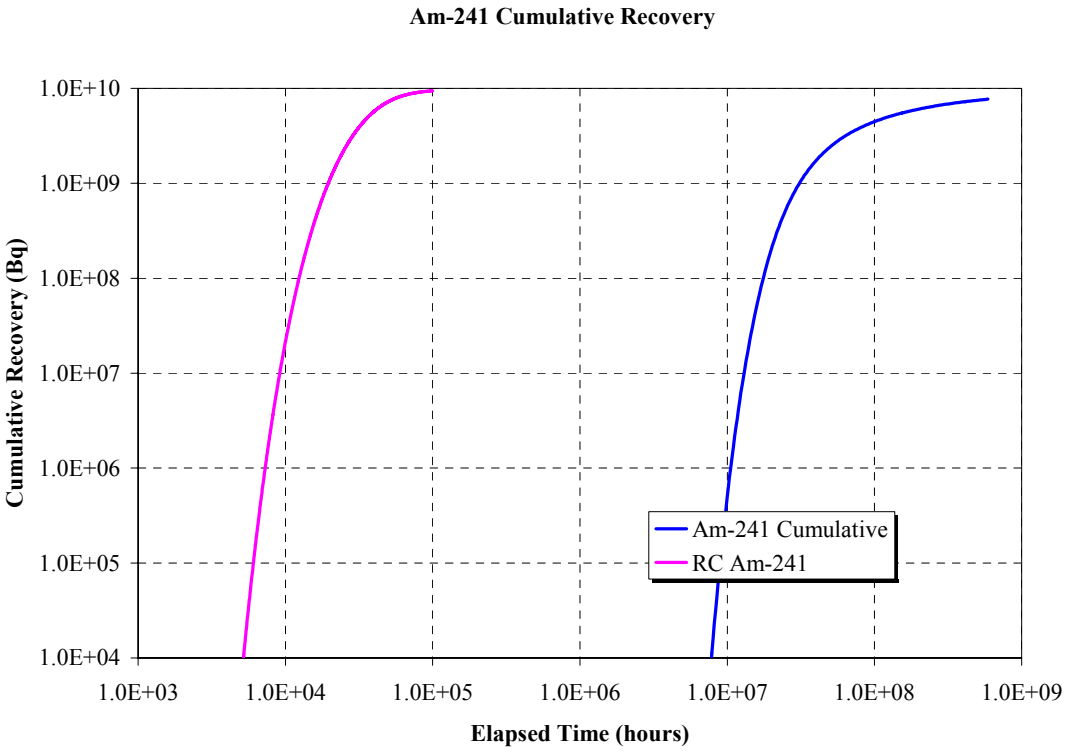

Figure 3-21 *Am-241 Tracer Breakthrough (RC and BG Boundary Conditions)*

Figure 4-22, Figure 4-24 and Figure 4-24 show the cumulative breakthrough for a Dirac injection function for a non-stationary transmissivity field, a geostatistical transmissivity field and a uniform transmissivity field respectively. The Dirac injection was selected because the injected mass goes through the system as a single pulse. For all three transmissivity fields, the breakthroughs for the BG boundary condition exhibit a single peak, although varying degrees of late time diffusion.

Figure 4-25 through Figure 4-30 illustrate results for a continuous injection boundary condition. The continuous injection was selected because this more closely models long term radionuclide releases. The response for the non-stationary continuum field is similar for continuous injection boundary conditions although the peak breakthrough becomes less profound as the sorption increases. This illustrates the pattern of breakthrough becomes smoother as time progresses.

3.2.3 Discussion

The simulations reported above provided a preliminary result for Task 6B2. These results illustrate a) the importance of assumed flow boundary conditions, b) the degree to which the heterogeneity of transmissivity on the fracture plane can be expected to influence tracer breakthrough, and c) the difference between assumed Dirac and Continuous tracer injections. These results will be used to support development of more detailed specifications for future Task 6B2
simulations.

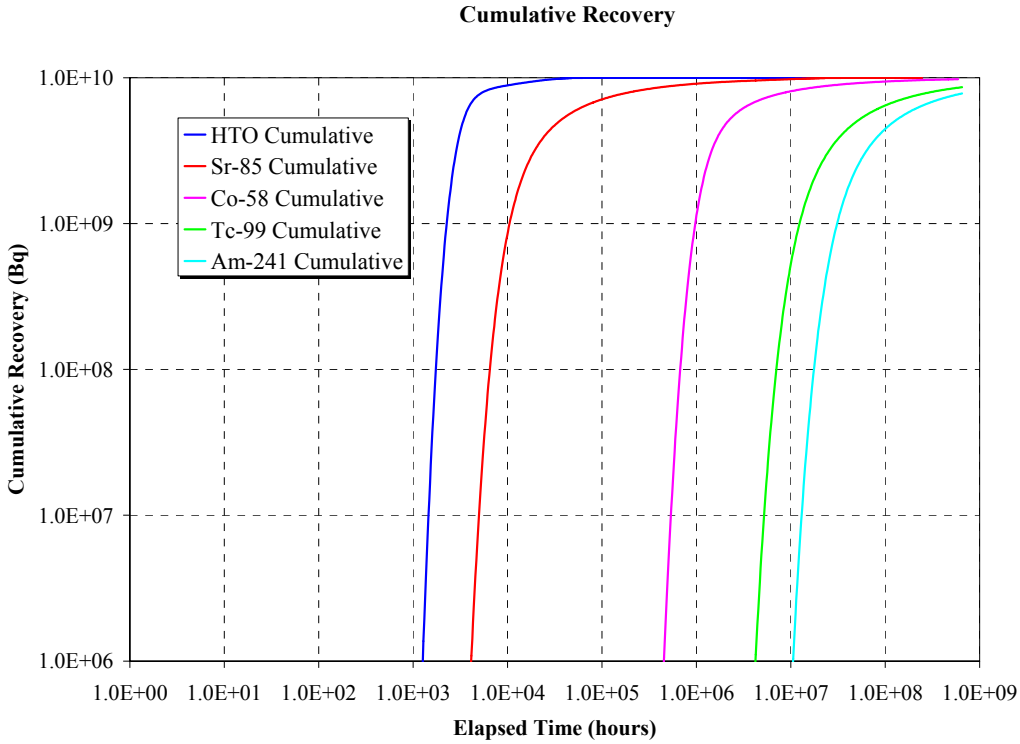

Figure 3-22 *Dirac Tracer Breakthrough, Non-Stationary Transmissivity Field*

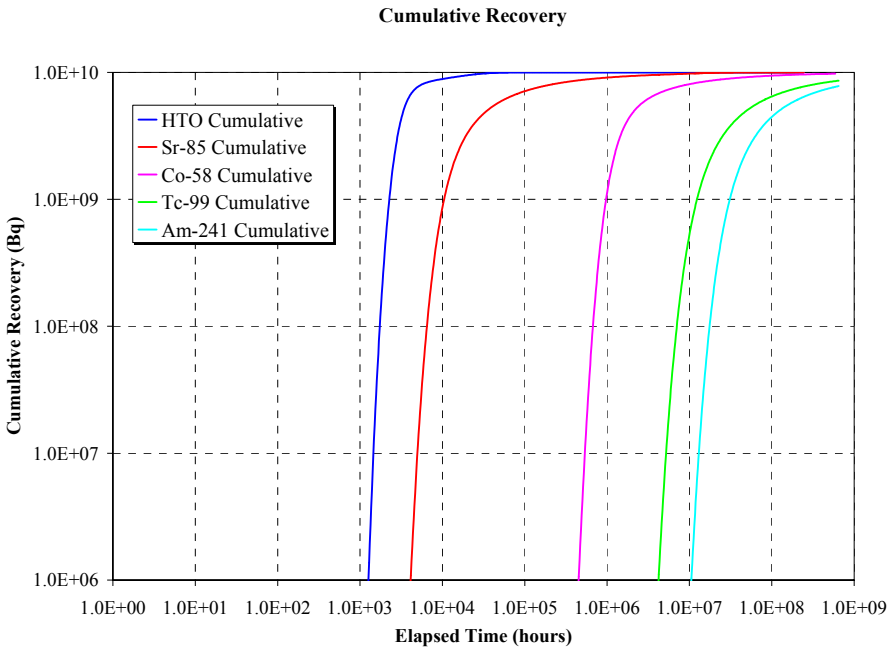

Figure 3-23 *Dirac Tracer Breakthrough, Geostatistical Transmissivity Field*

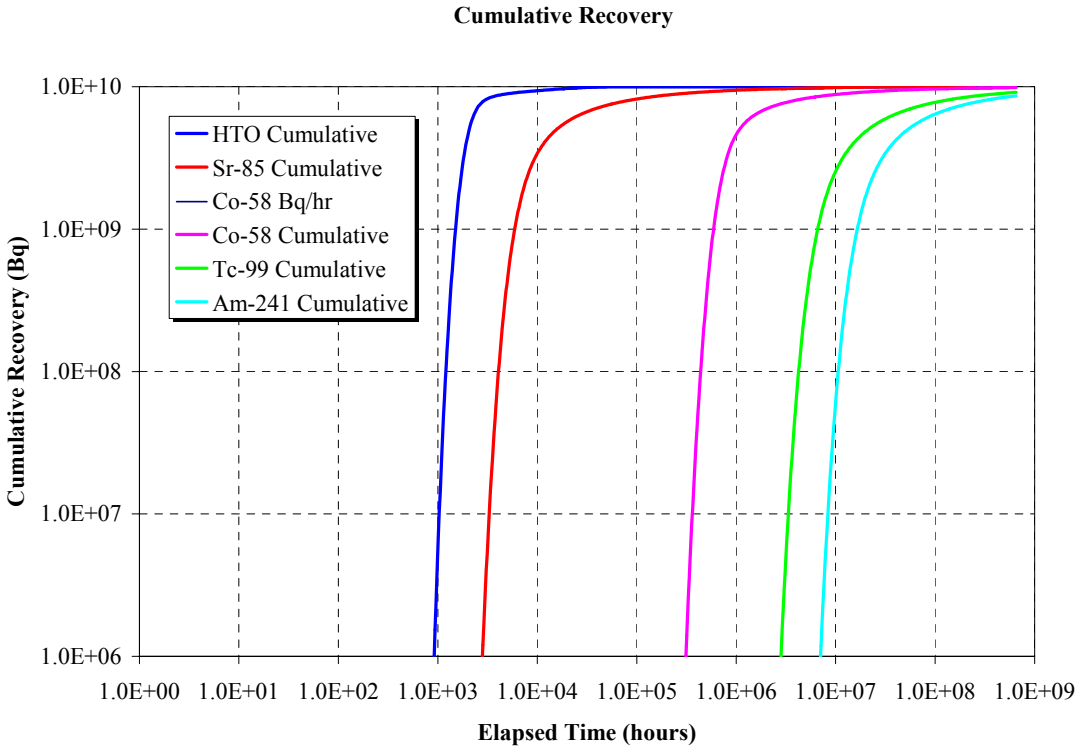

Figure 3-24 *Dirac Tracer Breakthrough, Uniform Transmissivity Field*

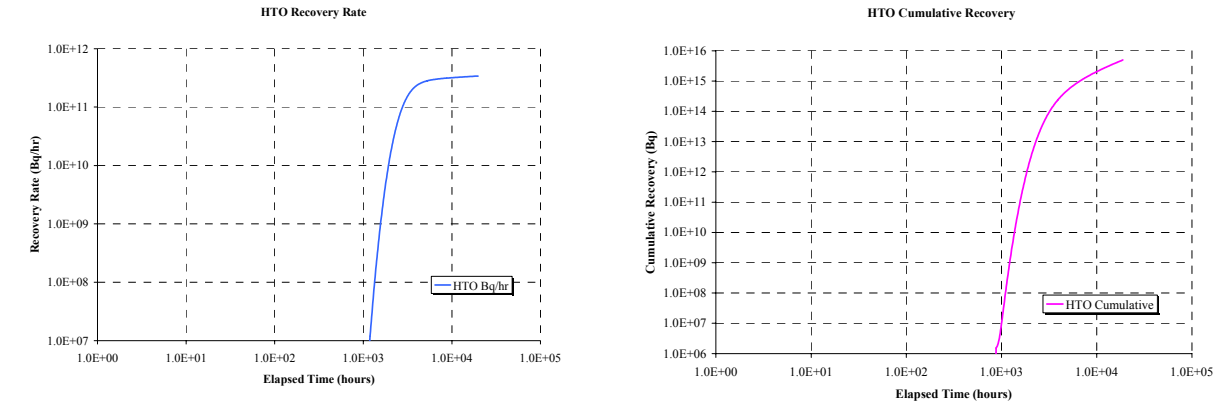

Figure 3-25 *Continuous Release HTO*

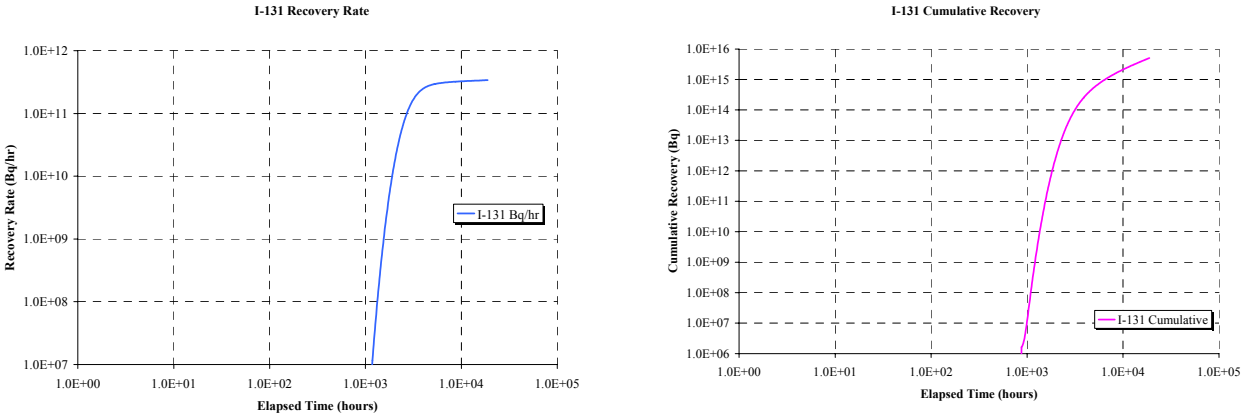

Figure 3-26 *Continuous Release I-131*

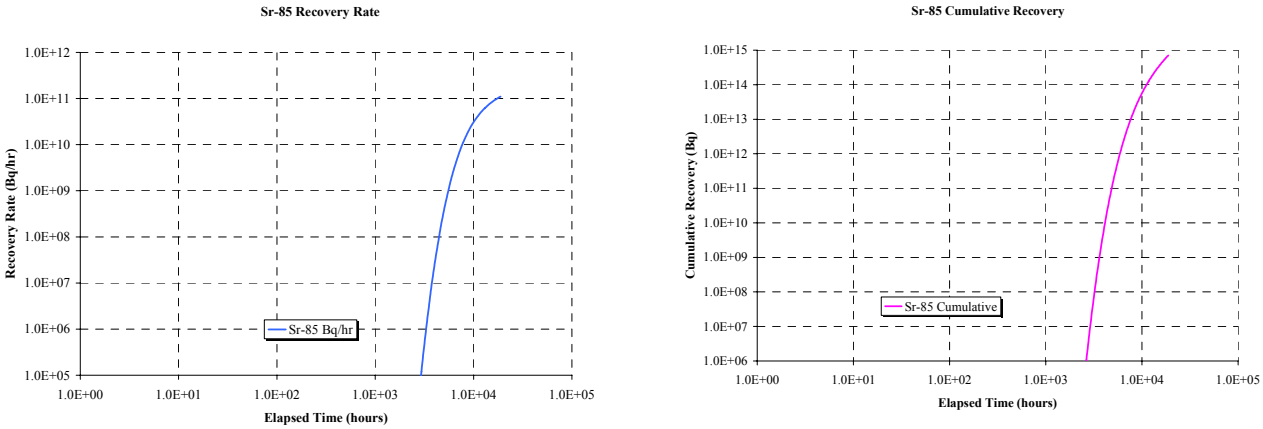

Figure 3-27 *Continuous Release Sr-85*

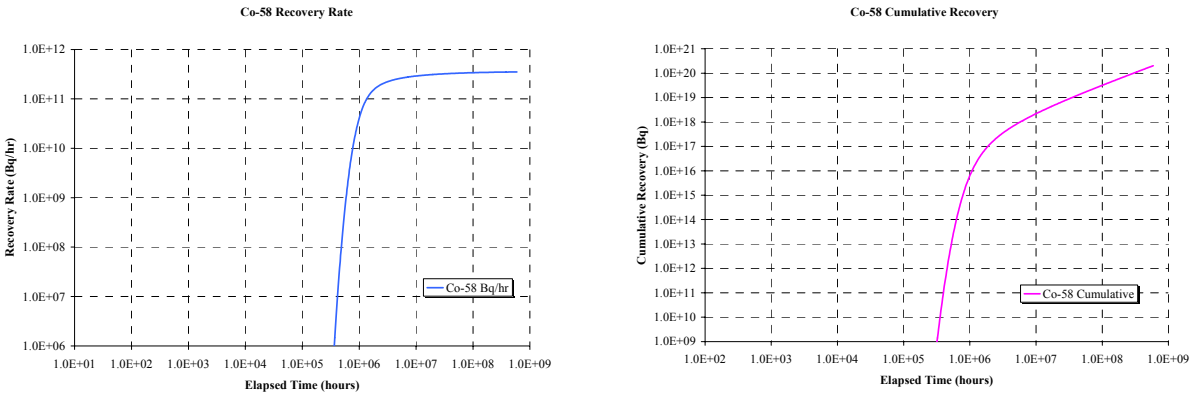

Figure 3-28 *Continuous Release Co-58*

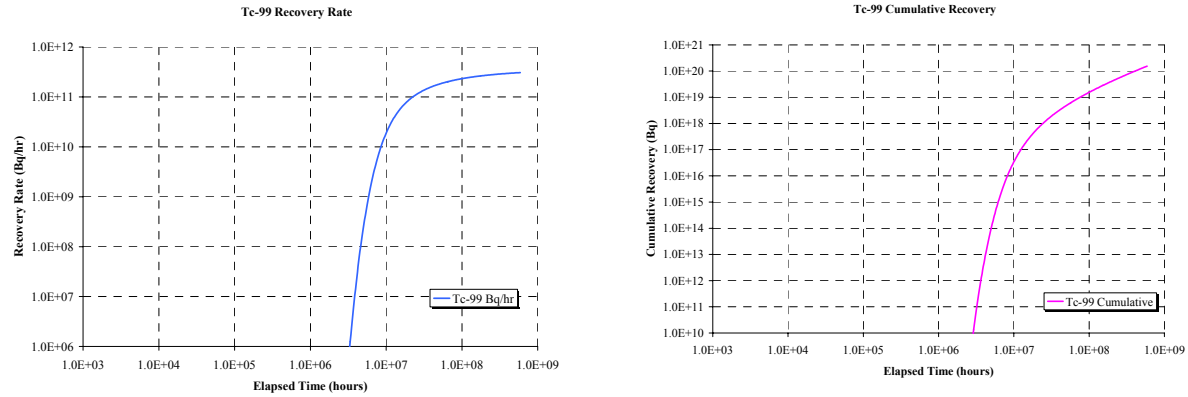

Figure 3-29 *Continuous Release Tc-99*

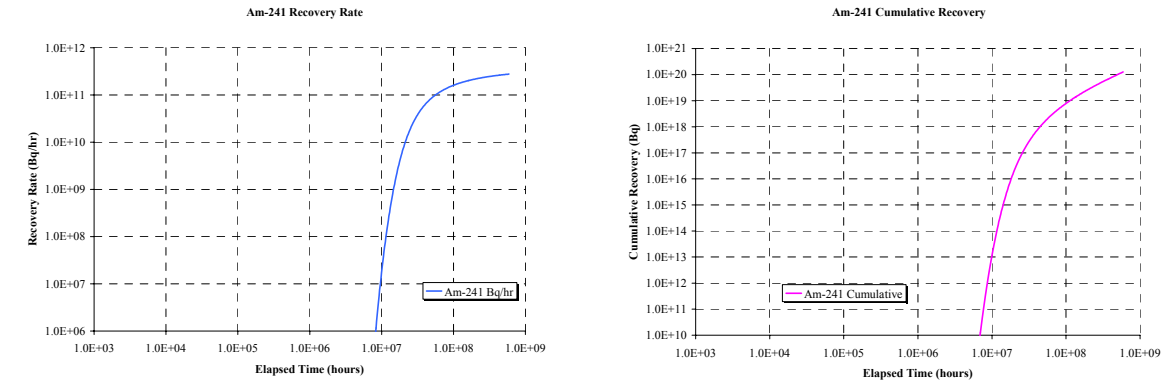

Figure 3-30 *Continuous Release Am-241*

3.3 Reference 2-D flow field

3.3.1 Assumptions

The study presented in Section 4.2 illustrates the ability of different 2-D spatial patterns of hydraulic properties to calibrate against measured tracer breakthrough. In this section, this approach was significantly extended by

a) building a more comprehensive set of stochastic continuum fields

b) implementing a more sophisticated microstructural model for these stochastic fields

c) calibrating each of the fields against the measured STT-1b tracer breakthrough

d) predicting solute transport in the calibrated fields using more realistic PA time scale boundary conditions.

3.3.2 Stochastic Fields

The different stochastic continuum fields used for this study are summarized in Table 3-2. Example realizations of the stochastic continuum fields are illustrated in Figures 4-31 through 4-34. The patterns were all produced using a Turning Bands geostatistical field generation algorithm, which explains the visible periodicity.

Table 3-2 Stochastic Continuum Fields

Case	Description	Stochastic Field	Parameters
1	Channeled aperture pattern, wide channels	Exponential Variogram	T_{mean} 10^{-6} T_{std} $5x10^{-6}$ Cov 2 Dimension 2
2	Channeled aperture pattern, narrow channels	Exponential Variogram	T_{mean} 10^{-6} T_{std} $5x10^{-6}$ Cov 1 Dimension 3
3	Homogeneous (unchannelled) with wide pattern	Exponential Variogram	T_{mean} 10^{-6} T_{std} 10^{-6} Cov 1 Dimension 2
4	Homogeneous (unchannelled) with narrow pattern	Null Variogram	T_{mean} 10^{-6} T_{std} 10^{-6}

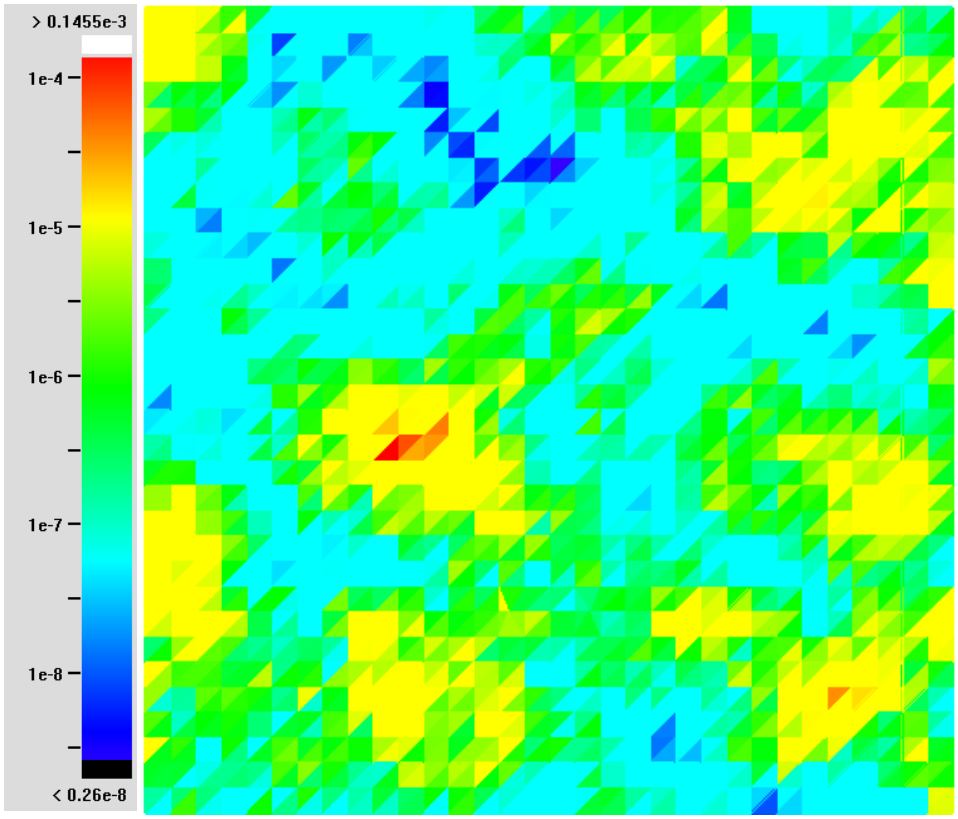

Figure 3-31 *Case 1, Channeled transmissivity pattern, wide channels*

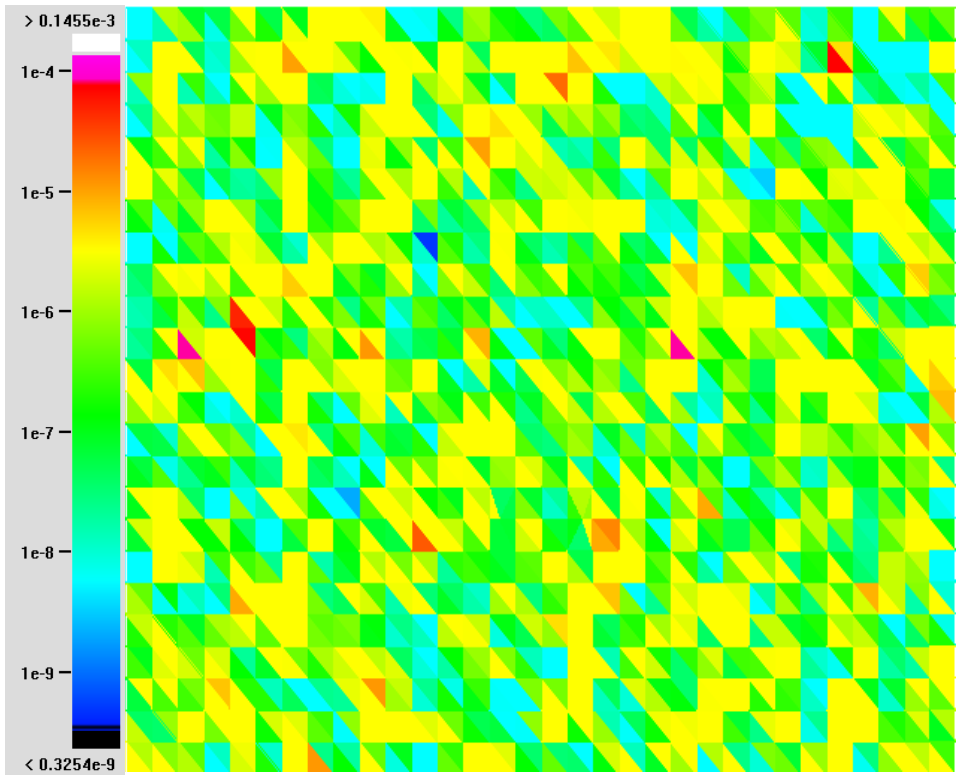

Figure 3-32 *Case 2, Channeled transmissivity pattern, narrow channels*

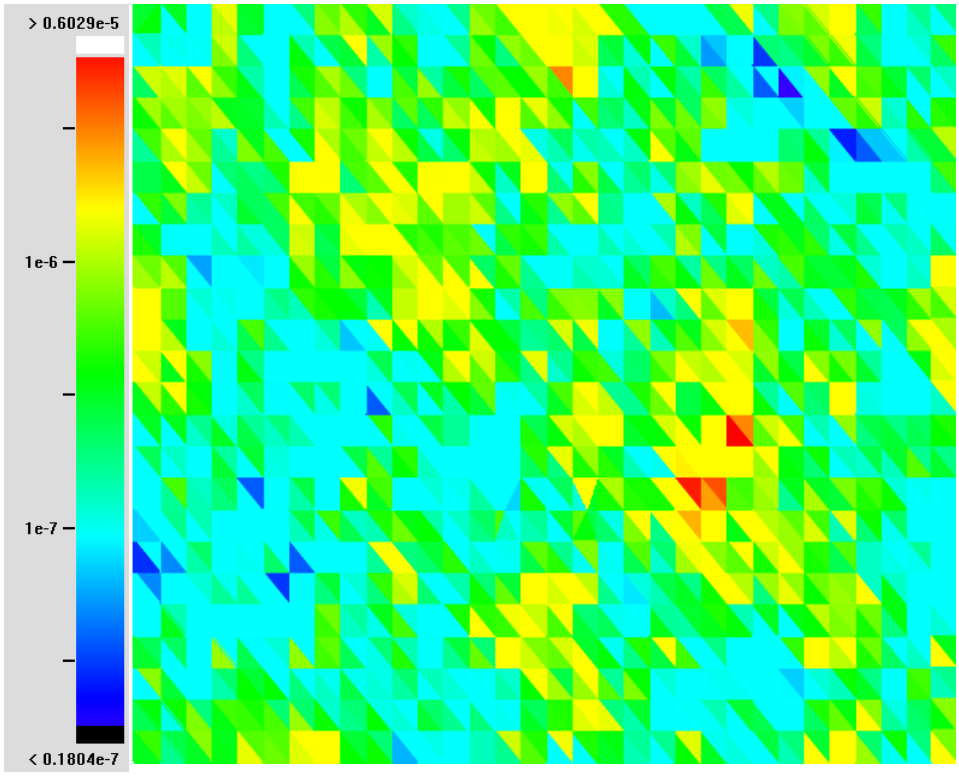

Figure 3-33 *Case 3, Homogeneous (unchannelled) transmissivity with wide pattern*

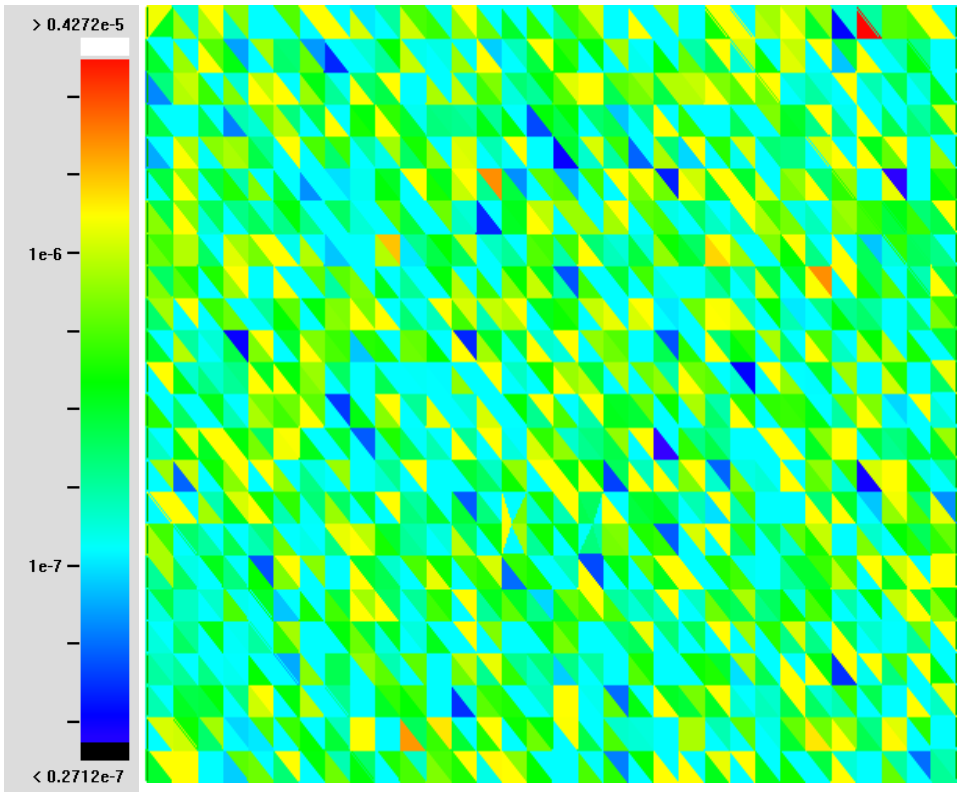

Figure 3-34 *Case 4, Homogeneous (unchannelled) transmissivity with narrow pattern*

Boundary Conditions

The reference 2-D flow field boundary conditions for Task 6B2 was established by Elert and Selroos (2001), based on the simulations carried out in Section 4.2 above. This boundary condition is illustrated in Figure 3-35. This boundary condition is based on an assumption of natural gradients at the PA time scale, with flow in an individual fracture driven by head gradients between different intersecting fractures. In this case, the fracture being simulated in "Feature A", and the two intersecting fractures are "Feature B" and NW-2' within the Äspö TRUE-1 hydrostructural model.

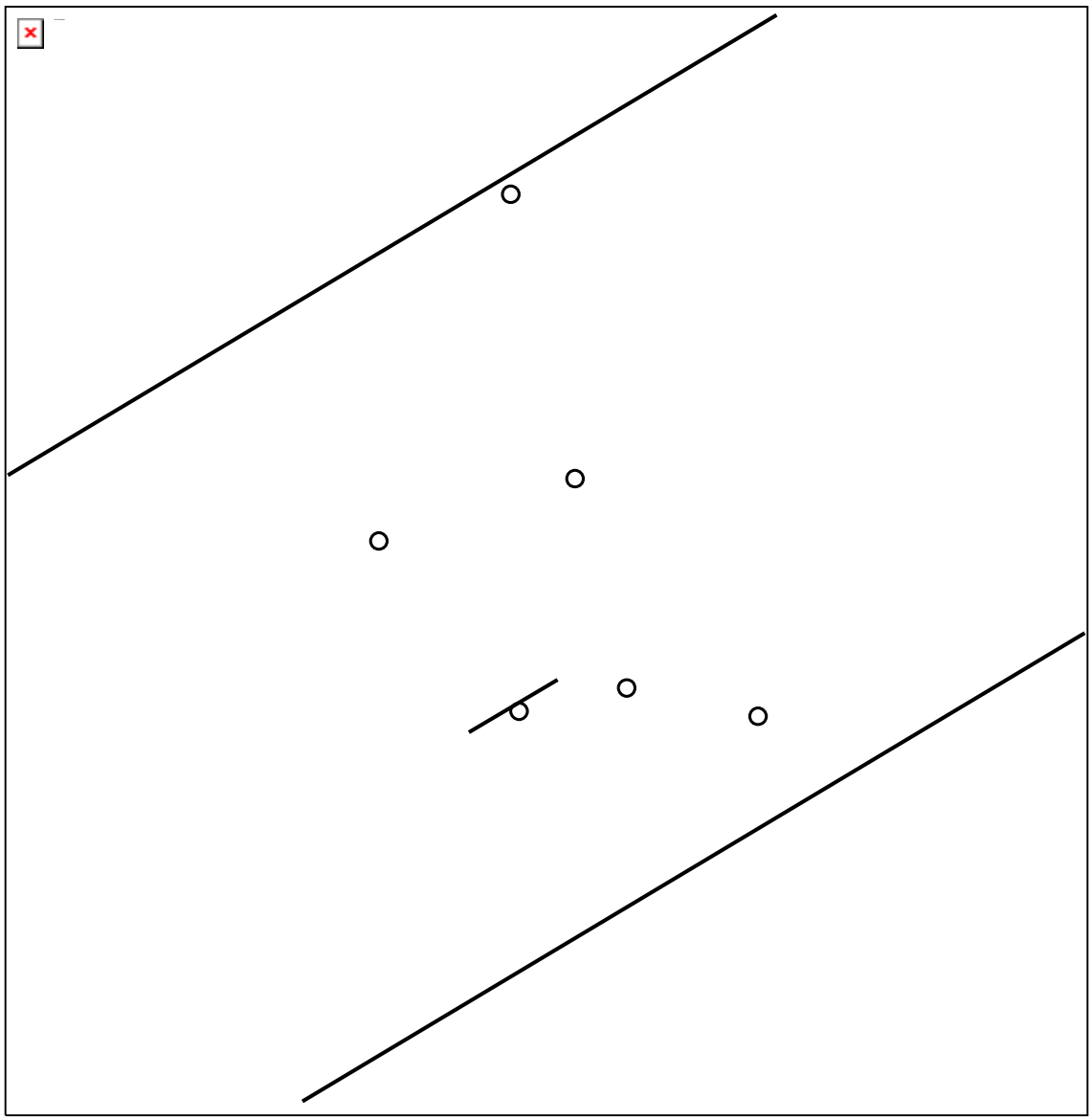

Figure 3-35 *Geometry of Task 6B2. Injection at line source at KXTT1 R2. Tracer collection at Fracture Y. (after Elert and Selroos, 2001)*

The 2-D flow field of Figure 3-35 is solved for flow using the FracMan/MAFIC finite element flow solver. The hydrological boundary conditions are constant heads at the intersecting fractures. The head difference between the two fractures is 0.015 meters, corresponding to a gradient of 0.1%.

Transport within this flow field is then solved using MAFIC/LTG as in the simulations described in Section 4.2 above. Two injection boundary conditions are assumed. In the first, injection is assumed to occur along a 2 meter long line source overlapping the position of borehole section KXTT1 R2. This 5 meter long transport pathway is similar to STT-1b pathway, and is therefore used with pumping at KXTT3 to calibrate the transport properties by comparison against STT-1b breakthrough.

The second injection boundary condition does not include pumping at KXTT3, and therefore provides a 10 meter long, true 2D transport pathway from a line source at Fracture X to a line sink at Fracture Y.

The tracers modeled in Task 6B2 are iodine, strontium, cobalt, technetium and americium,: Both tracer injections are simulated as a constant injection of 1 MBq/year and a Dirac pulse input (unit input). Radioactive decay is not considered

Microstructural Model

Spatial variability in the immobile zone microstructural model is the key to the JNC/Golder team approach to Task 6B2. The JNC/Golder conceptual model assumes that the variation in transmissivity over the fracture is primary due to variations in the microstructural model, rather than variations in "aperture". Thus, where transmissivity is low, the thickness of breccia and gouge infilling is high. This spatial correlation of the microstructural model has potential significance to the difference between 1-D and 2-D modeling. In 1-D, the "average" immobile zone properties are applied. In 2-D, the solute follows its own pathway, and accesses immobile zones related to that pathway.

The JNC/Golder microstructural model assumes a correlation between transmissivity and transport aperture of the form $e_t = c\ T^{b}$. Th value of b is generally assumed 0.5, and the value of c is obtained by calibration to the STT-1b breakthrough.

Calibration/Conditioning to STT-1b

As discussed in Chapter 3 above, site characterization attempts to constrain material properties and processes to reduce the uncertainty of PA time scale predictions. In Task 6B2, the individual stochastic fields were assumed in terms of transmissivity. The relationship between transmissivity and transport aperture and the relationship between transmissivity and immobile zone thickness were calibrated to match the STT-1b tracer breakthrough. The calibrated STT-1b tracer test results are illustrated in Figure 3-36 through Figure 3-52. Figure 3-53 through Figure 3-56 illustrate the microstructure model parameters from the calibration. The calibrated relationship between transport aperture- e_t and transmissivity for each of the stochastic fields were as follows:

- Case 1: $e_t = 2.6\ T^{0.5}$
- Case 2: $e_t = 1.025\ T^{0.5}$
- Case 3: $e_t = 1.7\ T^{0.5}$
- Case 4: $e_t = 3.2\ T^{0.5}$

The calibrated transport aperture e_t field for Case 1, 2, 3, and 4 are illustrated in Figure 3-57 through Figure 3-60. The transport properties assumed for each of the cases are provided in Tables 4-3 through 4-11.

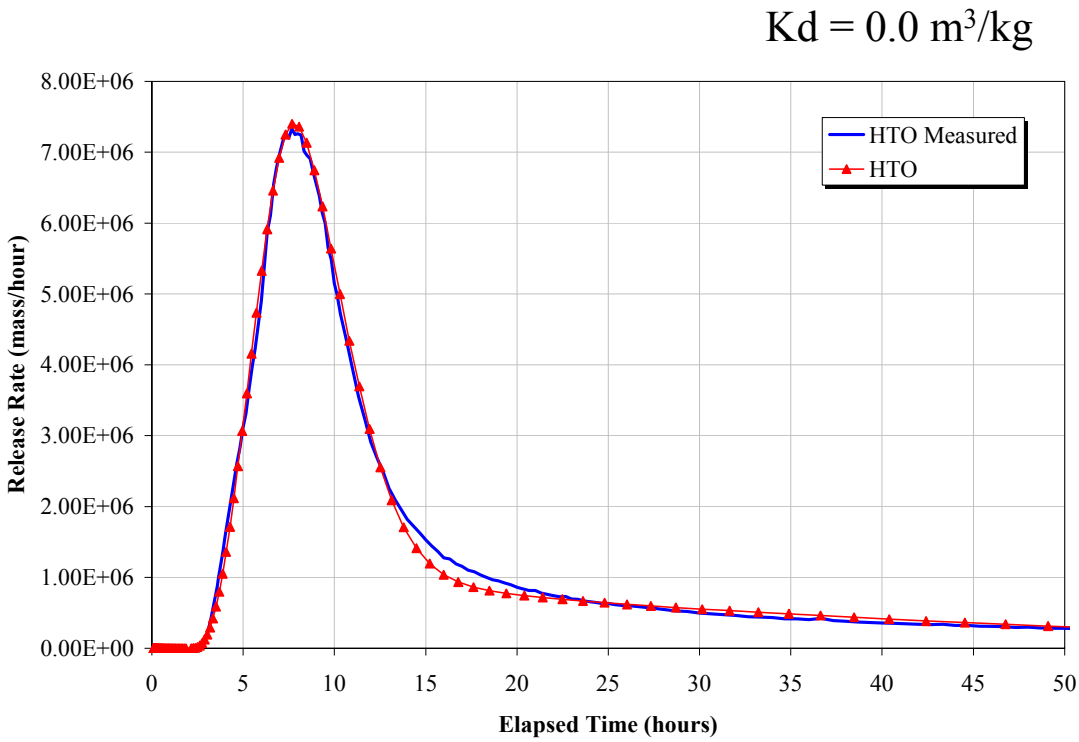

Figure 3-36 *STT-1b Calibration, HTO, Stochastic Field Case 1*

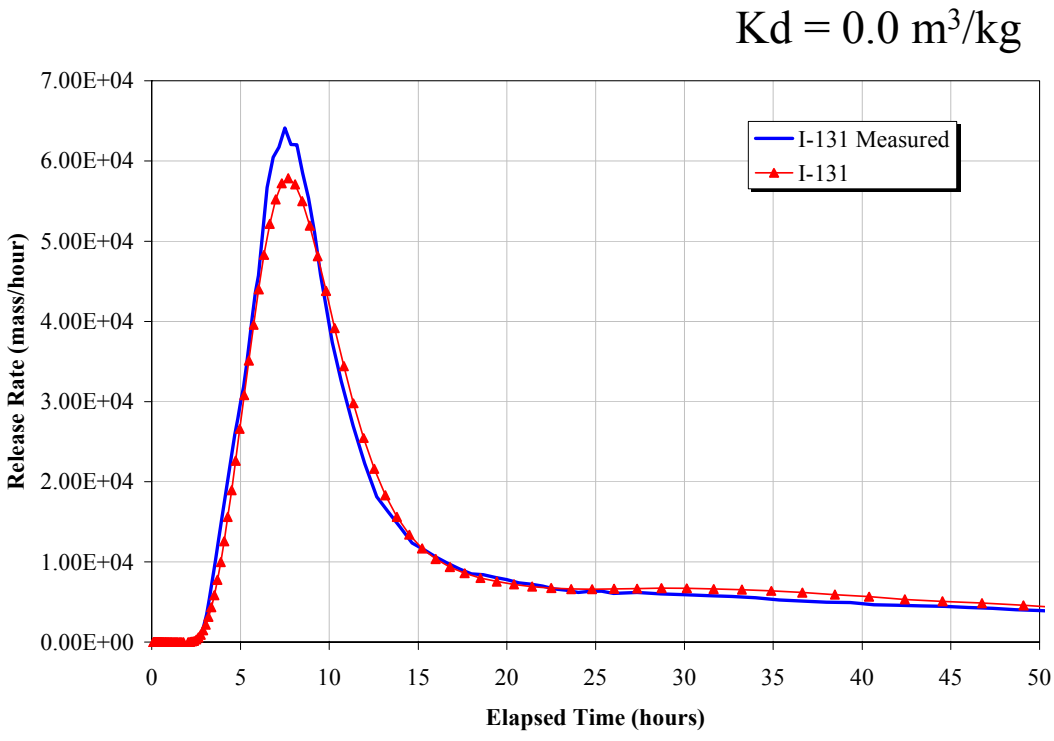

Figure 3-37 *STT-1b Calibration, I-131, Stochastic Field Case 1*

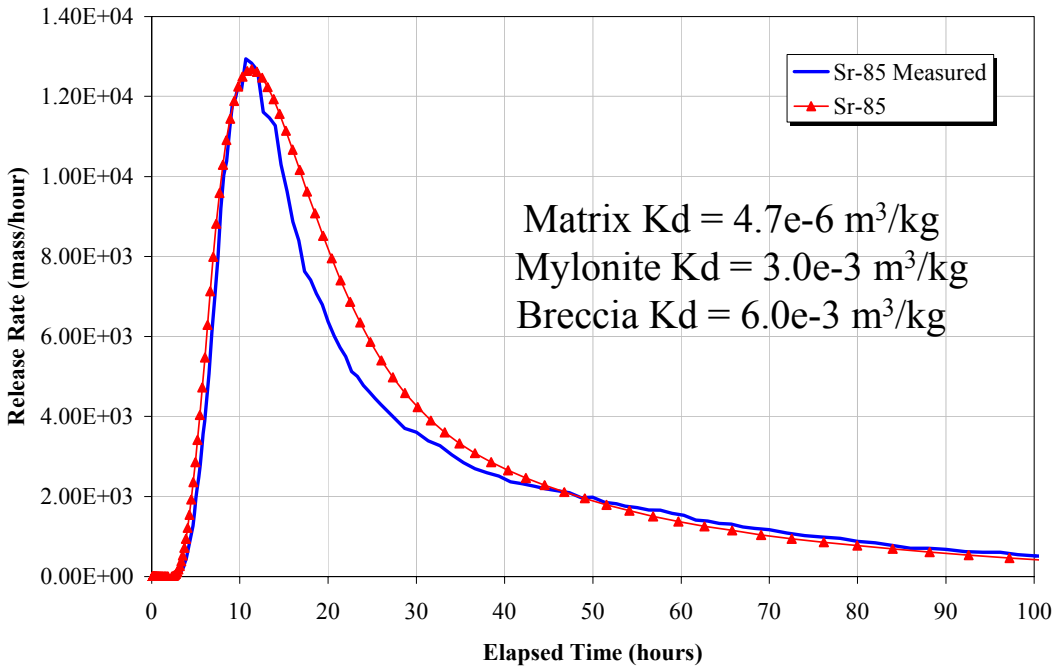

Figure 3-38 *STT-1b Calibration, Sr-85, Stochastic Field Case 1*

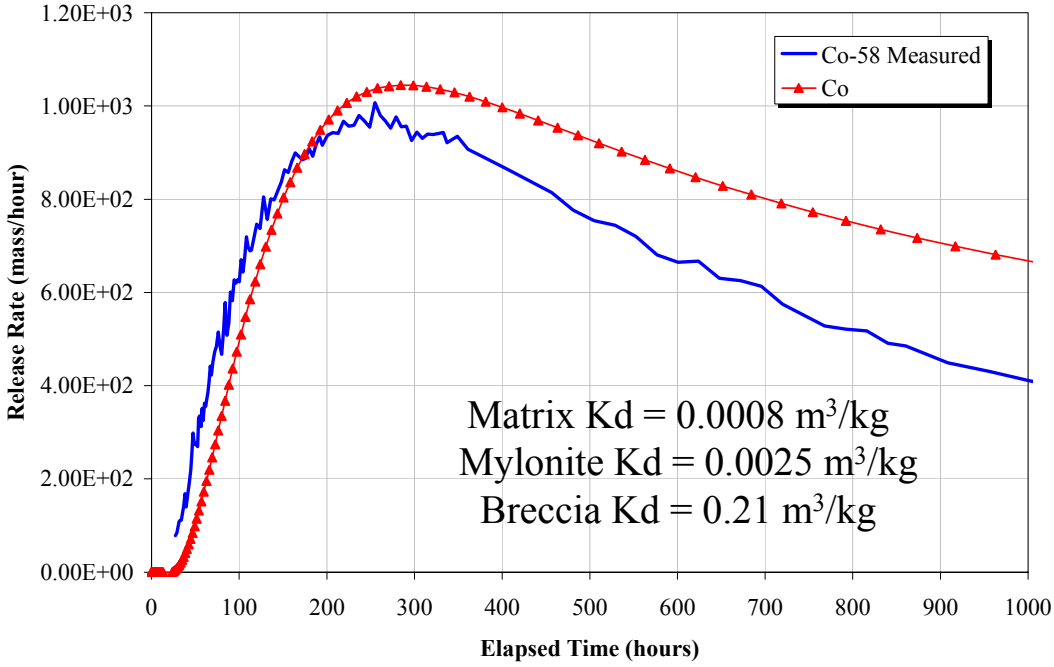

Figure 3-39 *STT-1b Calibration, Co-58, Stochastic Field Case 1*

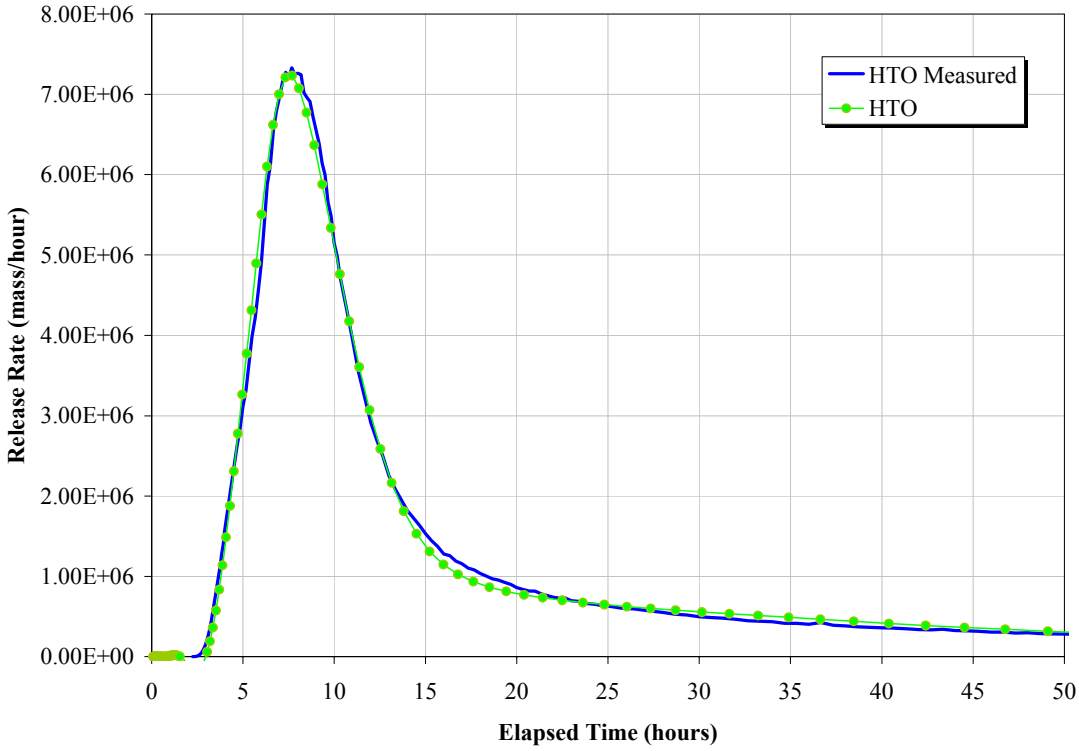

Figure 3-40 *STT-1b Calibration, HTO, Stochastic Field Case 2*

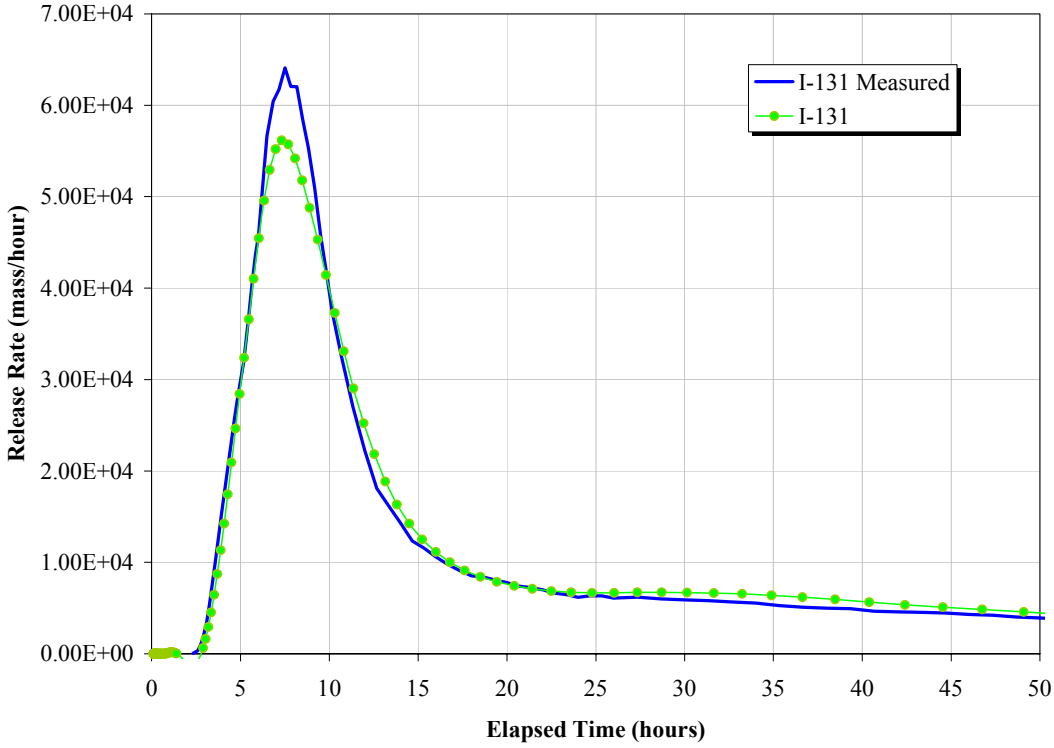

Figure 3-41 *STT-1b Calibration, I-131, Stochastic Field Case 2*

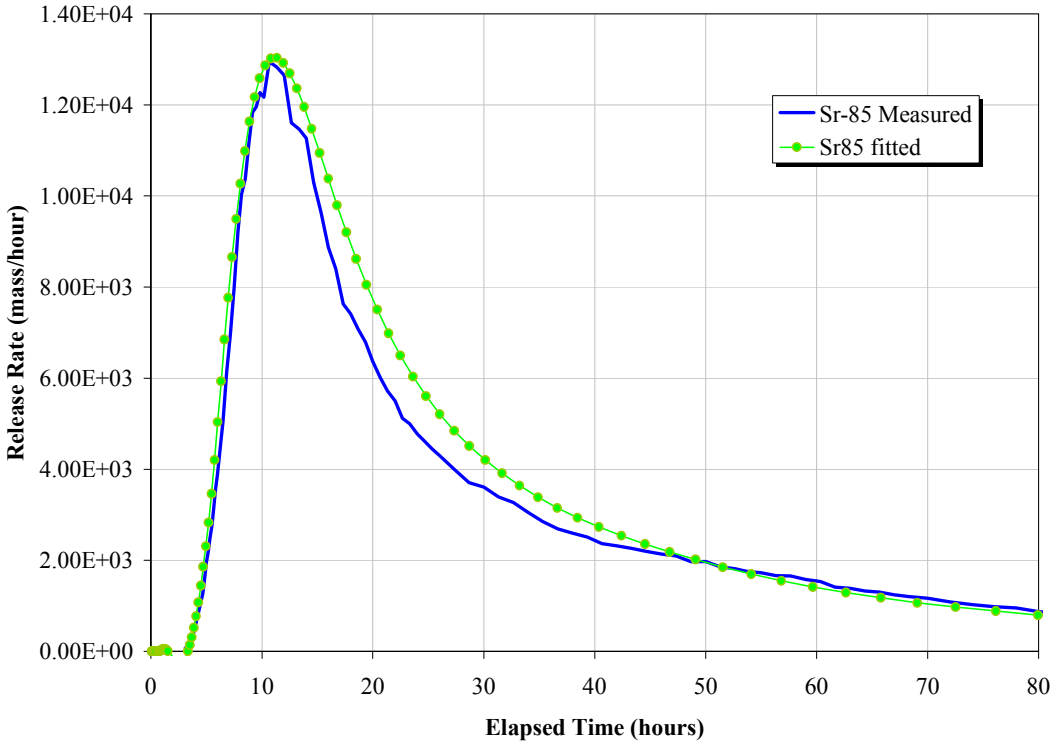

Figure 3-42 *STT-1b Calibration, Sr-85, Stochastic Field Case 2*

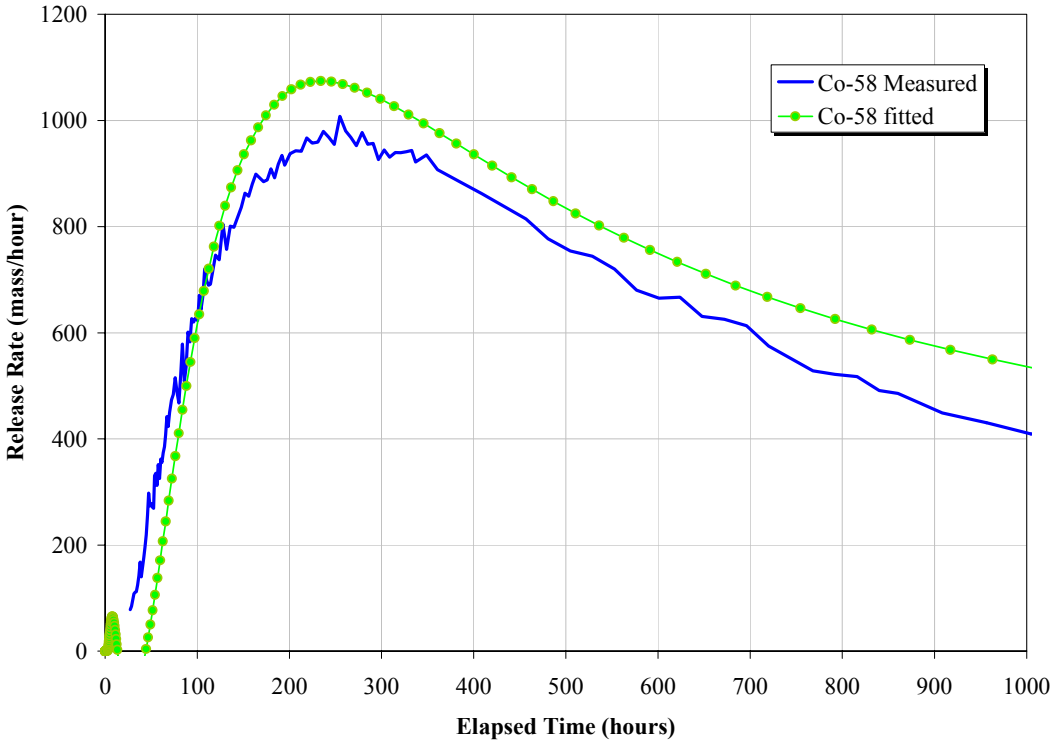

Figure 3-43 *STT-1b Calibration, Co-58, Stochastic Field Case 2*

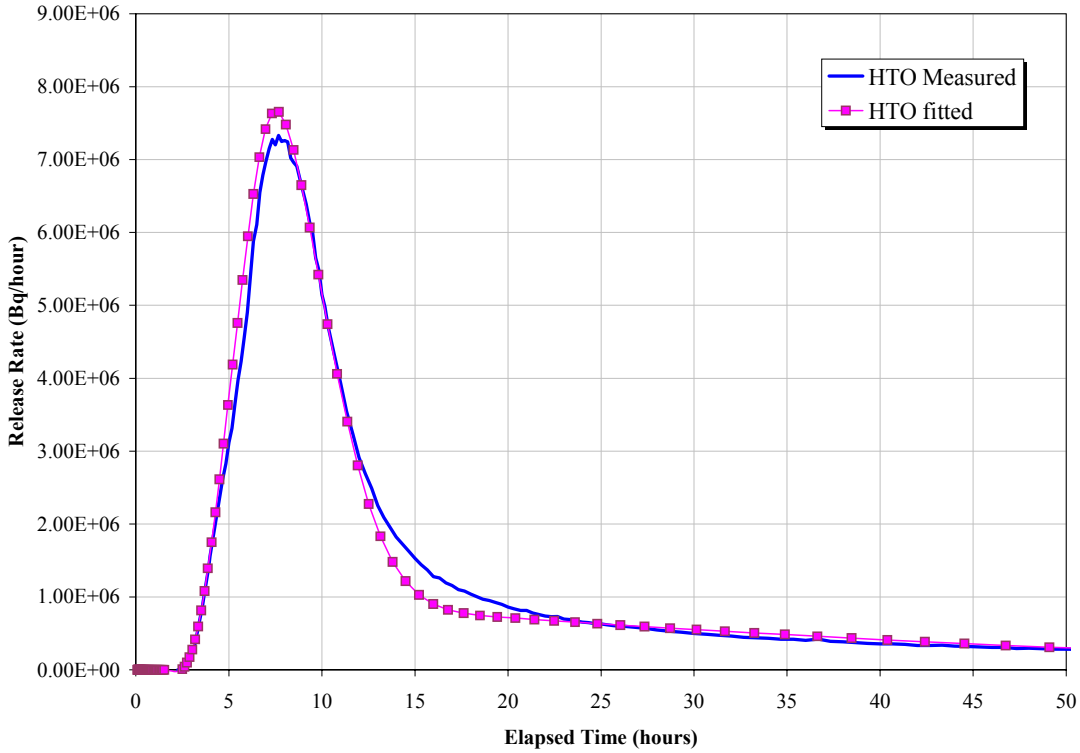

Figure 3-44 *STT-1b Calibration, HTO, Stochastic Field Case 3*

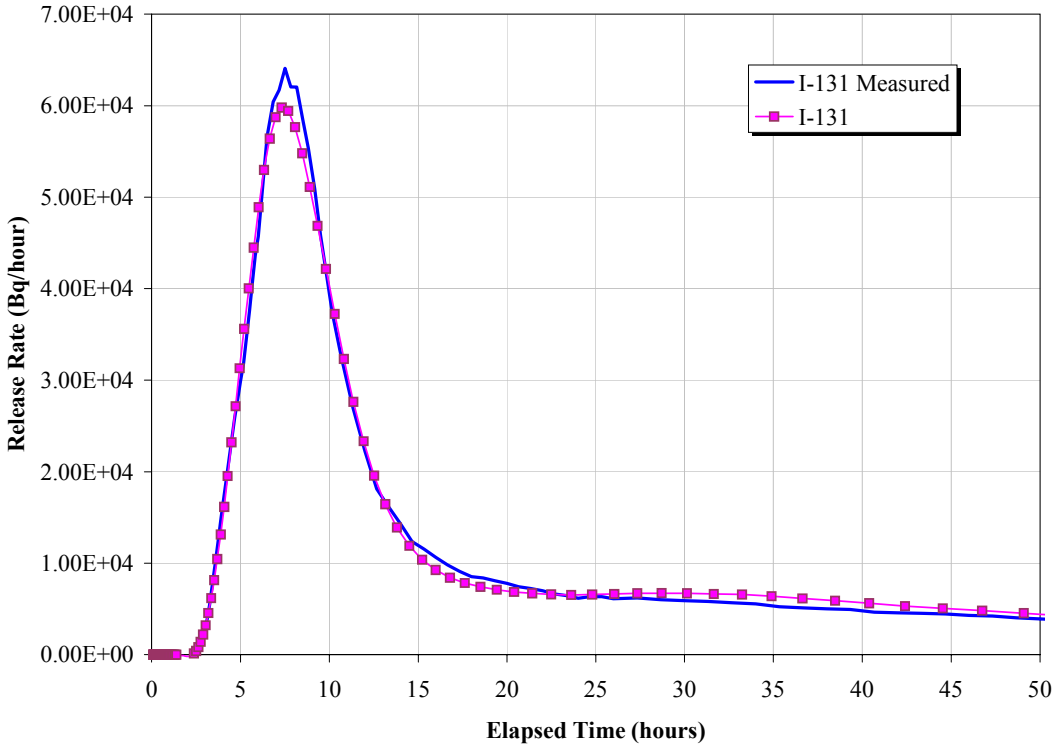

Figure 3-45 *STT-1b Calibration, I-131, Stochastic Field Case 3*

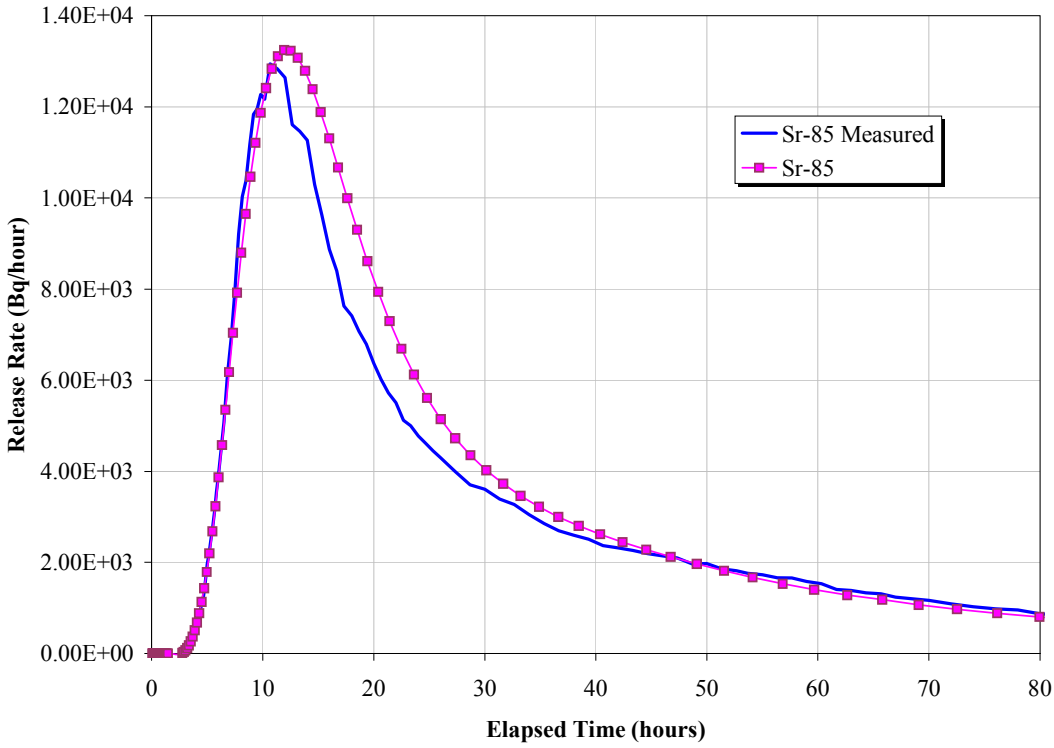

Figure 3-46 *STT-1b Calibration, Sr-85, Stochastic Field Case 3*

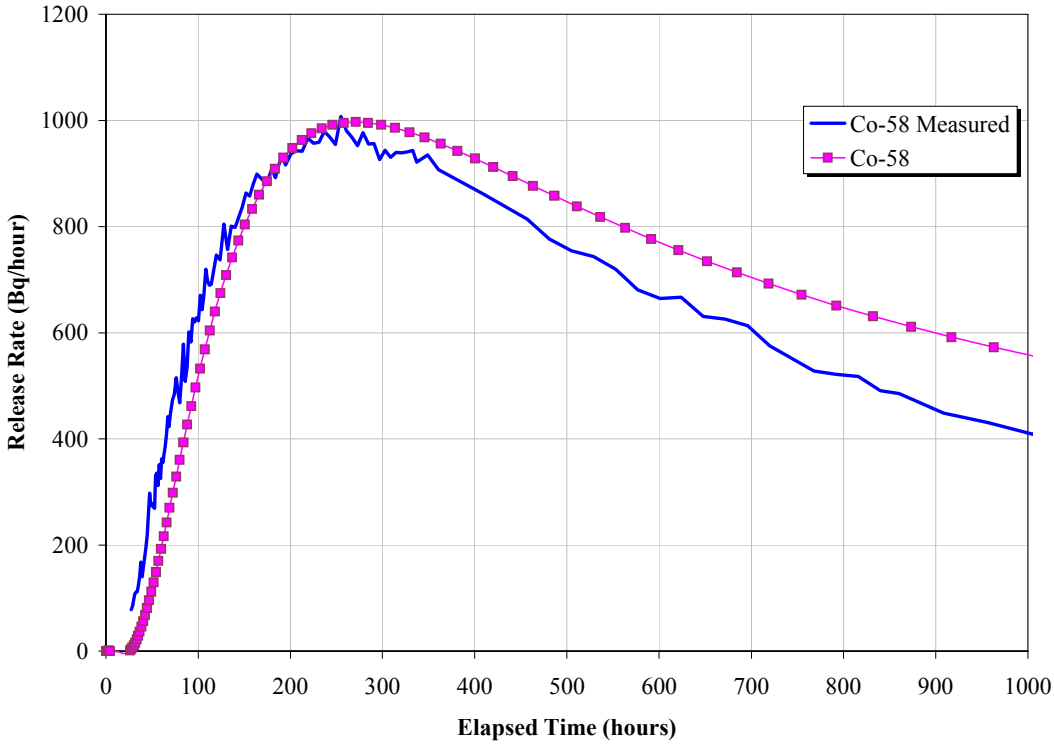

Figure 3-47 *STT-1b Calibration, Co-58, Stochastic Field Case 3*

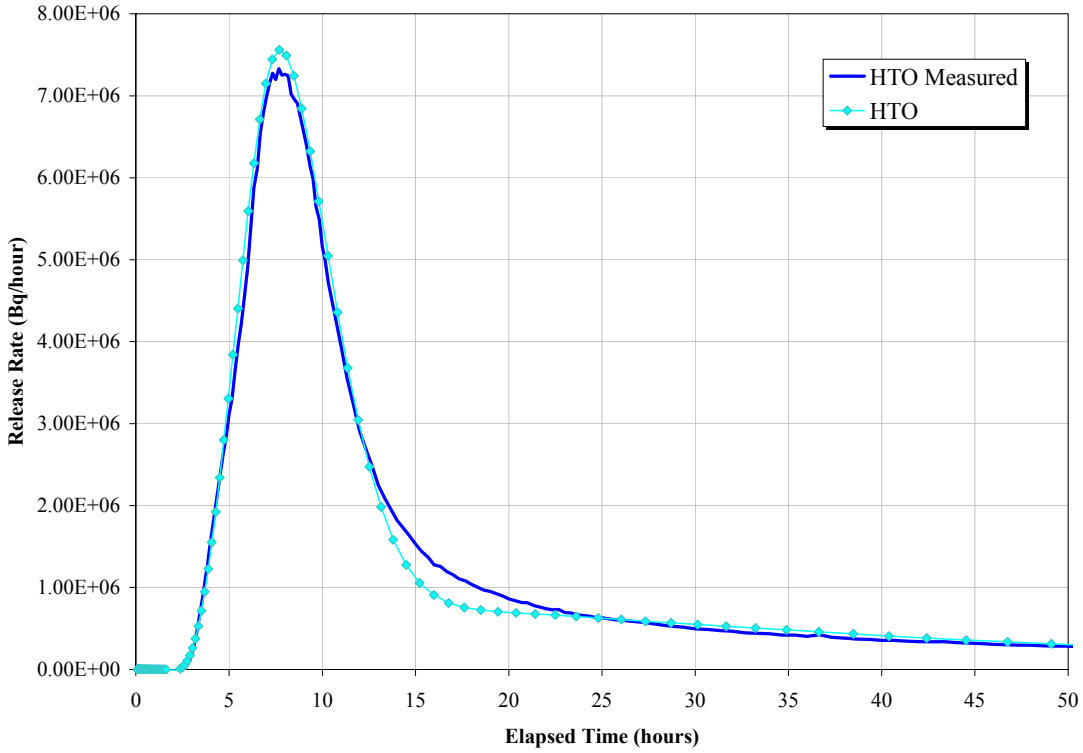

Figure 3-48 *STT-1b Calibration, HTO, Stochastic Field Case 4*

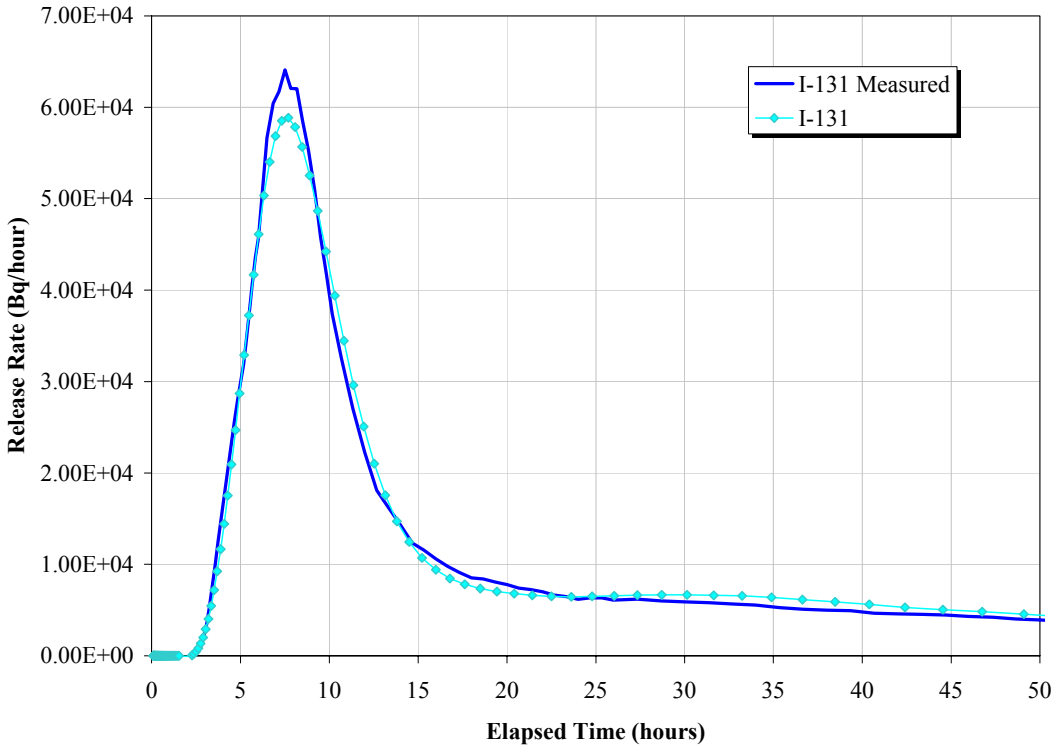

Figure 3-49 *STT-1b Calibration, I-131, Stochastic Field Case 4*

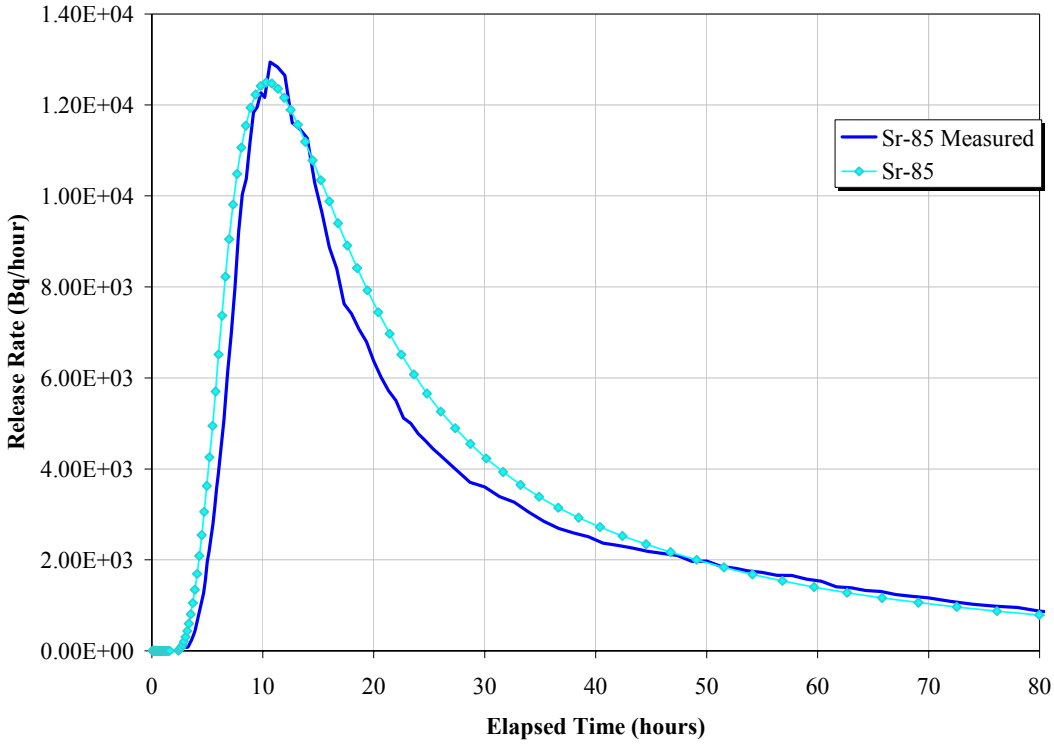

Figure 3-50 *STT-1b Calibration, Sr-85, Stochastic Field Case 4*

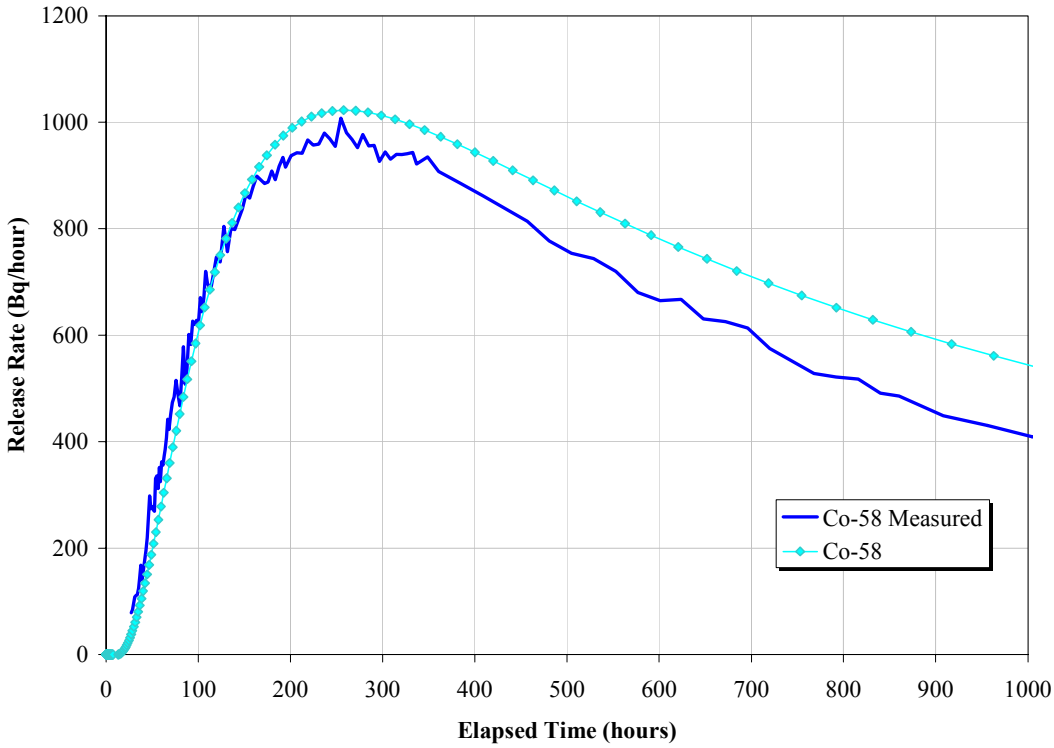

Figure 3-51 *STT-1b Calibration, Co-58, Stochastic Field Case 4*

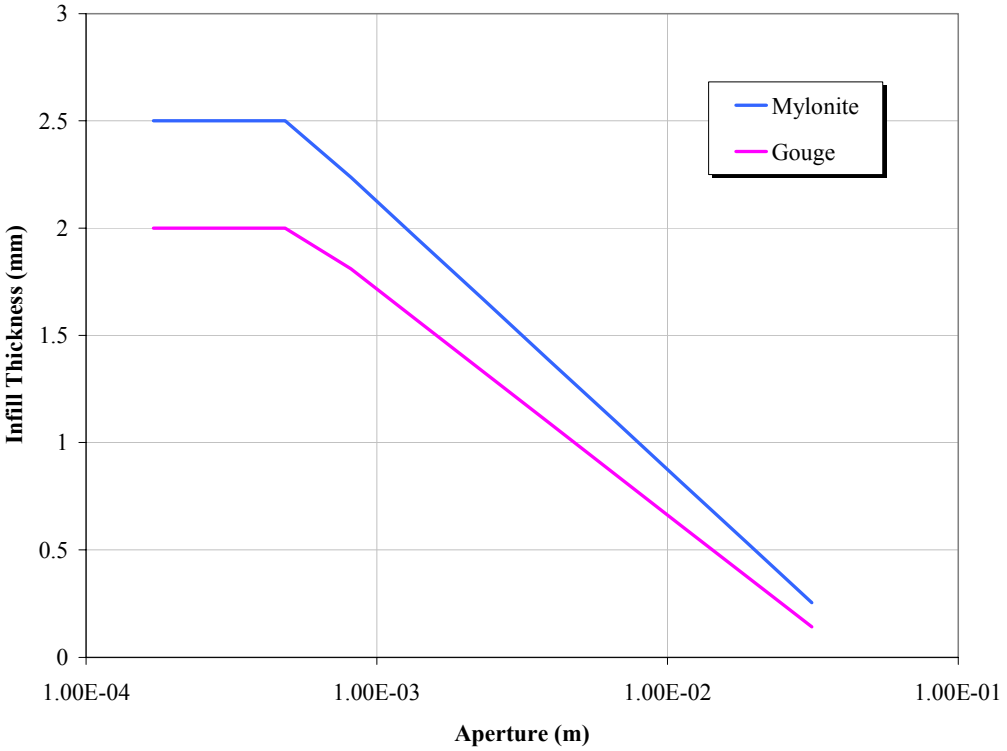

Figure 3-52 *STT-1b Calibration, Infill Thicknesses, Stochastic Field Case 1*

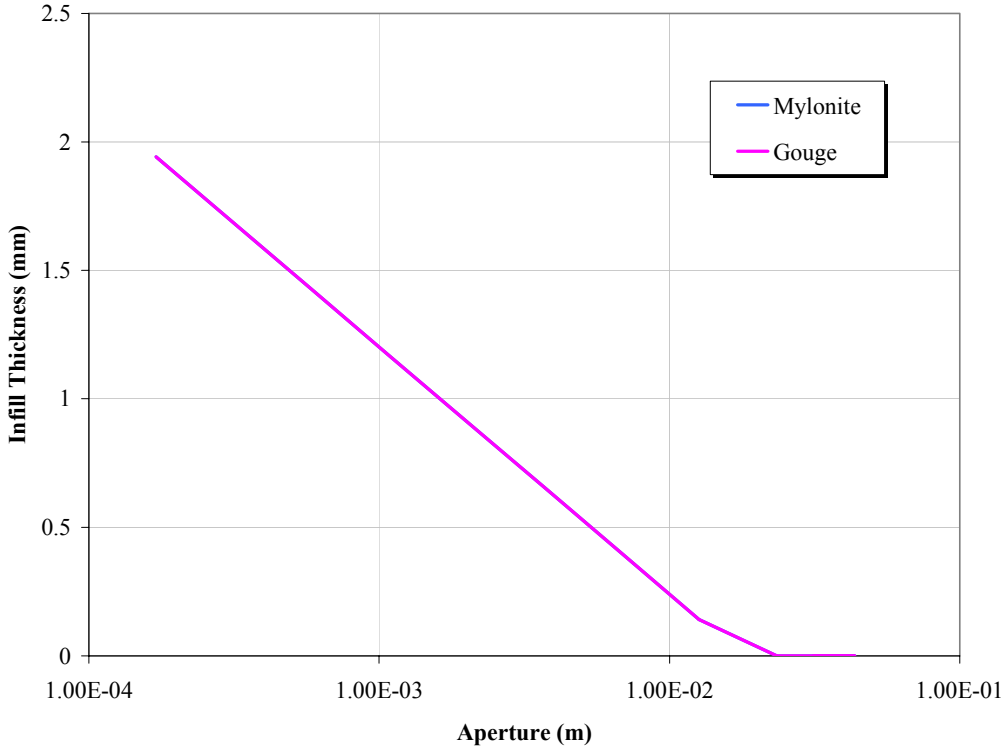

Figure 3-53 *STT-1b Calibration, Infill Thicknesses, Stochastic Field Case 2*

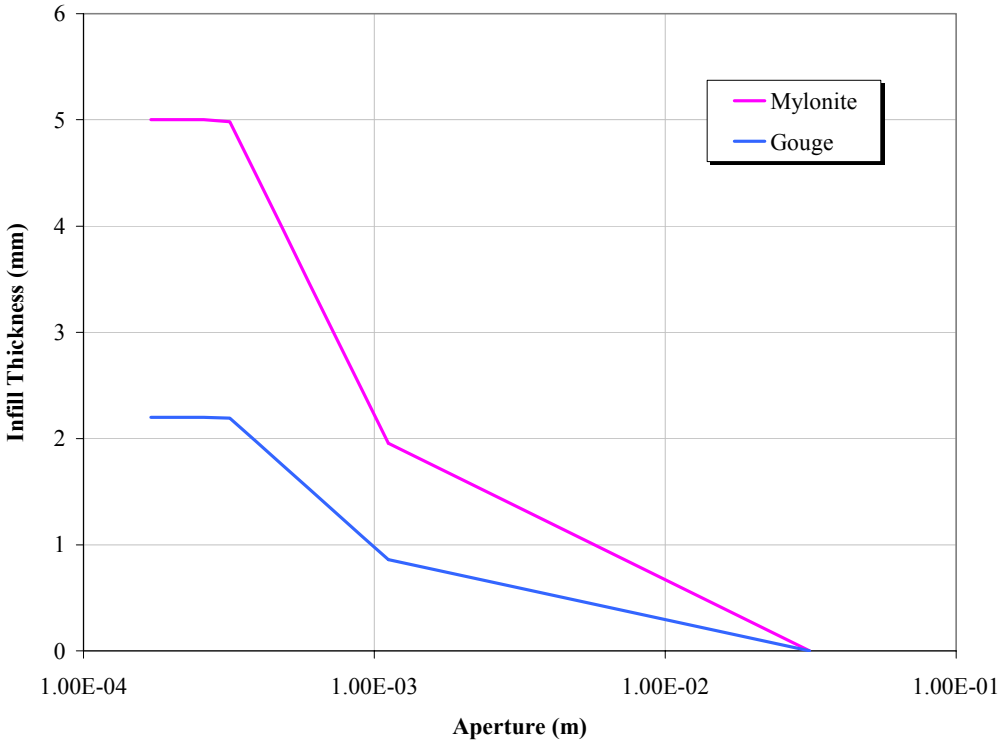

Figure 3-54 *STT-1b Calibration, Infill Thicknesses, Stochastic Field Case 3*

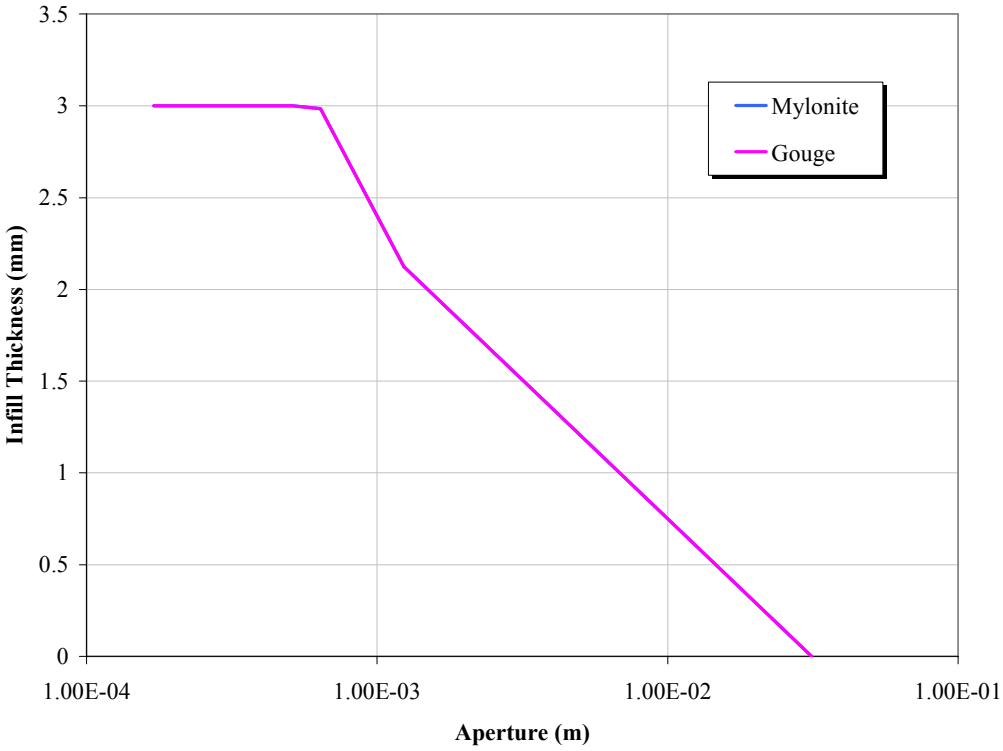

Figure 3-55 *STT-1b Calibration, Infill Thicknesses, Stochastic Field Case 4*

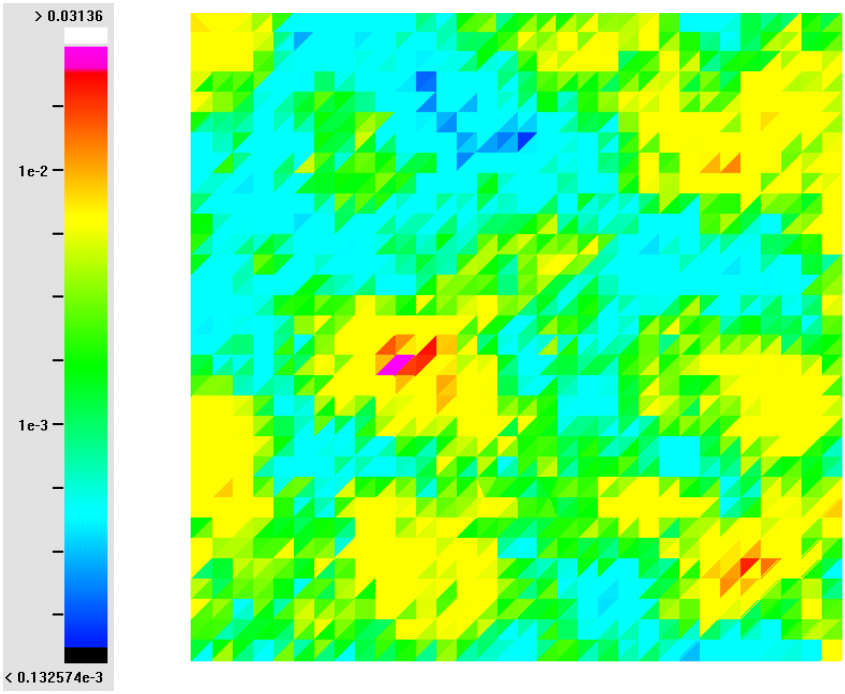

Figure 3-56 *Aperture Field Calibrated from Transmissivity Field, Stochastic Field Case 1*

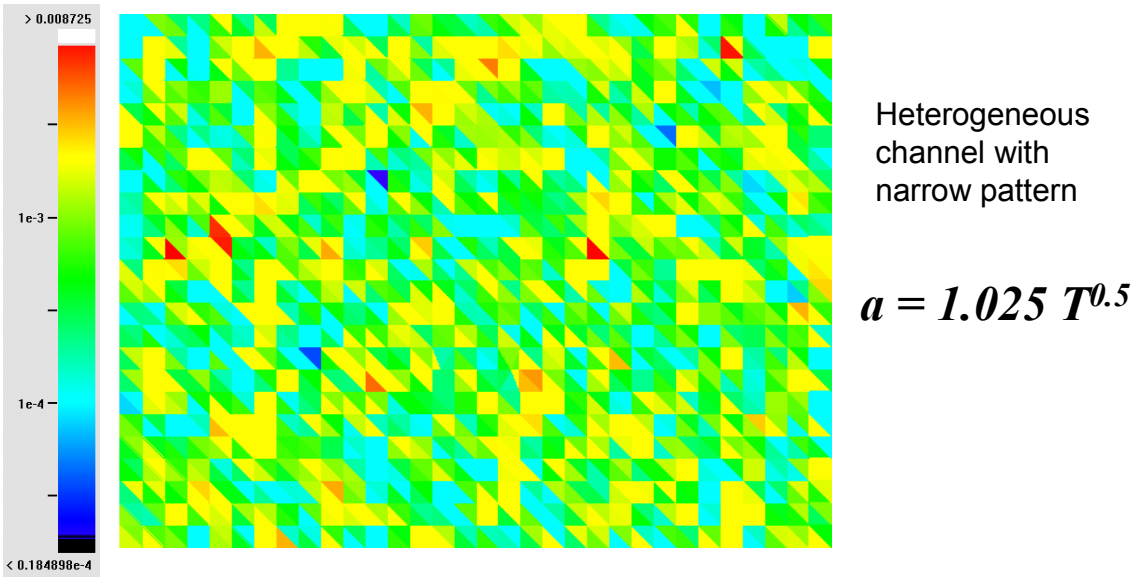

Figure 3-57 *Aperture Field Calibrated from Transmissivity Field, Stochastic Field Case 2*

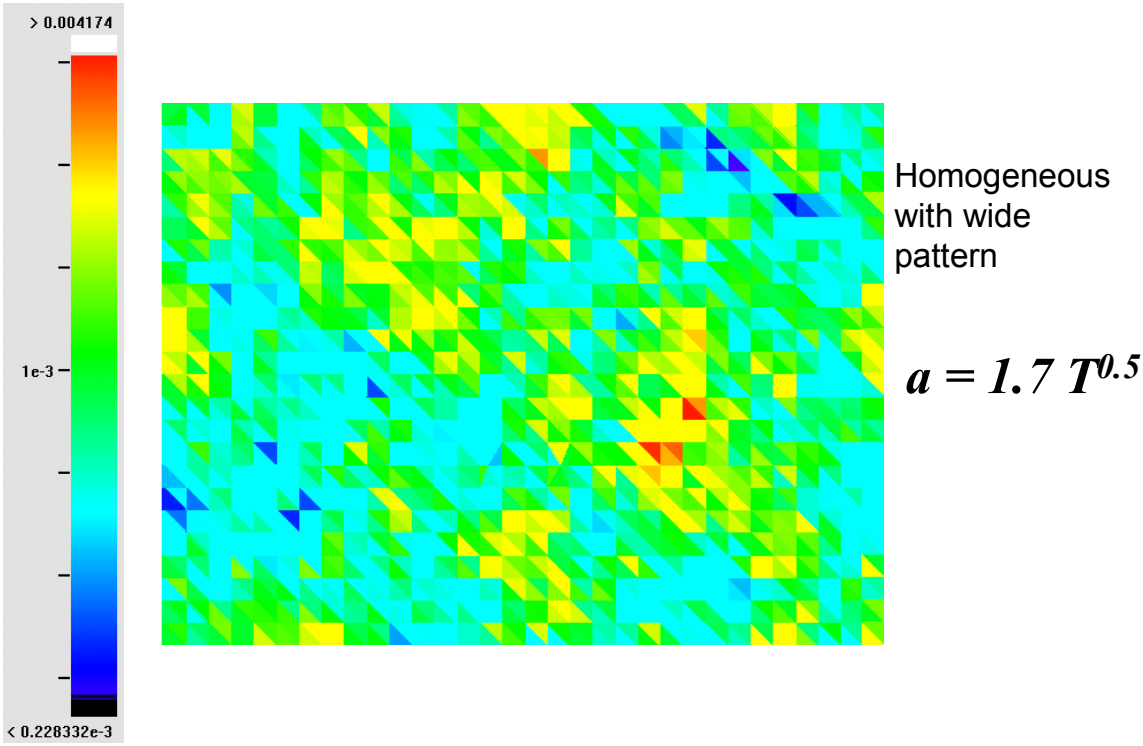

Figure 3-58 *Aperture Field Calibrated from Transmissivity Field, Stochastic Field Case 3*

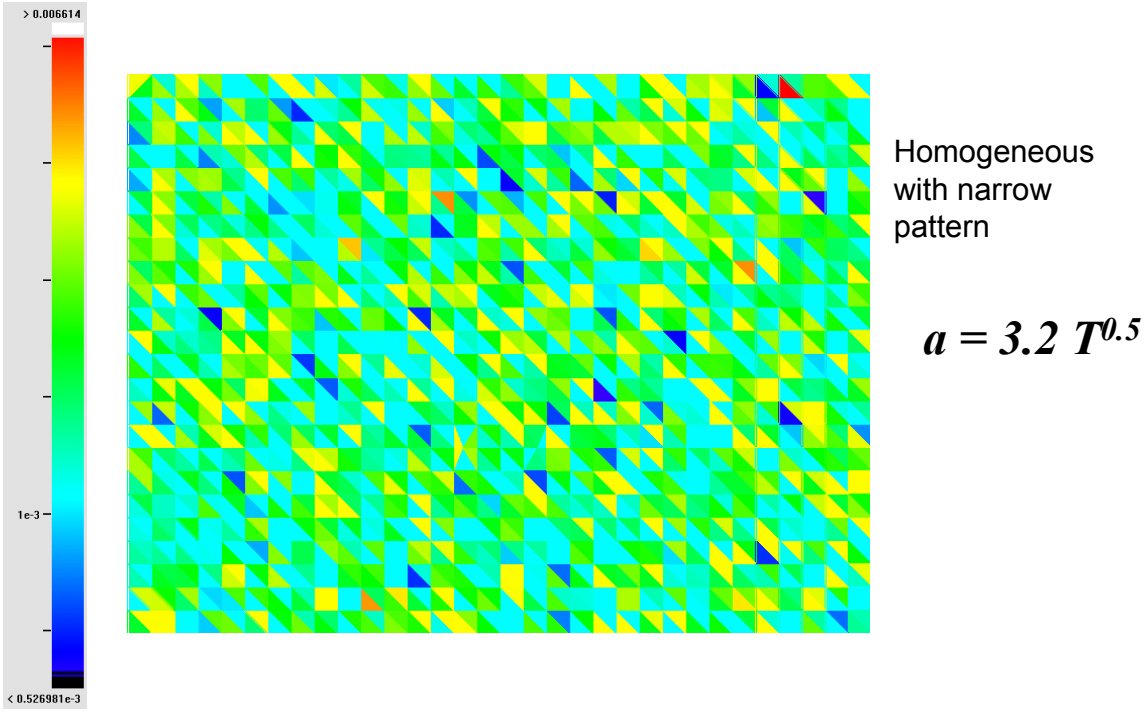

Figure 3-59 *Aperture Field Calibrated from Transmissivity Field, Stochastic Field Case 4*

3.3.3 Simulations – PA Time Scale

The four stochastic fields fracture cases calibrated in Section 4.3.1 above were simulated using Task 6B2 PA boundary conditions with dirac delta (1 Bq) and constant injection (1 MBq/year) boundary conditions. The tracers modeled for Task 6B2 were iodine, strontium, cobalt, technetium and americium, cf. Section 2.6. These tracers cover a range of sorption from none, weakly, moderately to strongly sorbing. Figures provides are as follows:

- Figures 4-60 through 4-64 Breakthrough curves for iodine, strontium, cobalt, technetium and americium
- Figures 4-65 through 4-69 Cumulative Breakthrough curves for iodine, strontium, cobalt, technetium and americium

Immobile zone properties for Iodine, Strontium, and cobalt for each of the four stochastic fields are identical to those derived by calibration. Values assumed for Technetium and Americium are as follows:

- Technicium,
  - Intact Granite Kd = 0.2 kg/m3
  - Mylonite & Disturbed Diorite Kd = 2.0 kg/m3
  - Gouge / Breccia Kd = 2.0 kg/m3
- Americium
  - Intact Granite Kd = 0.5 kg/m3
  - Mylonite & Disturbed Diorite Kd = 5.0 kg/m3
  - Gouge / Breccia Kd = 5.0 kg/m3

Breakthrough time T_5, T_{50}, and T_{95} are summarized in Table 4-12.

Table 3-3 Kd values Case 1 - GS6

Species	Rock Type	Kd value	Comment/Reference
HTO	all types	0.0 m^3/kg	Task 6A & 6B Modeling Task Specification
I-131	all types	0.0 m^3/kg	Task 6A & 6B Modeling Task Specification
Sr-85	Undisturbed Rock	4.7e-6 m^3/kg	Task 6A & 6B Modeling Task Specification
	Mylonite / Altered Diorite	3.0e-4 m^3/kg	TR98-18
	Breccia / Gouge	6.0e-4 m^3/kg	Higher than Altered diorite - Task 6A & 6B Modeling Task Specification page 5
Co-58	Undisturbed Rock	0.0008 m^3/kg	Task 6A & 6B Modeling Task Specification
	Mylonite / Altered Diorite	0.0025 m^3/kg	TR98-18
	Breccia / Gouge	0.21 m^3/kg	Higher than Altered diorite - Task 6A & 6B Modeling Task Specification page 5

Table 3-4 Free Water diffusivities – Case 1 (GS6)

Species	Free Water Diffusivity	Reference
HTO	2.40e-9 m^2/s	Task 6A & 6B Modeling Task Specification
I-131	1.66e-9 m^2/s	Task 6A & 6B Modeling Task Specification (calculated from D_{eff})
Sr-85	0.79e-9 m^2/s	Task 6A & 6B Modeling Task Specification
Co-58	0.58e-9 m^2/s	Task 6A & 6B Modeling Task Specification (calculated from D_{eff})

Table 3-5 Rock Properties

Rock	Porosity (%)	Thickness (mm)	Tortuosity	Density (kg/m^3)	Perimeter Fraction
Undisturbed Granite	0.15	1000	0.0125	2700	1.0
Mylonite / Disturbed Diorite	0.5	2.5	0.05	2700	1.1
Gouge / Breccia	20	2.0	1.0	2700	0.8

Table 3-6 Kd values Case 2 – GS9

Species	Rock Type	Kd value	Comment/Reference
HTO	all types	0.0 m^3/kg	Task 6A & 6B Modeling Task Specification
I-131	all types	0.0 m^3/kg	Task 6A & 6B Modeling Task Specification
Sr-85	Undisturbed Rock	4.7e-6 m^3/kg	Task 6A & 6B Modeling Task Specification
	Mylonite / Altered Diorite	1.0e-4 m^3/kg	TR98-18
	Breccia / Gouge	1.8e-4 m^3/kg	Higher than Altered diorite - Task 6A & 6B Modeling Task Specification page 5
Co-58	Undisturbed Rock	0.0008 m^3/kg	Task 6A & 6B Modeling Task Specification
	Mylonite / Altered Diorite	0.0025 m^3/kg	TR98-18
	Breccia / Gouge	0.085 m^3/kg	Higher than Altered diorite - Task 6A & 6B Modeling Task Specification page 5

Table 3-7 Free Water diffusivities – Case 2 (GS9)

Species	Free Water Diffusivity	Reference
HTO	2.40e-9 m^2/s	Task 6A & 6B Modeling Task Specification
I-131	1.66e-9 m^2/s	Task 6A & 6B Modeling Task Specification (calculated from D_{eff})
Sr-85	0.79e-9 m^2/s	Task 6A & 6B Modeling Task Specification
Co-58	0.18e-9 m^2/s	Reduced from Task 6A & 6B Modeling Task Specification to improve fit

Table 3-8 Kd values Case 3 – GS4

Species	Rock Type	Kd value	Comment/Reference
HTO	all types	0.0 m^3/kg	Task 6A & 6B Modeling Task Specification
I-131	all types	0.0 m^3/kg	Task 6A & 6B Modeling Task Specification
Sr-85	Undisturbed Rock	4.7e-6 m^3/kg	Task 6A & 6B Modeling Task Specification
	Mylonite / Altered Diorite	4.0e-4 m^3/kg	TR98-18
	Breccia / Gouge	2.75e-4 m^3/kg	Higher than Altered diorite - Task 6A & 6B Modeling Task Specification page 5
Co-58	Undisturbed Rock	0.0008 m^3/kg	Task 6A & 6B Modeling Task Specification
	Mylonite / Altered Diorite	0.0025 m^3/kg	TR98-18
	Breccia / Gouge	0.135 m^3/kg	Higher than Altered diorite - Task 6A & 6B Modeling Task Specification page 5

Table 3-9 Free Water diffusivities – Case 3 (GS4)

Species	Free Water Diffusivity	Reference
HTO	2.40e-9 m^2/s	Task 6A & 6B Modeling Task Specification
I-131	1.66e-9 m^2/s	Task 6A & 6B Modeling Task Specification (calculated from D_{eff})
Sr-85	0.79e-9 m^2/s	Task 6A & 6B Modeling Task Specification
Co-58	0.15e-9 m^2/s	Reduced from Task 6A & 6B Modeling Task Specification to improve fit

Table 3-10 Kd values Case 4 – GS1

Species	Rock Type	Kd value	Comment/Reference
HTO	all types	0.0 m^3/kg	Task 6A & 6B Modeling Task Specification
I-131	all types	0.0 m^3/kg	Task 6A & 6B Modeling Task Specification
Sr-85	Undisturbed Rock	4.7e-6 m^3/kg	Task 6A & 6B Modeling Task Specification
	Mylonite / Altered Diorite	4.0e-4 m^3/kg	TR98-18
	Breccia / Gouge	4.5e-4 m^3/kg	Higher than Altered diorite - Task 6A & 6B Modeling Task Specification page 5
Co-58	Undisturbed Rock	0.0008 m^3/kg	Task 6A & 6B Modeling Task Specification
	Mylonite / Altered Diorite	0.0025 m^3/kg	TR98-18
	Breccia / Gouge	0.31 m^3/kg	Higher than Altered diorite - Task 6A & 6B Modeling Task Specification page 5

Table 3-11 Free Water diffusivities – Case 4 (GS1)

Species	Free Water Diffusivity	Reference
HTO	2.40e-9 m^2/s	Task 6A & 6B Modeling Task Specification
I-131	1.66e-9 m^2/s	Task 6A & 6B Modeling Task Specification (calculated from D_{eff})
Sr-85	0.79e-9 m^2/s	Task 6A & 6B Modeling Task Specification
Co-58	0.25e-9 m^2/s	Reduced from Task 6A & 6B Modeling Task Specification to improve fit

Table 3-12 Task 6B2 Breakthrough Statistics

Case1	t5 (years)	t50 (years)	t95 (years)
I	1.21	2.07	4.31
Sr	3.47	6.80	18.68
Co	435.27	887.91	2691.41
Tc	9558.52	24728.56	133110.88
Am	14203.46	47534.03	2129303.24

Case2	t5 (years)	t50 (years)	t95 (years)
I	0.74	1.14	2.16
Sr	1.84	3.08	7.08
Co	310.86	530.60	999.93
Tc	15681.74	30746.82	146964.91
Am	25223.12	62720.23	193917.15

Case3	t5 (years)	t50 (years)	t95 (years)
I	0.77	1.24	2.29
Sr	3.08	6.54	14.44
Co	287.18	499.99	923.78
Tc	13384.22	30746.82	133110.88
Am	16315.31	49454.33	271531.11

Case4	t5 (years)	t50 (years)	t95 (years)
I	1.57	2.34	3.76
Sr	5.47	8.98	15.94
Co	1345.78	2039.75	3216.47
Tc	18741.16	33947.13	144083.52
Am	30143.96	67890.14	218382.26

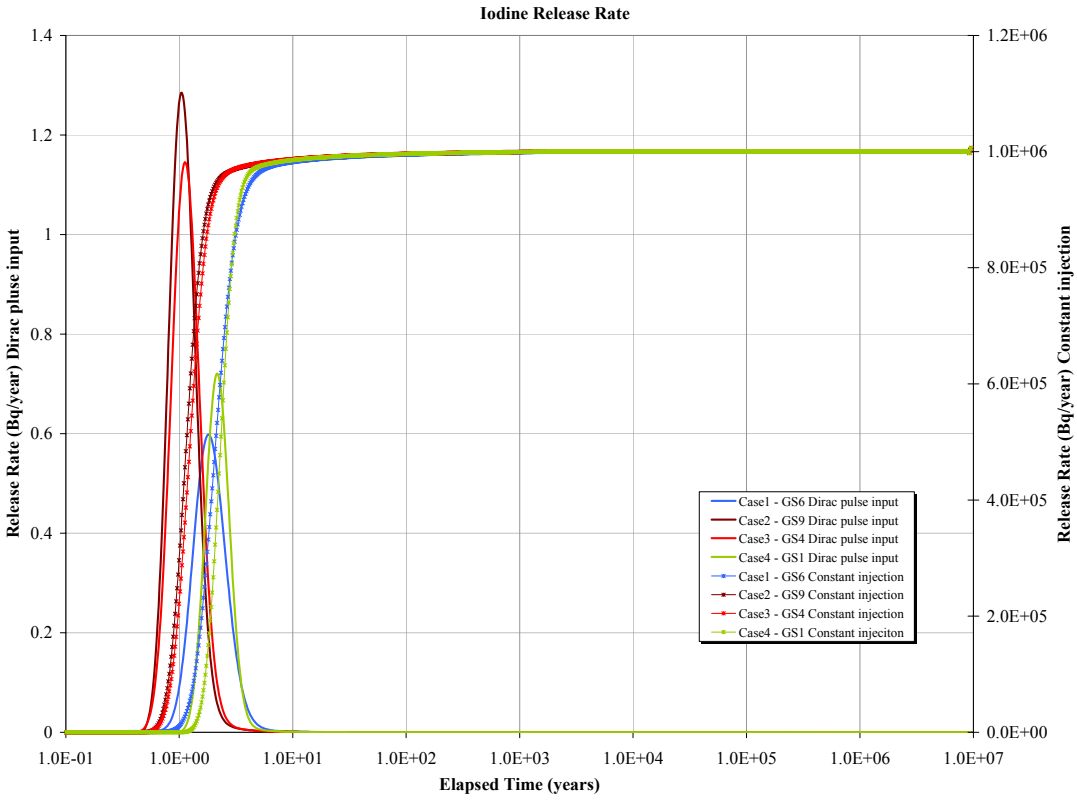

Figure 3-60 *PA Time Scale Breakthrough, Iodine*

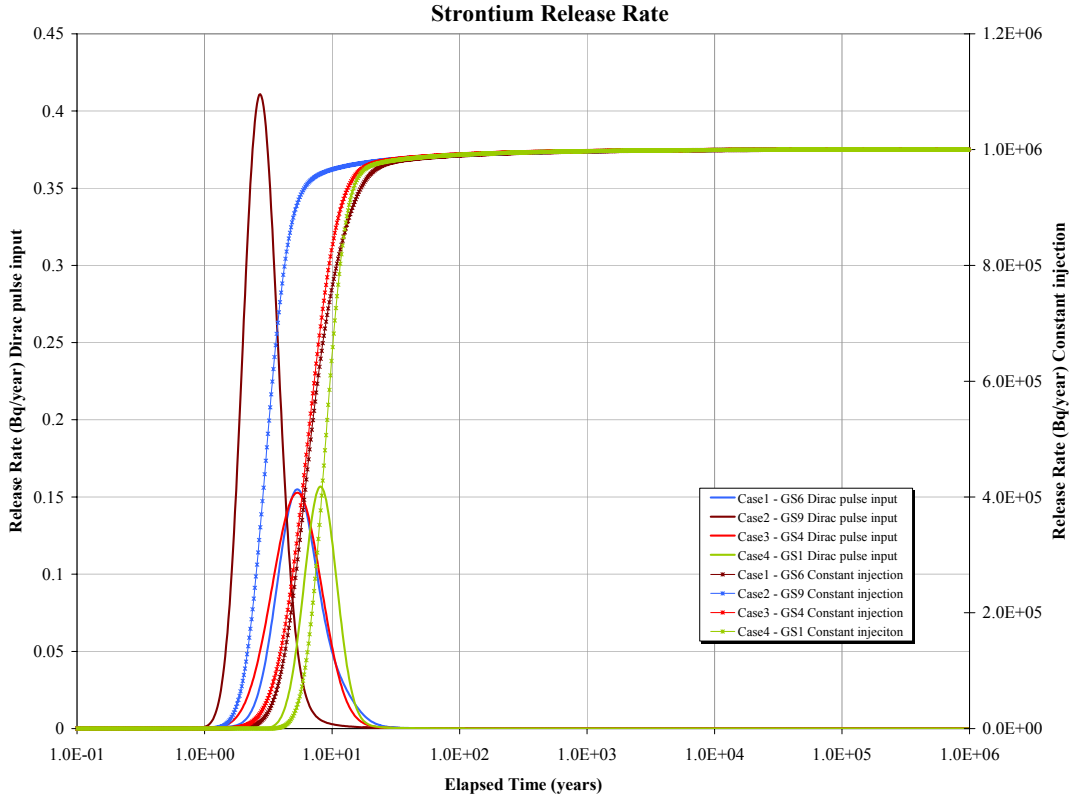

Figure 3-61 *PA Time Scale Breakthrough, Strontium*

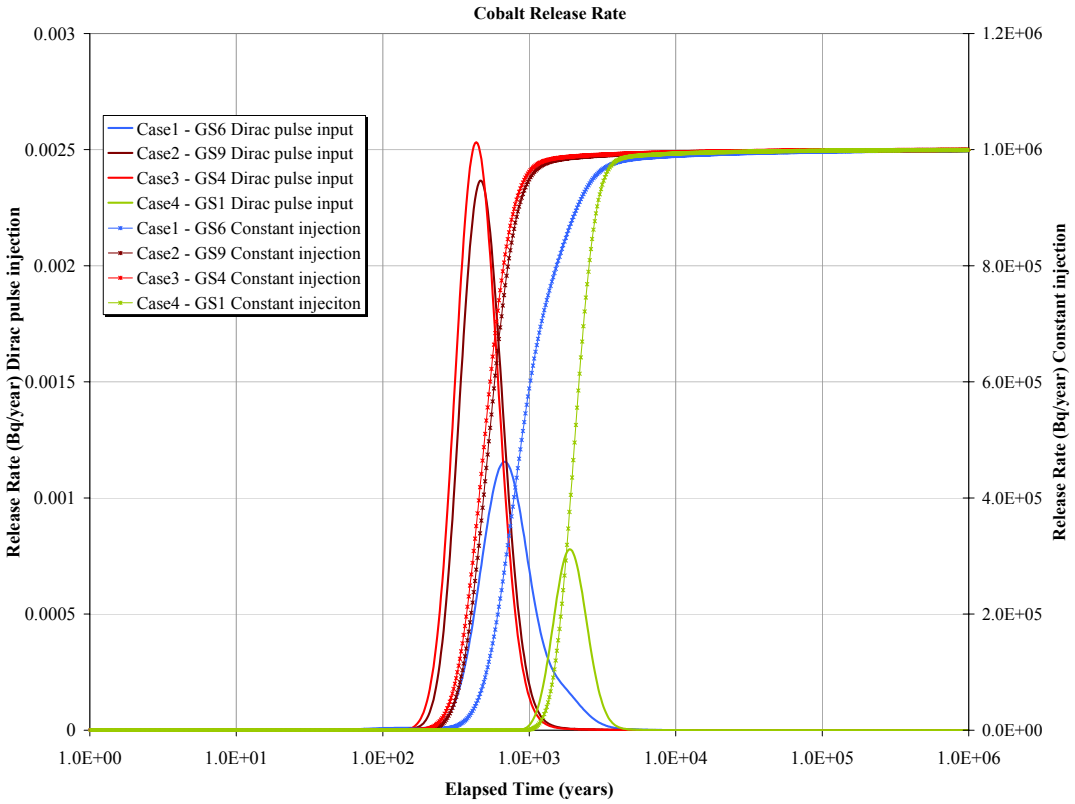

Figure 3-62 *PA Time Scale Breakthrough, Cobalt*

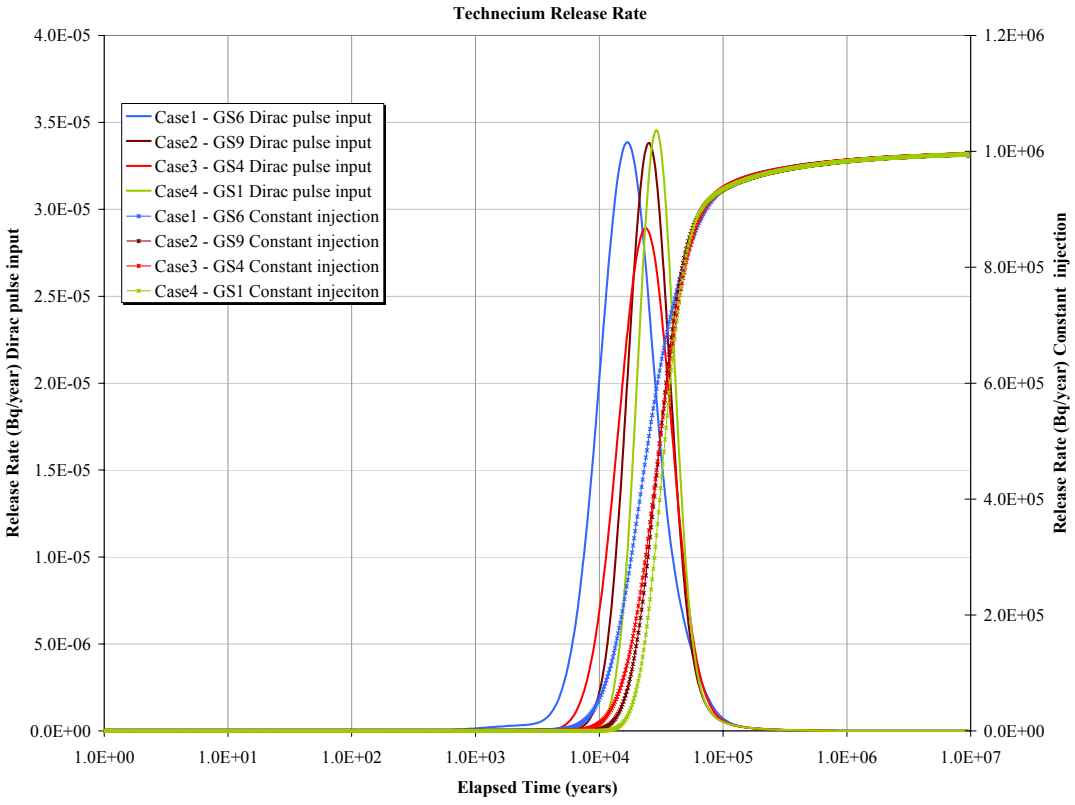

Figure 3-63 *PA Time Scale Breakthrough, Technetium*

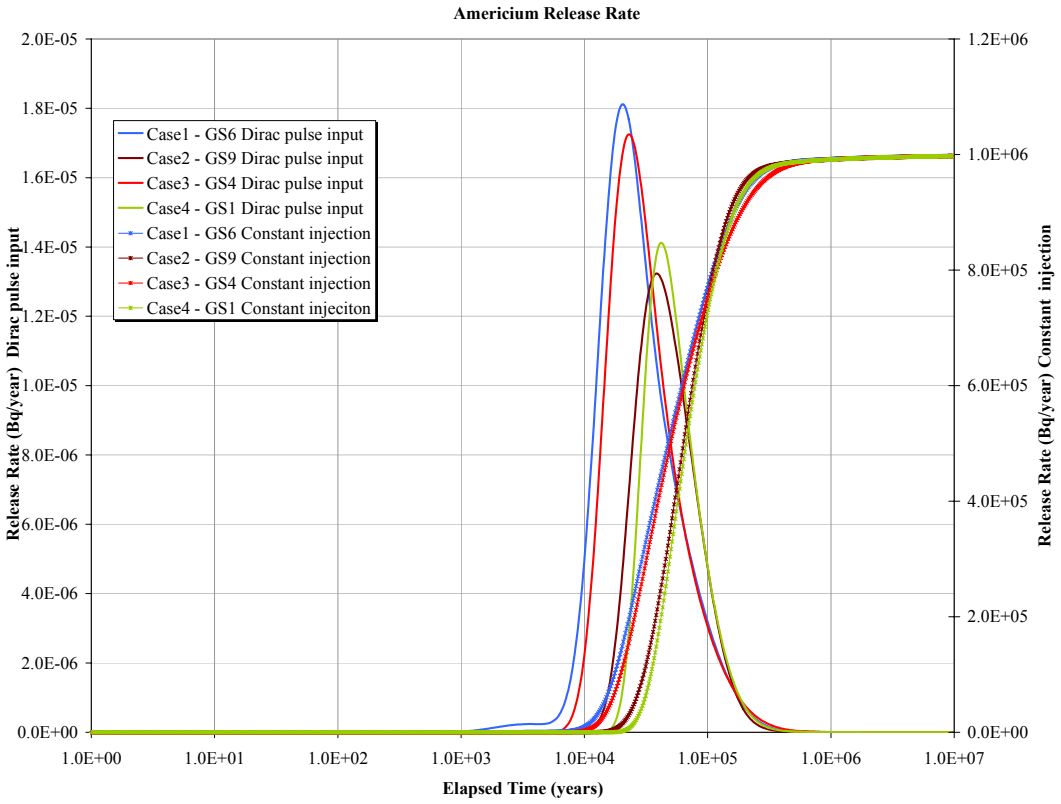

Figure 3-64 *PA Time Scale Breakthrough, Amerecium*

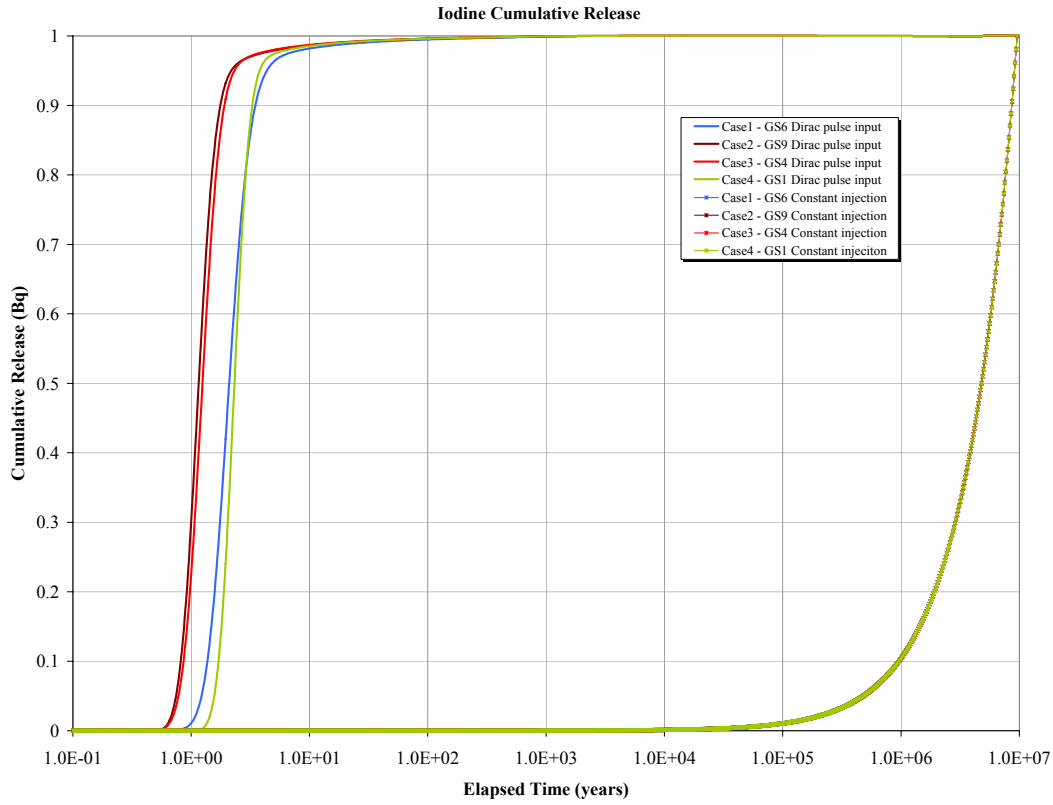

Figure 3-65 *PA Time Scale Cumulative Breakthrough, Iodine*

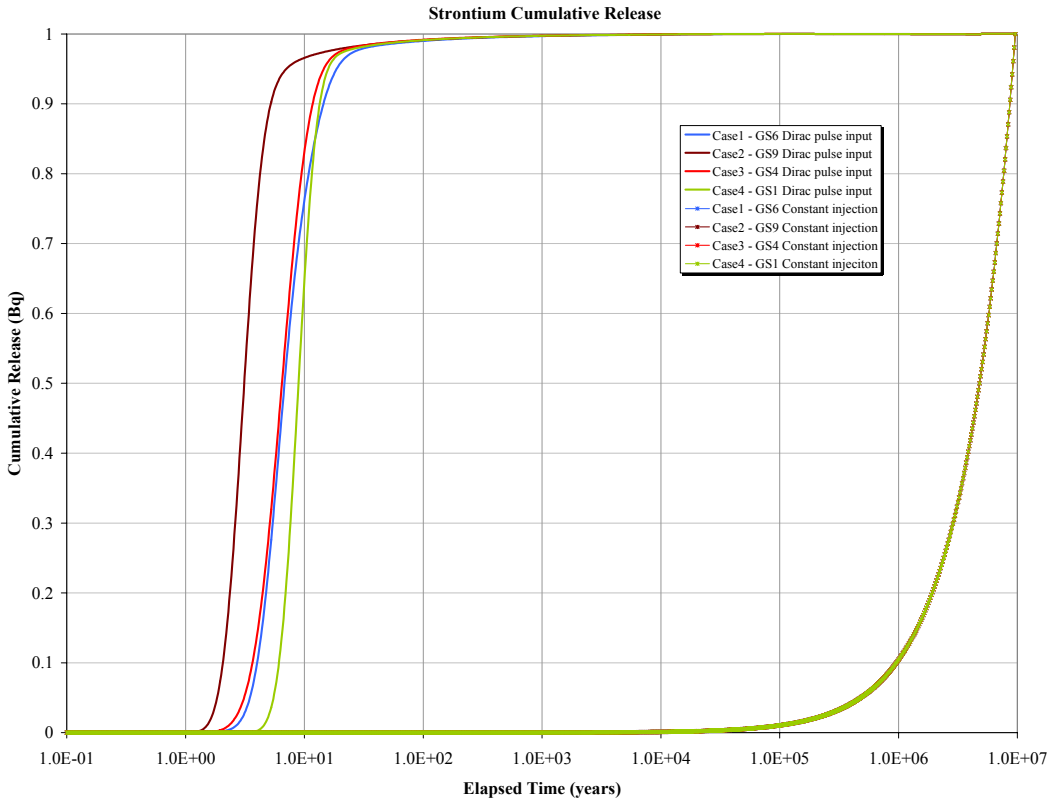

Figure 3-66 *PA Time Scale Cumulative Breakthrough, Strontium*

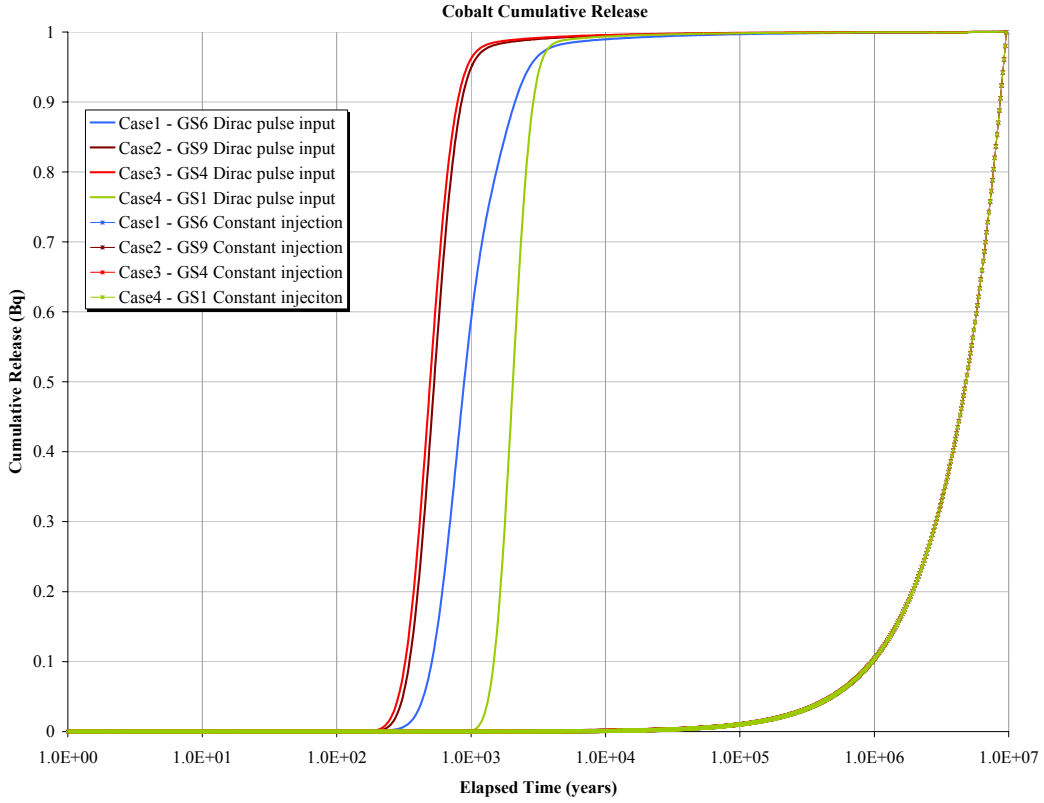

Figure 3-67 *PA Time Scale Cumulative Breakthrough, Cobalt*

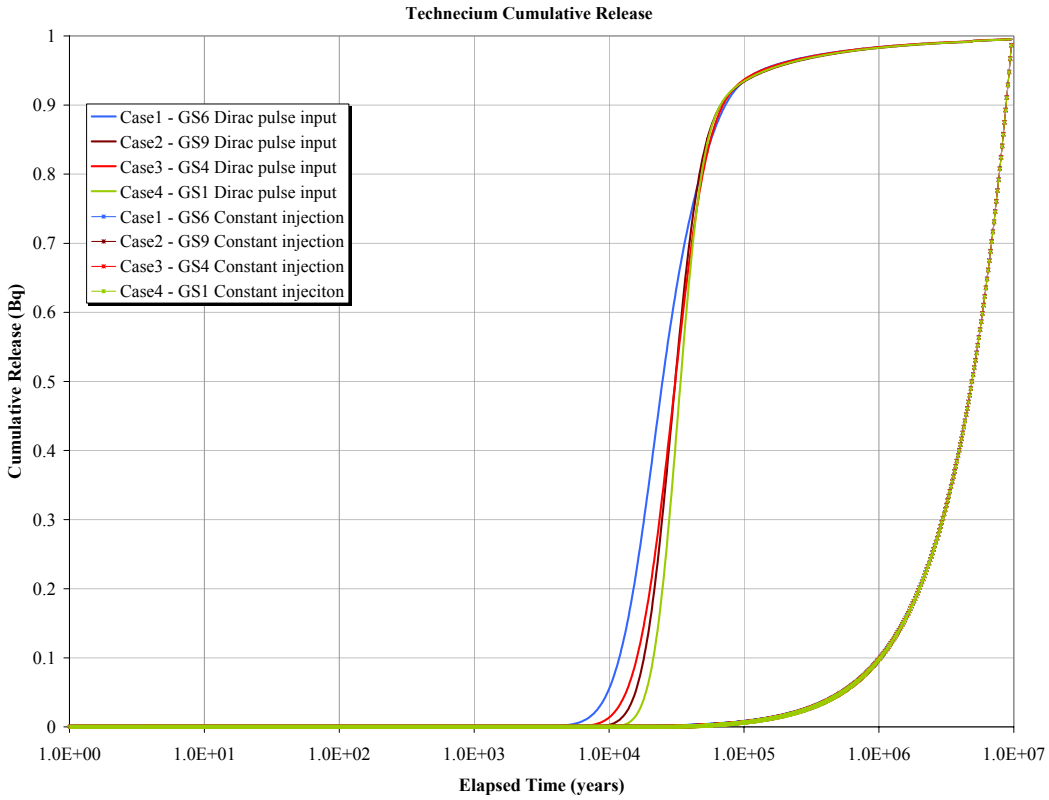

Figure 3-68 *PA Time Scale Cumulative Breakthrough, Technetium*

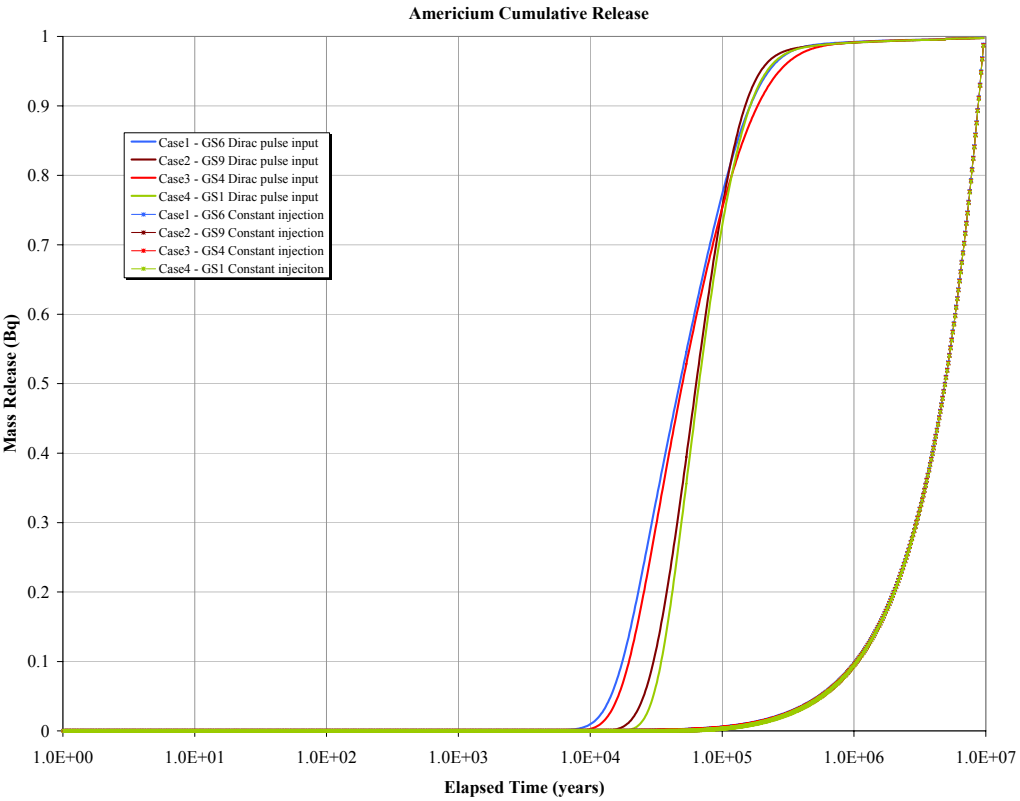

Figure 3-69 *PA Time Scale Cumulative Breakthrough, Amerecium*

3.3.4 Discussion

Despite the large difference between the stochastic fields assumed for Cases 1 through 4, and the limited constraining power of the STT-1b tracer transport experiment, very little difference between the various breakthrough curves is evident in Figure 3-60 through Figure 3-69. The greatest differences are on the scale of one order of magnitude, for iodine. The difference in breakthrough between different cases decreases as sorption activity increases.

4 Discussion

4.1.1 Conceptual issues

The simulations carried out for Task 6A and Task 6B directly addressed the ability of site characterisation approaches to constrain performance assessment. The PA code GoldSim was applied successfully for what is normally considered site characterisation modeling in Task 6A. The PA code matched the observed tracer breakthrough and also provided valuable insight concerning parameter uncertainty. The PA code had considerable flexibility for addressing the multiple immobile zones controlling transport at the site characterisation time scale.

It is important to note, however, that the site characterisation experiment studied in Task 6A was radially converging, which makes it particularly well suited for 1-D PA approaches. Simulations carried out for Task 6A demonstrated the value of PA type codes for rapid simulation and sensitivity studies to identify the range of consistent transport parameters, as opposed to the single "correct" set of parameters.

The simulations carried out for Task 6B propagated the residual parameter uncertainty from Task 6A to PA time scales. Where parameters were not sufficiently constrained by site characterization, the uncertainty at the PA time scales came back to the level of uncertainty based on the physically possible range of transport properties. In some cases, this range of uncertainties may still be acceptable for PA purposes. However, where this is not the case, Task 6B demonstrates the need for alternative site characterisation approaches to better constrain these parameters. Task 6B also demonstrates the importance of properly accounting for the residual uncertainty in transport parameters following site characterisation "calibration" exercises, rather than assuming that the single "best fit" parameters are "true".

Task 6B2 introduced the effect of (a) in plane heterogeneity not directly measurable in situ and (b) more realistic natural gradient PA boundary conditions. This combination has very significant effects on the spatial pattern of tracer breakthrough. Task 6B2 simulations addressed the issue as to whether site characterisation contrains in plane heterogeneity sufficiently to justify 2D PA calculations. Using widely varying stochastic continuum fields, it was still possible to calibrate 2D site characterization models to the STT-1b breakthrough using physically reasonable micro-structural model parameters. The PA scale time scale results for these different 2D hetereogenous models are significantly more similar than expected. This indicates that perhaps the level of uncertainty at the PA scale due to microstructural model uncertainty may not be sufficient to justify 2D modeling at PA time scales.

4.1.2 Lessons learned

The following lessons have been learned from the Task 6A, 6B, and 6B2 simulations:

- PA type probabilistic models can facilitate valuable sensitivity and uncertainty studies of site characterisation experiments.
- The STT-1b tracer experiment used to condition the Task 6A GoldSim model was not sufficient to constrain results at the PA time scale
- Two dimensional microstructural model heterogeneity can have a significant influence on tracer breakthrough. However, microstructure properties can be calibrated to match observed breakthrough under a wide variety of spatial heterogeneity assumptions.
- Uncertainty in the two dimensional spatial pattern of microstructural model heterogeneity can result in approximately 0.5 to 1 order of magnitude variation in PA time scale breakthrough.

References

Cvetkovic, V., Selroos, J-O., and H. Cheng. 1999. "Transport of reactive solute in single fractures." J. Fluid Mech. 318:335-356.

Dershowitz et al., 2002. Task 6C. A Semi-synthetic Model of Block Scale Conductive Structures at the Äspö Hard Rock Laboratory. SKB, Stockholm.

Dershowitz, W., Fox, A., Uchida, 2001. Understanding of Sorbing Transport in Fracture Networks at the 10-Meter Scale. SKB, International Cooperation Report ICR-01-XX, 2001.

Elert, Mark and Jan-Olof Selroos, 2001. TASK 6B2 Modeling task specification, Ver 1.0. SKB, Stockholm

Mazurek, M. and A. Jacob. 2001. "Evidence for matrix diffusion in the TRUE-1 Block at Äspö based on fracture characterization and modeling of tracer tests", Geological Evidence and Theoretical Bases for Radionuclide Retention. Workshop Proceedings, Oskarshamn, Sweden, 7-9 May 2001. OECD NEA, Paris.

Miller, I., 2002. GoldSim Pro, Version 751.1. User Documentation. Golder Associates Inc., Redmond, Washington.

Nagra, 1994. Kristallin-I Safety Assessment Report. Technical Report 93-22. Nagra, Wettingen, Switzerland.

Neretnieks, I., 1983. A Note on Fracture Flow Dispersion Mechanisms in the Ground. Water Resources Research Vol 19, pp 364-370.

Winberg, A., Andersson, P., Hermanson, J., Byegård, J., Cvetkovic, V. and L. Birgersson. 2000. "Final report of the first stage of the tracer retention understanding experiments. "Swedish Nuclear Fuel and Waste Management Company (SKB), Technical Report TR-00-07. ISSN 1404-0344.